



Faculty of Sciences  
Physics and Astronomy

# Human heart heterogeneity and its role in the onset and perpetuation of cardiac arrhythmias

Arne Defauw

Thesis submitted in fulfillment of the requirements for the degree of  
Doctor (Ph.D.) in Sciences: Physics

Year 2014-2015

Promotor : Prof. Dr. Alexander V. Panfilov

Co-Promotor: Prof. Dr. Peter Dawyndt







# Word of thanks

---

Men schrijft niet zomaar een doctoraatsthesis. Daarvoor is hulp nodig. Soms veel hulp, soms wat minder, af en toe ‘academische’ hulp, dan weer een goed gesprek met collega’s, vrienden of familie. Daarom grijp ik hier de gelegenheid aan om enkele mensen te bedanken die ervoor hebben gezorgd dat ik alles tot een goed einde kon brengen.

Allereerst wil ik mijn promotor Sasha Panfilov bedanken. Sasha, ik heb ontzettend veel van je geleerd de afgelopen vier jaar. Zowel op het gebied van (bio)fysica, als het leren schrijven van artikels en het opbouwen van onderzoek in het algemeen. Dit was bijzonder leerrijk voor mij. Ook kon ik, hoewel je het altijd razend druk hebt, altijd bij je terecht voor allerlei vragen. Het was een eer voor mij om de afgelopen vier jaar met jou te hebben mogen samenwerken.

Ik dank ook mijn co-promotor Peter Dawyndt voor de fijne samenwerking. Vooral dan om ons op weg te zetten bij het opstellen van een databank, waarvan we in deze thesis een prototype presenteren.

I also like to thank Prof. Efimov for the collaboration during this PhD, and for the hospitality during my visit at Washington University in St. Louis. I thank the research group of Prof. Efimov, and particularly Katherine Holzem for helping me setting up a structure for the database, and Bas Boukens for interesting discussions and showing me around in St. Louis. I also thank Alexey Glukhov for providing me with the data on which some of the results presented here are based.

Verder wil ik Bart Verheyde bedanken om me de basis van Drupal aan te leren, waardoor ik de database en corresponderende website, zoals beschreven in deze thesis, kon opstellen.

De simulaties beschreven in dit proefschrift werden hoofdzakelijk uitgevoerd op de STEVIN supercomputer van de Universiteit Gent. Ik dank daarom ook het High Performance Computing centrum van de UGent.

Ik dank ook mijn collega’s van de onderzoeksgroep biofysica. Ivan bedank ik om een fijne bureaugenoot te zijn, en om me enorm veel bij te leren over zo wat alles wat ik nodig had voor het onderzoek zoals het hier beschreven staat: van werken met Linux over programmeren in C en C++ tot (bio)fysica. Hans dank ik voor interessante discussies over de meer theoretische aspecten van (bio)fysica, vooral zeer nuttig bij het schrijven van het tweede hoofdstuk, en uiteraard ook om gedurende vier jaar een sympathieke bureaugenoot te zijn. Nele dank ik voor hulp bij zowel C, C++, Python als fysica problemen, en ook voor de leuke gesprekken tussendoor, en om met, bijvoorbeeld, planten allerlei en mini workshops over ‘positive thinking’, onze bureau op te fleuren. Ik dank ook de andere leden van onze onderzoeksgroep Sander, Tim, Sergei en Daniël voor raad, daad en onderonsjes. Ook dank aan Ilse van ‘de sterrenkunde’ voor de jarenlange vriendschap, de plezierige babbels tussendoor, en uiteraard ook voor het maken van lekkere desserts voor de hele vakgroep, die keren dat ik jarig was.

Esther Everaert dank ik voor het ontwerpen van de omslag van dit proefschrift.

---

Ik bedank ook twee heel bijzondere vrienden: Gertjan en Hannah. Gertjan, bedankt om al zoveel jaren een fantastische vriend te zijn. Er zijn weinig dingen die leuker zijn dan met jou een boom op te zetten over de meer occulte of afgestorven zijtakken van de wetenschap; wat Hegel nu juist bedoelde met ‘der Geist’; of wat een rare mens Franz Kafka moet zijn geweest. Hannah, bedankt om de warme mens te zijn die je bent, en om me altijd met open armen, verse soep, en het ‘lekkerste eten van de week’ te ontvangen bij huisje weltevree. Ik dank ook de rest van het Gentse team: Dave om het levende bewijs te zijn dat het helemaal OK is om naar Limp Bizkit te luisteren in 2014; Simon om me te doen inzien dat er ook zoiets bestaat als ‘clever use of game mechanics’; Fashion Queen Romany voor Fashion-advies; en Louis om de sympathieke notabele te zijn die je bent. De Brusselse connectie Kristien dank ik voor de vele updates uit het leven van Solange: nu ik begrijp dat zij het stijlvolle zusje is van Beyoncé, is mijn leven completer.

Mijn ouders kan ik niet genoeg bedanken. Ik weet amper waar te beginnen. Misschien om me de mogelijkheid te geven om wiskunde te studeren, of om altijd klaar te staan met een bemoedigend woord of een goed gesprek. Maar ik denk vooral om zowel Ineke als mij altijd te steunen, en voor een bijzonder warme plaats te zorgen waar wij altijd terecht kunnen. Mijn zus Ineke, Dries, Seppe en Tess bedank ik om een ontzettend lief en leuk gezinnetje te vormen; het doet me altijd veel plezier om bij jullie op bezoek te komen.

---

*...but I am a good Hegelian. If you have a good theory, forget about the reality.*  
Slavoj Žižek

*Je dis toujours la vérité: pas toute, parce que toute la dire, on n'y arrive pas. La dire toute, c'est impossible, matériellement: les mots y manquent.*  
Jacques Lacan

*'Mathematically, boy,' he told himself, 'if nobody else original comes along, they are bound to run out of arrangements some day. What then?' What indeed. This sort of arranging and rearranging was Decadence, but the exhaustion of all possible permutations and combinations was Death.*  
Dudley Eigenvalue in V., Thomas Pynchon

*En dit noem jij ontoegankelijk?!*  
Het geheim van het verdwenen mysterie, Gumbah.





# Dutch Summary - Nederlandse Samenvatting

---

We present here a Dutch Summary of this thesis.

## Inleiding

---

Golven die een systeem van de ene toestand in de andere brengen, worden veel gezien in de natuur. Een klassiek voorbeeld van zo'n 'trigger' golf is de propagatie van een verbrandingsfront. Het vuur (bijvoorbeeld langs droog gras) schakelt het systeem om naar een andere toestand. Inderdaad, gedurende een zekere tijd zal het niet mogelijk zijn om een nieuwe verbrandingsgolf te initiëren. Er zijn veel voorbeelden van dergelijke golven van excitatie. Zo werden ze onder meer geobserveerd in de Belousov-Zhabotinsky reactie; spelen ze een rol bij de elektrische activiteit gedurende een epileptische aanval; en werden deze (spiraal)golven ontdekt tijdens de morfogenese van bepaalde types amoeba.

In deze thesis focussen we op een van de meest intrigerende voorbeelden van zulke golven van excitatie, namelijk elektrische golven van excitatie in het (menselijk) hart. Deze propagerende elektrische golven initiëren de contractie van het hart, waardoor bloed door het lichaam wordt gepompt. Indien dergelijke excitatiegolven worden verstoord, dan kunnen er afwijkingen ontstaan in de timing, volgorde en coördinatie van de contractie van de hartspier. In dat geval spreken we van hartritmestoornissen. Er zijn veel soorten aritmieën, gaande van meestal ongevaarlijke hartkloppingen, tot hartritmestoornissen die in enkele minuten dodelijk kunnen zijn. Hartritmestoornissen zijn dan ook een van de meest voorkomende doodsoorzaken. In deze thesis zullen we dergelijke aritmieën onderzoeken door gebruik te maken van numerieke simulaties van wiskundige modellen. We zullen met name elektrische weefselheterogeniteiten bestuderen, en hun effect op het ontstaan en de dynamica van hartritmestoornissen.

## Het hart als een exciteerbaar medium

---

Het hart is een holle spier dat door samen te trekken het bloed doorheen het lichaam pompt in een gesloten, circulatoir systeem. Zowel zoogdieren als vogels hebben een dubbel-geluste bloedsomloop. Daarom omvat het hart van deze soorten een linker-en een rechterhelft, elk bestaand uit een ventrikel (kamer) gekoppeld aan een atrium (boezem). Eerst trekken de beide atria samen, zodat het bloed uit de atria naar de ventrikels wordt gepompt. Vervolgens trekken de ventrikels samen. Het rechterventrikel pompt zuurstofarm bloed naar de longen; het linkerventrikel pompt zuurstofrijk bloed, via de aorta, naar de rest van het lichaam. De samentrekking van individuele hartcellen wordt getriggerd door een elektrisch signaal dat *excitatie* of *actiepotentiaal* wordt genoemd. De actiepotentiaal wordt gevormd door ionstromen die door ion-kanalen gelegen in het celmembraan van een hartspiercel lopen, en geeft vervolgens een signaal aan de hartspiercel om samen te trekken.

In de wand van de rechterboezem bevindt zich een stukje weefsel, de sinusknop genoemd, met speciale hartcellen: ze genereren spontaan een actiepotentiaal met een bepaalde frequentie. Normale hartspiercellen bezitten deze eigenschap niet, ze kunnen enkel gestimuleerd worden door een elektrisch stroompje van een buurcel. Doordat hartspiercellen elektrisch aan elkaar gekoppeld zijn, geven deze sinusknopcellen, op het moment dat ze een actiepotentiaal genereren, een elektrisch stroompje door aan de omliggende hartspiercellen, waardoor zij ook een actiepotentiaal ontwikkelen. Op die manier ontstaan golven van elektrische activiteit die zich voortplanten in het hartweefsel. Eerst worden de boezems geëxciteerd, waardoor deze

---

samentrekken en het bloed naar de kamers wordt gepompt. Vervolgens plant de excitatiegolf zich, met een kleine vertraging, voort naar de kamers, waarna deze samentrekken en bloed naar de longen en de rest van het lichaam wordt gepompt. Bij de meeste hartritmestoornissen is een afwijking in de propagatie van deze excitatiegolf de oorzaak voor de verstoorde contractie van de hartspier.

## **Abnormale excitatie van het hart: hartritmestoornissen**

---

Een hartritmestoornis is een situatie waarbij het hart onregelmatig samentrekt. In rust bedraagt de hartslag van een volwassen persoon zo'n 60-100 slagen per minuut. Als de hartslag, in rust, hoger wordt dan 100 slagen per minuut, dan spreken we van *tachycardie*. Stijgt de hartslag tot boven de 250 slagen per minuut, dan wordt gesproken van *fibrillatie*. Tijdens fibrillatie trekken de atria of de ventrikels niet langer synchroon samen, waardoor de pompwerking van het hart wordt verstoord. Bij ventrikelfibrillatie werken de ventrikels niet langer als een effectieve pomp, met als gevolg dat er bijna geen bloed meer uit de kamers wordt gepompt. Omdat hierdoor de zuurstofvoorziening van het lichaam stilvalt, is ventriculaire fibrillatie binnen een paar minuten dodelijk.

Twee mechanismen worden beschouwd als de hoofdoorzaak voor het ontstaan van hartritmestoornissen: ectopische activiteit, gelijkaardig aan de pacemaker activiteit van de sinus-knoop; en abnormale regimes van activatie. In deze thesis focussen we ons op het tweede mechanisme. Meer bepaald op deze hartritmestoornissen veroorzaakt door abnormale *reentrant* propagatie van excitatiegolven: een zeer gevaarlijke en veel voorkomende categorie hartritmestoornissen.

Uit studies in het begin van de vorige eeuw, is het idee naar voren gekomen dat hartritmestoornissen worden gedreven door dergelijke cirkelgeleiding. Ook wel *reentry* genoemd. Tijdens reentry draait de excitatiegolf rond in een cirkel, waarbij de kop van het signaal voortdurend de staart volgt. In twee en drie-dimensionale weefsels kan een excitatiegolf ronddraaien om een niet-exciteerbaar anatomisch obstakel, en zo een golf vormen in de vorm van een spiraal. Dit wordt anatomische reentry genoemd. Dergelijke spiralen kunnen echter ook roteren rond hun eigen kern. In dat geval spreken we van functionele reentry. Spiralen roteren met een hoge frequentie, en exciteren bij elke omwenteling het medium, wat telkens voor een contractie van het hartweefsel zorgt. Als een dergelijke spiraalgolf ontstaat in de ventrikels, dan wordt de excitatie, en dus ook de contractiefrequentie, niet langer bepaald door de sinusknop, maar door de spiraalgolf. Dit zorgt voor een verhoogde hartslag: tachycardie. Bij tachycardie is er dus maar één spiraalgolf aanwezig. Tijdens fibrillatie daarentegen, zijn er meerdere spiraalgolven tegelijkertijd aanwezig die voortdurend interageren met elkaar en fragmenteren in nieuwe spiralen. Hierdoor ontstaat een chaotisch excitatiepatroon dat zorgt voor een asynchrone samentrekking. Tachycardie kan overgaan in fibrillatie als een spiraal opbreekt in verschillende spiralen. Deze opbreking van een enkele spiraal in verschillende spiralen kan veroorzaakt worden door dynamische instabiliteiten van het hartweefsel, of door interactie van de spiraal met weefselheterogeniteiten.

Voor de volledigheid merken we op dat tachycardie en fibrillatie ook kan veroorzaakt worden door focale getriggerde activiteit, in het bijzonder in harten leidend aan cardiomyopathie. Dit type hartritmestoornissen, dus niet gedreven door reentry, zal niet bestudeerd worden in deze thesis.

---

## Deze thesis

---

In deze thesis bestuderen we het effect van (weefsel)heterogeniteiten op elektrische golven van excitatie in het menselijk hart. Dit met behulp van een wiskundig model voor de elektrische excitatie van het hart. In het bijzonder, in een groot deel van deze thesis, bestuderen we heterogeniteiten op het vlak van de duur van de actiepotential (APD) in hartweefsel, alsook de rol ervan op initiatie van spiraalgolven, en de invloed op spiraalgolfdynamica. We onderzoeken ook het effect van een (dynamische) heterogeniteit, gecreëerd door een tijdelijke blokkade van golfpropagatie, op zowel vlakke golven, als op spiraalgolfdynamica. De resultaten hiervan gebruiken we vervolgens om de resultaten uit de vorige hoofdstukken beter te begrijpen. We introduceren en bespreken ook een prototype van de databank die we ontwikkelden om data bekomen uit experimenten op menselijke harten, zoals gebruikt in deze thesis, in op te slaan.

In **hoofdstuk 2**, onderzoeken we het effect van celkoppeling op APD heterogeniteit in menselijk hartweefsel. Het is algemeen geweten dat de omvang van heterogeniteit sterk kan verschillen tussen het weefsel en het eencellige niveau, en het is belangrijk om de relatie te kennen tussen de twee, bijvoorbeeld om deze soorten heterogeniteiten te modelleren, zoals we doen in **hoofdstuk 3 en 4**. We tonen dat het effect van celkoppeling op APD heterogeniteit wiskundig kan beschreven worden door gebruik te maken van een convolutie met Gaussische functies. Gebruik makend van deze benadering lossen we zowel het voorwaartse probleem op (bepalen van weefselheterogeniteit, startend van celheterogeniteit), als het inverse probleem (bepalen van ceileigenschappen, gebaseerd op metingen uitgevoerd op weefsel). De oplossing van het voorwaarts en inverse probleem wordt geïllustreerd aan de hand van verschillende voorbeelden van 1D en 2D systemen. Het voorwaartse probleem kunnen we oplossen met een behoorlijk grote nauwkeurigheid. Zelfs voor steile gradiënten in heterogeniteit kunnen we de maximale waarde van de APD in het gekoppelde systeem voorspellen, welke belangrijk is om de omvang van de heterogeniteit te karakteriseren. Betreffende het inverse probleem, is onze oplossing ook veelbelovend. Hoewel, voor steile gradiënten, heeft onze oplossing een oscillatoire component, waardoor we de maximale amplitude niet met genoeg zekerheid kunnen bepalen. Dergelijke oscillatoire component is een gekende eigenschap van oplossingen van inverse problemen. Maar, we merken op dat we een van de eenvoudigste methoden voor de oplossing van inverse problemen gebruikten, en dat het inverse probleem, zoals hier geformuleerd, een van meest bestudeerde is in het onderzoeksgebied van de toegepaste wiskunde. Onze oplossing kan dus zeker nog verbeterd worden. Bijvoorbeeld, andere normen zouden kunnen gebruikt worden voor Tikhonov regularizatie. Dit zou echter specifiek onderzoek vergen, en de ontwikkeling van speciale software, wat buiten het bestek van deze thesis valt. De waarde van dit hoofdstuk voor toepassingen, is dat we heterogeniteit op cellulair niveau relateren aan heterogeniteit op weefsel niveau. We kunnen dus eigenschappen van hartcellen voorspellen uit metingen uitgevoerd op weefsel en omgekeerd. Merk op dat dit geen triviaal probleem is, want heterogeniteit op cellulair niveau kan 200 tot 500 % groter zijn dan op weefselniveau.

In **hoofdstuk 3** gebruiken we het TP06 model [139] voor menselijk hartweefsel om APD heterogeniteiten met kleine afmetingen te modelleren, zoals geobserveerd door Glukhov et al. [40] tijdens experimenten op wigvormige preparaten uit het menselijk linkerventrikel. Om een initiële schatting van de onderliggende eigenschappen van de cellen binnen deze heterogeniteiten te maken, gebruiken we de methode ontwikkeld in **hoofdstuk 2**. We bestuderen het effect van dit type heterogeniteiten op de initiatie van spiraalgolven, en de dynamica van spiraalgolven rond deze heterogeniteiten. We vinden dat er spiraalgolven kunnen worden

---

gevormd rond deze heterogeniteiten als we het hartweefsel met een voldoende hoge frequentie stimuleren. Deze nieuwe bronnen worden hier niet enkel gevormd door een breuk in het golffront, zoals klassiek beschreven in [73, 102], maar ook door interactie van deze breuken (in de excitatiegolf) met andere golven, uiteindelijk leidend tot de formatie van een spiraalgolf verankerd rond de heterogeniteit. We bestuderen de dynamica van deze verankerde spiraalgolven, en vinden twee verschillende periodes van excitatie: een voor cellen die zich binnenin de heterogeniteit bevinden, en een voor deze buiten de heterogeniteit. We tonen ook aan dat elk van deze periodes hoofdzakelijk bepaald wordt door eigenschappen van het hartweefsel in de corresponderende regio: verhoging van de refractorische periode resulteert in een verhoging van de periode. Interessant is ook dat bij dergelijke verhoging van de refractorische periode, de verhoging van de periode niet gradueel is. We vinden dus een bifurcatiepunt. In het bifurcatiepunt verhoogt de periode plots 1.3 keer.

In vorige modelleerstudies [1, 102, 2], was het belangrijkste effect van weefselheterogeniteit op spiraalgolfdynamica de drift van de spiraal langs de grens van de heterogeniteit. Hier is het belangrijkste effect de ankering van de spiraal aan de heterogeniteit. Ook krijgen we in ons geval een electrocardiogram (ECG) dat gelijkenissen vertoont met ECGs zoals opgenomen tijdens periodes van torsades de pointes en polymorfische tachycardie. Hoewel, in ons geval is het een gevolg van de verschillende excitatiefrequenties binnen en buiten de heterogeniteit, en niet een gevolg van de drift van de excitatiegolf in het weefsel.

Ankering van spiraalgolven aan obstakels werd al intens bestudeerd, zowel in 2D als in 3D [22, 142, 152, 81, 156, 81, 131]. Maar in al deze studies werden spiralen bestudeerd die zich verankerden aan niet exciteerbare obstakels. In **hoofdstuk 3** tonen we aan dat een heterogeniteit die exciteerbaar is ook spiralen kan ankeren, en dat deze ankering resulteert in meer complexe dynamica in vergelijking met ankering rond niet-exciteerbare obstakels, door de invloed van de heterogeniteit op spiraalgolfrotatie.

Onze resultaten omtrent de dynamica van spiraalgolven rond een heterogeniteit zijn algemeen, en gelden ook voor heterogeniteiten met een verschillende grootte, vorm, en gemiddeld door de aanpassing van verschillende parameters van ons model. Ook bekwamen we dezelfde resultaten na toevoeging van rotationele anisotropie aan ons medium.

In **hoofdstuk 3** beschrijven en verklaren we dus mogelijke golfdynamica rond realistische heterogeniteiten zoals gemeten in menselijke harten. Dit in termen van formatie van nieuwe bronnen van hartritmestoornissen in 2D modellen van hartweefsel.

In **hoofdstuk 4** vervolgen we ons onderzoek naar het effect van ionische heterogeniteiten met kleine afmetingen op spiraalgolfdynamica. Opnieuw modelleren we heterogeniteiten met een omvang en grootte zoals gemeten door Glukhov et al. [40], maar nu zowel in 2D als in een anatomisch model voor de menselijke ventrikels. We tonen aan dat zulke heterogeniteiten niet enkel spiralen kunnen ankeren, zoals we leren uit **hoofdstuk 3**, maar ook spiralen kunnen aantrekken die op een substantiële afstand van de heterogeniteit roteren. In het bijzonder, in 2D kunnen deze soort heterogeniteiten spiralen aantrekken, en uiteindelijk ankeren, op een afstand van 6 cm langs de vezelrichting, 4 cm dwars op de vezels, en rond de 5 cm bij een hoek van 45 graden met de vezels. In ons anatomisch model is de spiraal altijd verankerd (of verwijderd), indien de heterogeniteit groot genoeg is. De regio waarin spiralen kunnen aangetrokken worden door heterogeniteiten is dus aanzienlijk in vergelijking met de typische grootte van het hart (ongeveer 10 cm hoog). Interessant genoeg is deze aantrekking over grote afstanden een eigenschap die enkel ionische heterogeniteiten lijken te bezitten: niet exciteerbare obstakels trekken spiralen niet aan over zo'n grote afstanden. Verder tonen we aan, in ons anatomisch model van de ventrikels, dat als de heterogeniteit gelokaliseerd is dicht

---

bij de basis van het hart, deze niet enkel spiralen kan aantrekken en ankeren, maar ze ook kan verwijderen. Dit is een interessant resultaat, want het suggereert dat sommige types heterogeniteit een anti-aritmisches effect hebben.

Het is logisch dat we in onze simulaties vinden dat spiralen aangetrokken worden naar regio's met een langere APD. Immers, in vroegere studies werd aangetoond dat spiralen de neiging hebben om naar de regio met een langere rotatieperiode te driften [116, 102, 138], welke geassocieerd wordt met een langere APD [100, 138]. Hoewel, we merken op dat het aantrekkingsproces, zoals hier geobserveerd, geen continu proces is waarbij de spiraal traag in de richting van de heterogeniteit beweegt, zoals gerapporteerd in deze vorige publicaties, maar een stapsgewijs proces waarbij de spiraal naar de heterogeniteit toe wordt geduwd door een complexe interactie met de heterogeniteit.

In [123, 122] werd eerder al onderzoek gedaan naar de dynamica van spiralen in hartweefsel in de aanwezigheid van grote, vierkante ionische heterogeniteiten en niet-exciteerbare obstakels. Afhankelijk van de positie van de heterogeniteit in het weefsel, werden verschillende regimes geobserveerd. Een van deze regimes was, net zoals in onze studie, de verankering van de spiraal rond de heterogeniteit. Het zou interessant zijn om na te gaan welke van deze regimes worden gevonden als heterogeniteiten met een grootte en vorm zoals geobserveerd in experimentele studies, zouden worden gebruikt. Uit andere studies van dezelfde groep [81, 80], blijkt ook dat heterogeniteiten die een kortere APD hebben dan het omliggende hartweefsel, spiralen zouden kunnen ankeren. Hoewel, dit resultaat moet nog verder onderzocht worden om uitsluitend te bieden hieromtrent.

Samengevat bestuderen we in **hoofdstuk 4** of een bestaande spiraal kan ankeren rond een heterogeniteit met realistische afmetingen. Dit is een vervolg op het onderzoek beschreven in **hoofdstuk 3**, maar nu gefocust op het mogelijke ankeren van spiralen, hierbij gebruik makend van accurate anatomische modellen. Een nieuw onverwacht resultaat is dat dergelijke heterogeniteiten spiralen kunnen aantrekken, en dat in sommige gevallen zo'n aantrekking leidt tot de beëindiging van de hartritmestoornis.

Vervolgens bestuderen we in **hoofdstuk 5** dynamische heterogeniteiten in homogeen hartweefsel gecreëerd door APD-restitutie effecten. We tonen aan dat een regio van tijdelijke blok van golfpropagatie kan resulteren in dynamische Wenckebach 'blocks' die groeien in de ruimte. Dit type instabiliteit noemen we een globale alternans instabiliteit (GAI). Deze GAI heeft belangrijke effecten op spiraalgolfdynamica: het kan leiden tot de formatie van nieuwe spiralen, of de eliminatie van reeds bestaande spiralen. Restitutie-eigenschappen van hartweefsel worden al geruime tijd beschouwd als gerelateerd aan geobserveerde instabiliteiten, die aan de basis liggen van de initiatie of het opbreken van spiraalgolven. In het bijzonder, verschillende studies [62, 112, 114, 36] demonstreerden dat een steile helling van de restitutiecurve kan resulteren in dynamische instabiliteiten, mogelijk leidend tot fibrillatie. In **hoofdstuk 5**, laten we zien dat ook substantiële restitutie-effecten kunnen verwacht worden op globaal niveau. Dus we tonen aan dat, hoewel een steile restitutiecurve aanleiding geeft tot dynamische instabiliteiten, het geen noodzakelijke conditie is: ook de globale vorm van de restitutiecurve speelt een belangrijke rol.

Terugkijkend naar **hoofdstuk 3** en **4**, kunnen we nu ook begrijpen waarom een initiële kleine ionische heterogeniteit zich uitbreidt in de ruimte onder stimulatie met een hoge frequentie: het mogelijke mechanisme achter deze groei, waardoor spiralen kunnen geïnitieerd worden, of aangetrokken, is GAI. Ook kan dit beschreven mechanisme essentieel zijn bij het opstellen van een algemene theorie voor hartritmestoornissen, bijvoorbeeld om de ritmestoornissen te verklaren die zich voordoen tijdens parasymphatische stimulatie van het hart, zoals

---

gerapporteerd in [125].

In **hoofdstuk 6** ten slotte, introduceren we een prototype van een databank om data in op te slaan afkomstig van experimenten op menselijke harten. Data zoals gebruikt in de vorige hoofdstukken om modellen mee te ontwikkelen. Om deze databank op te bouwen gebruikten we het content management systeem Drupal. Het prototype is gebaseerd op data afkomstig van de groep van Prof. Efimov. We overlopen de algemene structuur van de databank, en leggen uit hoe gebruikers data kunnen opladen en downloaden. Dit systeem is nog altijd in ontwikkeling, hoewel, alle belangrijke componenten van de databank en corresponderende website zijn reeds getest, en zullen binnenkort met data worden gevuld.

## Conclusie

---

In deze thesis onderzochten we APD heterogeniteit van hartweefsel en het effect ervan op spiraalgolfdynamica. In het laatste hoofdstuk van deze thesis, bestudeerden we ook (dynamische) heterogeniteiten gecreëerd door APD restitutie-effecten. We bekwamen verschillende interessante resultaten. In het eerste deel van deze thesis, toonden we aan dat het effect van celkoppeling op APD heterogeniteit wiskundig kan beschreven worden door gebruik te maken van Greense functies met een Gaussische kern. Via deze benadering kunnen we eigenschappen van hartcellen voorspellen uit metingen uitgevoerd op weefsel, en omgekeerd. Dit is een niet-triviaal probleem, aangezien heterogeniteit op cellulair niveau 200 tot 500 % groter kan zijn dan op weefselniveau. We denken dat dit een boeiend resultaat is, aangezien dit het probleem van elektrotonische interacties verbindt met een breed scala aan klassieke problemen in de fysica, chemie en biologie, waarvoor robuuste methoden bestaan. Dus, hoewel onze methode geen perfecte oplossing biedt voor het (inverse) probleem, geloven we dat ze veelbelovend is. In het volgende hoofdstuk modelleerden we kleine ionische heterogeniteiten, zoals geobserveerd in experimenten, en toonden aan dat deze heterogeniteiten pro-aritmisches kunnen zijn als het hartweefsel gestimuleerd wordt onder hoge frequentie. Interessant genoeg vonden we dat deze spiralen ankerden rond deze kleine regio's van verhoogde APD. Verder vonden we ook dat deze heterogeniteiten spiralen kunnen aantrekken die roteren op een substantiële afstand van de heterogeniteit, zowel in 2D als in een anatomisch model voor de menselijke ventrikels. We toonden ook aan hoe een tijdelijke blokkade van de golfpropagatie belangrijke effecten kan hebben op het ruimtelijke excitatiepatroon en spiraalgolfdynamica. In het bijzonder demonstreerden we dat het resulteert in dynamische Wenckebach 'blocks' die zich uitbreiden in de ruimte, door ons globale alternans instabiliteit genoemd (GAI). We illustreerden dat GAI het mogelijke mechanisme is dat aan de basis ligt van de groei van de kleine ionische heterogeniteiten, leidend tot spiraalgolf initiatie of aantrekking, geobserveerd in vorige hoofdstukken. Ten slotte introduceerden en bediscussieerden we een prototype van een databank die we ontwikkelden om data in op te slaan. Data zoals bekomen uit experimenten op menselijke harten, en die we gebruikten in deze thesis om modellen te bouwen.

<b>Word of thanks</b>	<b>iii</b>
<b>Dutch Summary</b>	<b>vii</b>
<b>1 Introduction</b>	<b>1</b>
1 The heart as an excitable medium . . . . .	3
1.1 Anatomy and function of the heart . . . . .	3
1.2 Cellular basis for electrical activation . . . . .	4
2 Abnormal excitation of the heart: cardiac arrhythmias . . . . .	5
2.1 Mechanisms of reentrant cardiac arrhythmias . . . . .	7
2.2 Mechanisms of atrial and ventricular fibrillation . . . . .	10
3 Modeling in cardiac electrophysiology . . . . .	13
3.1 The need for modeling in cardiac electrophysiology . . . . .	13
3.2 Model formalism . . . . .	13
3.3 From phenomological to ionic models . . . . .	14
4 Thesis outline . . . . .	15
<b>2 APD heterogeneity of cardiac tissue can be evaluated from cell properties using Gaussian Green’s function approach</b>	<b>17</b>
1 Introduction . . . . .	17
2 Materials and Methods . . . . .	18
3 Results . . . . .	19
3.1 1D step-wise heterogeneity . . . . .	19
3.2 The forward problem . . . . .	21
3.3 The inverse problem . . . . .	25
4 Discussion . . . . .	28
<b>3 Initiation and dynamics of a spiral wave around an ionic heterogeneity in a model for human cardiac tissue</b>	<b>35</b>
1 Introduction . . . . .	35
2 Materials and methods . . . . .	36
3 Results . . . . .	37
3.1 Baseline model . . . . .	37
3.2 Periods . . . . .	41
3.3 Period increase bifurcation . . . . .	43
3.4 Modifications of baseline model . . . . .	43
4 Discussion . . . . .	48
<b>4 Small size ionic heterogeneities in the human heart can attract spiral waves</b>	<b>51</b>
1 Introduction . . . . .	51
2 Materials and methods . . . . .	52
3 Results . . . . .	55
3.1 Ionic heterogeneities as attractors of spiral waves in 2D cardiac tissue . . . . .	55
3.2 Ionic heterogeneities as attractors of spiral waves in an anatomical model of the heart . . . . .	60

## CONTENTS

---

4	Discussion . . . . .	65
<b>5</b>	<b>Global alternans instability and its effect on non-linear wave propagation: dynamical Wenckebach block and self-terminating spiral waves.</b>	<b>69</b>
1	Introduction . . . . .	69
2	Materials and methods . . . . .	71
3	Results . . . . .	71
	3.1 GAI in 1D . . . . .	71
	3.2 Mechanism of GAI . . . . .	74
	3.3 GAI in 2D . . . . .	77
4	Discussion . . . . .	80
<b>6</b>	<b>Setting up a database structure for modeling the human heart</b>	<b>83</b>
1	Introduction . . . . .	83
2	Structure of the database . . . . .	84
3	Features of the database . . . . .	85
	3.1 Upload data . . . . .	85
	3.2 Download data from the website . . . . .	89
4	Conclusion and future perspective . . . . .	92
<b>7</b>	<b>Summarizing discussion</b>	<b>93</b>
1	A review . . . . .	93
2	Model complexity and limitations . . . . .	96
3	Future directions . . . . .	97
4	Conclusion . . . . .	100



---

# 1

## Introduction

Waves which switch a system from one state to another are often seen in usual life. A classical example of such a, so-called, trigger wave is the propagation of a combustion front. The fire (for example along dry grass) switches the system to another state. Indeed, for a certain time it will not be possible to get a new wave of burning: we will only be able to initiate a new wave when the grass has been burned out, and new grass has grown. This recovery time of the system (i.e. the time after which we can initiate another propagating wave) is called the refractory period (see Fig. 1.1).



**Figure 1.1: Wave propagation in an excitable medium.** Figure shows a schematic representation of the main states during wave propagation in an excitable medium: the resting state (white), excited state (red) and the refractory state (green). The arrow shows direction of wave propagation.

One of the most famous physico-chemical systems in which such propagating waves were observed is the Belousov-Zhabotinsky (BZ) reaction. This is a reaction in which some organic reductants are oxidated by bromic acid, catalized by transition-metal ions. Boris Belousov found that when cerium is used as a catalyst and citric acid as a reductant, the colour of the reaction oscillated between colourless and yellow. Later, citric acid was replaced by malonic acid by Anatol Zhabotinsky. At first, the BZ reaction was just an example of oscillatory dynamics, in which the main demonstration was the periodic change of colour in the glass. Later, when doing experiments in petri dishes of thin layers of the reaction, waves, vortices and target patterns (when a train of waves originates from a point) were found. In Fig. 1.2 we show the original pictures from the paper about the discovery of spiral waves in the BZ reaction by Zhabotinsky and Zaikin in 1971. Important phenomena first discovered in the BZ reaction were waves in 3D, vortices in 3D (called scroll waves), and filaments.

Another example of such waves, but of completely different origin, were discovered in 1944 by Aristides Leão when studying electrical activity during epilepsy in rabbit brains [75]. He used several electrodes to simulatenously record the electrical activity of the brain, and found that during epilepsy the normal electrical activity is suppressed. But interestingly, he found that this suppression was spreading from electrode to electrode in a wave-like way. Also the recovery occurred in a wave-like way. In the same way as in the previous example, these waves can form spiral waves. Waves of spreading depression were later found in different parts of



**Figure 1.2: Spiral waves in the Belousov-Zhabotinsky reaction.** Figure shows initiation of vortices or spiral waves in the BZ reaction. Taken from the paper by Zhabotinsky and Zaikin from 1971 [157].

the brain, and turned out to be extremely important, for example for its close association with migraine.

There are many other examples of non-linear waves and spiral waves of excitation: they play a role during heterogeneous catalysis [59, 3]; spiral waves of cAMP during morphogenesis of *Dictyostelium discoideum amoebae* were found in [38, 129]; and calcium waves in *Xenopus oocytes* were described in [76, 27].

In this thesis, we will focus on one of the most intriguing examples of such waves of excitation, namely electrical waves of excitation in the (human) heart. In the next section, we will discuss how contraction of the heart is initiated by these electrical waves propagating through cardiac tissue. As in the aforementioned systems, spiral waves were also observed in the heart [6, 21, 22], and they underlie life-threatening cardiac arrhythmias. This will be the topic of the second section of this introduction. As in this thesis we use mathematical models to study cardiac arrhythmias, we discuss briefly the importance of modeling in cardiac electrophysiology; the model formalism; and the model we will use. At the end, we provide a short outline of the modeling studies described in this thesis.

## 1 The heart as an excitable medium

### 1.1 Anatomy and function of the heart

In 1628 William Harvey was the first to discover that the heart pumps the blood around in a closed circulatory system [50]<sup>1</sup>. Both mammals and birds have a double-looped circulatory system. Therefore, the heart of these species comprises a right and a left half, each consisting of a ventricle connected to an atrium. The right atrium and ventricle function as a pump for the pulmonary circulation, whereas the left atrium and ventricle function as a pump for the systemic circulation.

The heartbeat is initiated and controlled by electrical impulses that are generated and conducted by myocardial cells in the heart. Under normal conditions the excitation wave of the heart originates in the sino-atrial (SA) node, located in the upper right atrium. The SA node thus functions as the cardiac pacemaker. The wave of excitation propagates through atrial myocardial cells to the right atrium, and then to the left atrium, after which they contract and blood is pumped to the ventricles. We thus see that there should be some delay in cardiac activation and contraction between the atria and the ventricles. Indeed, the ventricles should contract after being filled with blood supplied by the atria and hence after atrial contraction. This delay is regulated by the atrio-ventricular (AV) node. It is the only place where the atria and ventricles are electrically coupled. The very low conduction velocity in the cells of the AV node is causing the required delay. From the AV node, the signal is passed to the AV bundle. This is a rapidly conducting structure made up of special type of cells, namely Purkinje cells. The AV bundle splits into right and left bundle branches. Eventually the electrical signal conducted through these bundle branches reach the ventricular myocardium via the His-Purkinje system, which is a network of rapidly conducting cells that synchronizes ventricular activation. This causes the ventricles to contract, and blood is pumped into the arteries.

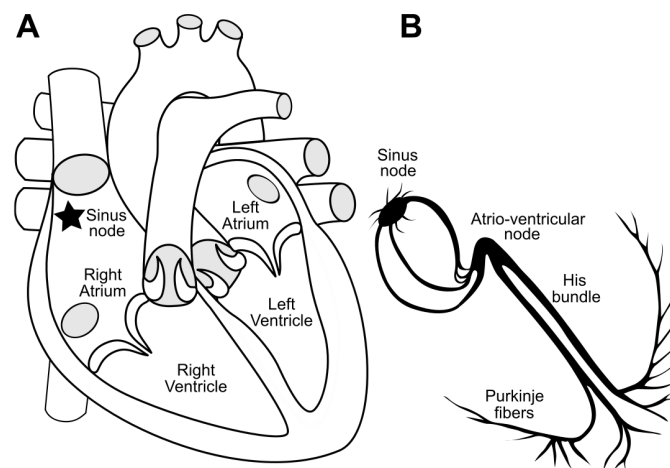


**Figure 1.3: The human heart.** In A we show a schematic central view on a cross section of the heart, and in B we show the conduction system of the heart. Figure taken from [145].

<sup>1</sup>His theories about treating migraine are a little more controversial: he recommended trepanation as a treatment for this [20] - if only he had known the connection between cardiac excitation and severe headache...

The adaptation of cardiac output to the oxygen demands of the organism is regulated by the autonomous nervous system. Both heart rate and contraction force are regulated by this system. Heart rate is regulated by changing the firing frequency of the SA node and the rate of transmission of the AV node. Contraction force is regulated by adapting intracellular calcium handling and tissue restitution properties.

### 1.2 Cellular basis for electrical activation

In the second paragraph of this section, we will focus on the cellular basis of this electrical signal propagating through the heart. As was clear from the previous paragraph, this electrical signal, usually called action potential (AP), serves as a trigger for the contraction of the cardiac muscle cells. Of course to obtain a propagating wave, the cells need to have a way to communicate to each other. This communication is done by the gap junctions which electrically couple the cells. These gap junctions are channels composed of two connexons (or hemichannels) which connect across the intercellular space. Because of these channels, connecting neighbouring cells, an action potential generated in a particular cell serves as a current source for adjacent cells, after which this cell also generates an AP and contracts. Due to the strength of this electrical coupling, the waves of electrical activity can propagate fast through cardiac tissue, which leads to almost synchronous contraction of the cardiac muscle cells.

Now we will discuss by which processes this AP can be described. Therefore we first should take a look to the cell when in its resting state. Because a (cardiac) cell is surrounded by a lipid membrane which acts as a barrier with different permeability for the various ions, in its resting state, a (cardiac) cell is in a dynamic equilibrium in which the magnitude of the chemical force is equal and opposite to the magnitude of the electrical force. This balance between all ionic fractions results in a resting potential around  $V_m \approx -80 \text{ mV}$ , in which we defined, by convention, the transmembrane potential as the potential inside the cell, with respect to the extracellular potential:

$$V_m = V_{int} - V_{ext} . \quad (1.1)$$

For a cardiac cell in its resting state, the dominant ions in the extracellular space are  $Na^+$  and  $Cl^-$ , while inside the cell  $K^+$  has the highest concentration. Despite its small concentrations both inside as outside the cell (although higher outside the cell), also  $Ca^{2+}$  is an important ion for the generation of the AP.

So when does a cardiac cell generate an AP? For this, the cell needs to receive some current (for instance from an adjacent cell via the gap junctions), which increases the membrane potential. If the membrane potential reaches a certain threshold, the permeability of the membrane to  $Na^+$  increases, and they flow into the cell via the  $Na^+$  channels. This increases the membrane potential further, which triggers the opening of other channels and a complete action potential is generated. A typical cardiac AP consist of five phases which we briefly discuss:

**Phase 0: Action potential upstroke.** Once the transmembrane potential of the cell reaches a certain threshold of approximately  $-65 \text{ mV}$ , membrane  $Na^+$  channels suddenly open. Because the concentration of  $Na^+$  is significantly larger in the extracellular space than in the intracellular space, this leads to a rush of ions into the cell.  $Na^+$  ions are positively charged, thus the membrane potential rapidly becomes less negative (also called depolarization) which results in the upstroke or phase 0 of the AP.

---

## 2. ABNORMAL EXCITATION OF THE HEART: CARDIAC ARRHYTHMIAS

---

**Phase 1: Rapid repolarization.** At a transmembrane potential level of  $20\text{ mV}$  the  $Na^+$  channels close and a new current arises. During this phase, the potassium conductance increases, and via the transient outward current ( $I_{to}$ )  $K^+$  ions flow out of the cell, causing  $V_m$  to decrease. A decrease of the transmembrane potential is also called repolarization. The transient outward current inactivates very rapidly, and its contribution to the other phases is small.

**Phase 2: Action potential plateau.** Other voltage-dependent channels are also activated by an increase in transmembrane voltage, but because they activate at a slower rate, they contribute to the AP only several milliseconds after the end of the upstroke phase 0. In a simplified way, the two dominant currents during this phase are the inward calcium current and the delayed rectifier potassium outward current. Due to the concentration gradient, the opening of calcium channels leads to depolarization; opening of potassium channels lead to repolarization. During the plateau phase, the membrane potential thus depends on the balance between the inward calcium and the outward potassium current. This balance leads to a nearly constant membrane potential, which generates a plateau phase between 200 to 300 ms. There are actually several currents which are calcium or potassium dependent, and which are active in this phase. The most important of them are the L-type calcium current  $I_{CaL}$  and the fast ( $I_{Kr}$ ) and slow ( $I_{Ks}$ ) delayed rectifier potassium current.

**Phase 3: Final repolarization.** After approximately 200 to 300 ms the calcium channels inactivate, and only the repolarizing potassium channels remain active. The delayed rectifier currents close as the cell repolarizes, and the current which dominates during this phase is the inward rectifier current  $I_{K1}$ .

**Phase 4: Diastolic potential.** The inward rectifier current remains the dominant current at rest, and sets the resting potential. In atrial and ventricular myocytes the potential remains at a constant level until a new stimulus brings the transmembrane potential to threshold and a new AP is initiated.

In Fig. 1.4, we show a typical action potential for ventricular cells and denote the different phases and most important currents active during each phase.

As we already discussed in the first part of this introduction, cardiac tissue has a certain *refractory period* (we refer to Fig. 1.1) during which a new propagated AP can not be initiated. This refractory period is determined by the slow time course of channel reactivation (complete recovery of the  $Na^+$  channels for instance takes up to 100 ms). The refractory period is divided into two phases. During the first phase, called the *absolute refractory period* (ARP), no stimulus, whatever its strength, can initiate a propagated response. Then follows the *relative refractory period* (RRP), when only stimuli that exceed the normal threshold can initiate a propagated response. We also refer to Fig. 1.5 for a schematic representation.

---

## 2 Abnormal excitation of the heart: cardiac arrhythmias

---

Cardiac arrhythmias are conditions in which a failure occurs in the timing and or coordination of cardiac contraction. Arrhythmias may arise from abnormalities in the formation of the excitation wave (abnormal automaticity or triggered activity); alterations in the propagation of the excitation wave; or a combination of both [61]. Because arrhythmias can be caused and maintained by these various factors, there are many different forms of rhythm disturbances. The main focus of this thesis, however, will be on arrhythmias caused by abnormal reentrant propagation of excitation waves: a category of arrhythmias which is one of the most frequently

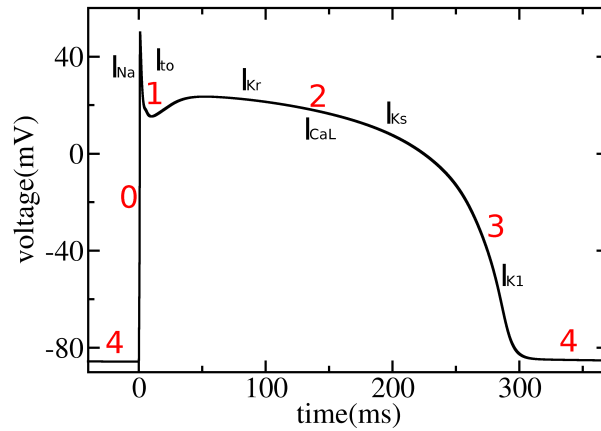


**Figure 1.4: Action potential for cardiac cells.** Figure shows the action potential for (epicardial) ventricular cells simulated using the TP06 model [139]. In red we denote the different phases as described in the text. We also show, schematically, the most important currents during each phase ( $I_{Na}$  during phase 0;  $I_{to}$  during phase 1;  $I_{Kr}$ ,  $I_{Ks}$  and  $I_{CaL}$  during phase 2;  $I_{K1}$  during phase 3 and 4).

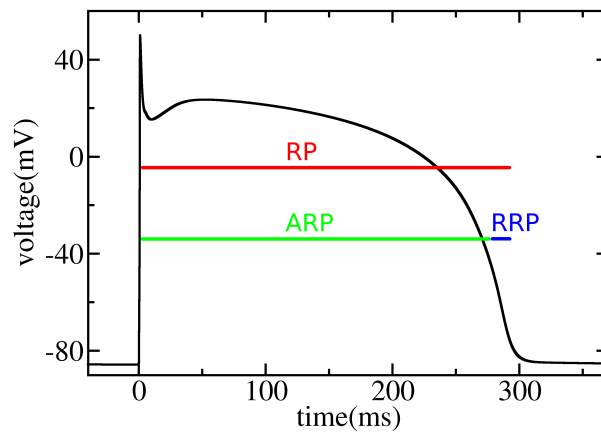


**Figure 1.5: Refractory periods.** Figure shows the action potential for (epicardial) ventricular cells simulated using the TP06 model [139]. In red, green and blue we show, resp., the refractory period, the absolute refractory period and the relative refractory period.

occurring and dangerous. We will briefly introduce and discuss this type of arrhythmias in the next paragraph.

### 2.1 Mechanisms of reentrant cardiac arrhythmias

The first known experiments which showed reentry in excitable tissue were conducted in 1906 by Mayer in jellyfish rings and turtle ventricular muscle [83]<sup>2</sup>. He showed that an excitation wave could circulate in an isolated ring of muscle for long periods of time. Some years later, studies by Mines and Garrey [84, 85, 37] in rings of canine ventricular muscle confirmed these results, which formed the basis for the concept of (anatomical) reentry. This circulation of an excitation wave in a ring is also known as *circus movement reentry*. It is the 1D equivalent of spiral waves in 2D, already briefly discussed in the first section of this introduction. We give a schematic representation of this type of reentry in Fig. 1.6. In response to a point

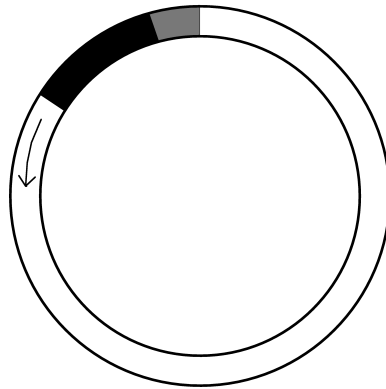


**Figure 1.6: Circus movement reentry.** Schematic representation of reentry in a ring of excitable tissue. Arrow shows the direction of propagation.

stimulus in such a ring of excitable tissue, two propagating waves will be produced which move in opposite directions away from the stimulus site. If, however, one of these waves is blocked due to, for instance, incomplete recovery of the tissue after the passing of the previous wave, we end up with only one wave travelling along the circular path. This wave will make a complete loop in a time  $t = \frac{l}{v}$ , with  $v$  the speed of the wave and  $l$  the length of the ring. If the period  $t$  is larger than the refractory period of the tissue, the wave will continue to move along the circle ‘forever’. Important to note is that such a reentrant pattern will lead to an increased heartbeat if this period  $t$  is smaller than the period of the natural pacemaker (i.e. the S.A. node).

In the seminal work by Wiener and Rosenblueth from 1946 [148] this 1D reentry was extended to two dimensions. They used numerical experiments to postulate that spiral wave rotation in 2D around an inexcitable obstacle was a necessary condition to initiate and maintain arrhythmias. We refer to Fig. 1.7, where we show the rotation of a spiral wave around an inexcitable obstacle for different time frames. Later, in 1948, Selfridge showed, through a modification of the model by Wiener and Rosenblueth, that spirals don’t necessarily need an anatomical obstacle around which they rotate [121]. He demonstrated that they can also rotate around their own spiral *core*, formed in the center of the spiral due to refractory properties of the excitable medium. This spiral core is thus a virtual, excitable obstacle around which the spiral rotates. In Fig. 1.8 we show such free rotating spiral wave for different time frames. The period of a (free rotating) spiral wave is two to three times smaller than the

---

<sup>2</sup>For a thorough review on the topic of history of reentry we refer to [60].

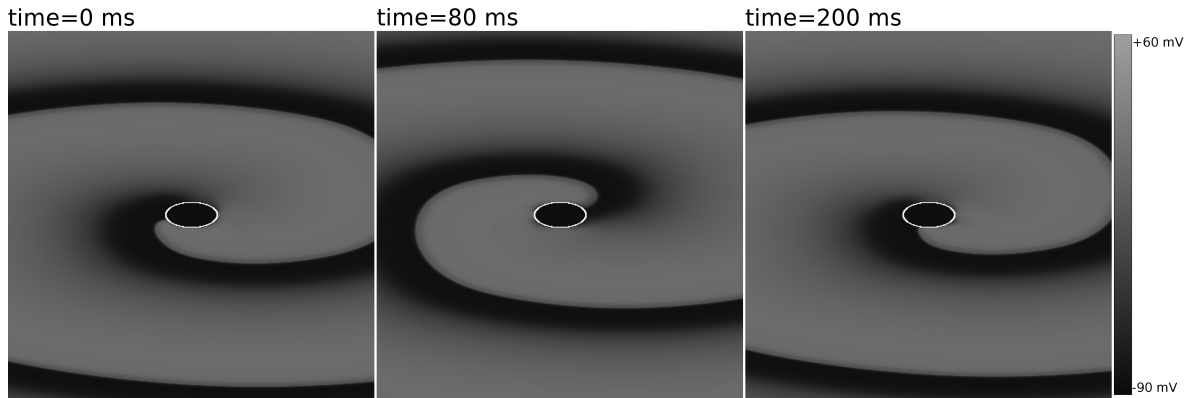


**Figure 1.7: Anatomical reentry.** Spiral wave reentry around an inexcitable obstacle. Simulated using the TP06 model for human ventricular tissue [139]. White line shows size of the inexcitable obstacle. Total size of the medium is 9 cm by 9 cm.

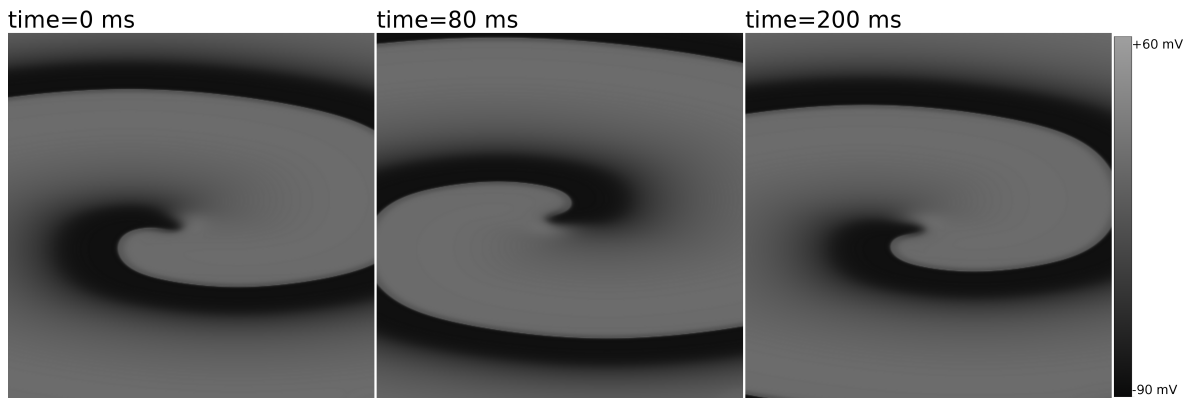


**Figure 1.8: Functional reentry.** Free rotating spiral wave. Simulated using the TP06 model for human ventricular tissue [139]. Total size of the medium is 9 cm by 9 cm.

period of the S.A. node <sup>3</sup>, therefore the spiral wave will take over the role of the natural pacemaker. Because of this the heart will contract more rapidly. Such an increased heart rate is called a *tachycardia*.

In the case of functional reentry, one sees from Fig. 1.8 that a special location is the unique point where the wave front and the wave back meet. This point is called the spiral tip. It is also called the phase singularity point (PS) of the spiral wave, because the spiral tip has no clearly defined phase in the activation cycle.

The trajectory of the PS during spiral wave rotation is also important, because it is one of the main factors which determine the type of (reentrant) cardiac arrhythmia. The simplest example of such a trajectory is circular. It is clear that in that case, this trajectory is just along the circular core of the spiral. The rotation of the spiral is stationary, or in other words: the period of rotation is constant. However, because the core remains excitable during spiral wave rotation, changes in, for instance, the excitability of the tissue may lead to shifts in the trajectory of the wavebreak with activation of the core area, also called meandering. We

<sup>3</sup>In the case of anatomical reentry, the period of the spiral wave depends on the size of the obstacle.



## 2. ABNORMAL EXCITATION OF THE HEART: CARDIAC ARRHYTHMIAS

refer to Fig. 1.9, where we show changes in the trajectory of the spiral tip under increasing excitability of the tissue. This shift, or drift, of the spiral tip can also be caused due to

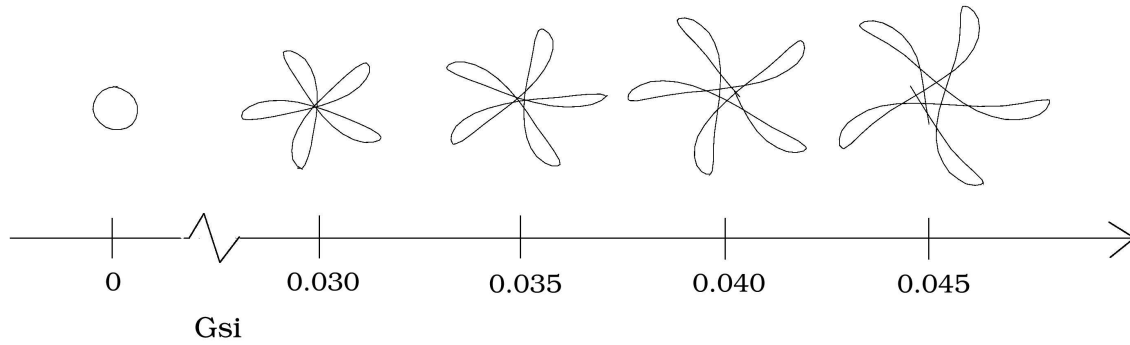


**Figure 1.9: Meandering of the spiral tip.** Trajectory of the PS under increasing excitability of the tissue. Simulations were performed in the Lou-Rudy phase 1 model for ventricular cells [78]. Figure taken from [138].

heterogeneity of cardiac tissue. Both in experiments as in computer models it was shown that spatial gradients in either action potential duration (APD) or conduction velocity may be responsible for drift [116, 29, 102, 22, 138]. These studies showed that the direction of drift is toward the longer APD and toward the region of slower conduction velocity. We will come back to this in **chapters 3 and 4** of this thesis.

As already noted, the trajectory of the spiral tip is an important factor in determining the type of cardiac arrhythmia that will occur. A stationary rotation of the spiral is associated with monomorphic tachycardias. Such rotation leads to a periodic electrocardiogram (ECG). Non stationary spiral rotation can cause polymorphic tachycardias and torsade de pointes, leading to complex non periodic ECG's.

In the previous paragraphs, we have limited our discussion to the 2D case. Although this approximation may reasonably well represent the thin walls of the atria, the thicker walls of the ventricles form essentially a 3D structure. Three dimensional vortices (called scroll waves) in an excitable medium, predicted using simple models such as the FitzHugh-Nagumo model, were first observed by Arthur Winfree in 1973 in thick layers of the BZ-reaction [151]. A scroll wave can be produced by stacking spiral waves on top of each other to fill the third dimension. Scroll waves are normally characterized by their *filaments*, which is an extension of the notion of the spiral wave tip into 3D. To obtain a filament, one just needs to connect the tips of the spiral waves in each of the sections of the scroll wave. A filament is thus the 3D equivalent of a PS. We note that a filament does not need to be a straight line. Albeit, one substantial constraint is that filaments can only end on the medium boundaries [105]. It is also possible that the filament forms a closed loop; the corresponding scroll wave is in that case called a scroll ring.

### 2.2 Mechanisms of atrial and ventricular fibrillation

Fibrillation is the rapid, irregular and unsynchronized contraction of muscle fibers. With regard to the heart we can have both atrial and ventricular fibrillation. As we saw in section 1.1, all electrical impulses from the atria to the ventricles pass through the AV node. Because this AV node has a limited conduction velocity the rate at which impulses reach the ventricles is reduced. Therefore not all impulses produced during atrial fibrillation (AF) are passed through the ventricles, which makes AF not a life threatening arrhythmia. On the other hand, fibrillation in the ventricles (VF) is the leading cause of sudden cardiac death, accounting for more than 400000 deaths per year in the United States alone [41]. The mechanisms behind AF and VF are believed to be slightly different, hence we will divide this section into two parts: first we will give a brief introduction into the processes which are responsible for AF; then we will talk about VF.

Despite years of research, the mechanisms behind AF are still not completely understood. Also the treatment of this disease remains suboptimal. Yet, there is some consensus on the general mechanisms behind AF. Also, the success rate of several treatments has increased over the years due to better understanding of this disease. Historically, the *multiple wavelet hypothesis* of AF postulated by Moe in 1962 [86] and tested using a computer model in 1964 [87] was a key breakthrough into understanding AF. In these papers, Moe suggested that multiple propagating wavelets gave rise to the turbulent atrial activity observed during AF. Experimental proof for this was first given by Allesie in 1985 [7]. However, there is no consensus on how these wavelets arise. Although, since the work by Haïssaguerre [47], it is generally accepted that most cases of paroxysmal AF in humans are initiated by ectopic focal discharges in the pulmonary veins (PV). He showed that isolating these PV can cure a significant proportion of patients with AF. The precise nature of these foci, however, is still unknown. These foci could be (micro-)reentrant patterns, triggered (i.e. delayed and early afterdepolarizations) or the result of abnormal automaticity. On the other hand, in the case of chronic AF, also evidence for reentrant patterns at other positions in the atrium [120] was found.

The reentrant patterns observed during AF can be initiated by a wavebreak formed by the interaction of a wave front, of any origin, with an anatomical obstacle or heterogeneously recovered tissue. In Fig. 1.10 we show how two counter rotating spirals can be initiated by interaction of a wave front with a piece of tissue having a longer refractory period. A mechanism first described by Krinsky in 1966 [73] using a computer model. When such a spiral wave is formed, these electrical vortices, swirling at high speed, propagate through the atrium and can interact with other anatomical and/or electrophysiological obstacles, which causes fragmentation of the spiral wave and new wavelet formation. This process is also called *fibrillatory conduction*. The driving source of AF in this case is thus a spiral wave or rotor (known as the *mother rotor*), generating wavelets due to its interaction with various obstacles in its path. In this way we see that the multiple propagated wavelets observed during AF are not completely unpredictable, but share some deterministic components. Recently, clinical studies showed that localization and subsequent ablation of these driving rotors of fibrillation could terminate or slow AF [88, 89]. We will come back to this in **chapter 4**.

As we already mentioned in the first paragraph of this section, VF is a much more dangerous arrhythmia than AF. For, VF prevents synchronous ventricular contraction, which is needed for efficient pumping of blood to the body. When no electrical defibrillating shocks are applied, VF is lethal within minutes. Similar as for AF, rotors play an important role in

## 2. ABNORMAL EXCITATION OF THE HEART: CARDIAC ARRHYTHMIAS

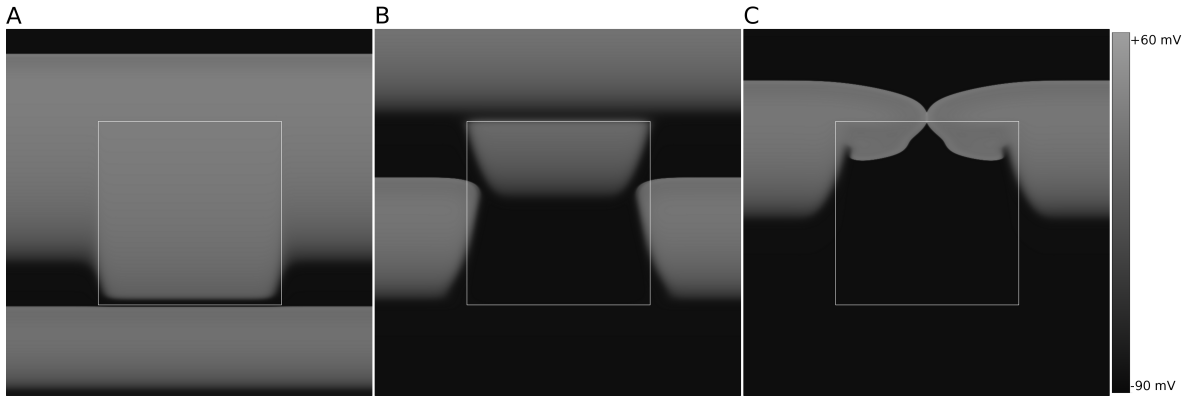


**Figure 1.10: Reentry caused by interaction of a wave front with heterogeneously recovered tissue.** A: Stimulation of the tissue at the bottom of the medium results in propagating waves. Due to the longer refractory period of a rectangular region (obtained by decreasing the conductance of the  $I_{Ks}$  channel inside this region with 80%; white lines), it takes longer for the cells inside this region to recover after passing of the first wave. B: When the second wave reaches this heterogeneity, these cells with a longer refractory period have not recovered and we observe wavebreak. C: After some time the rectangular region becomes excitable again, and the wavebreaks enter the heterogeneity resulting in two counter rotating spiral waves. Simulated using the TP06 model for human ventricular tissue [139]. Total size of the medium is 16 cm by 16 cm.

the generation and maintenance of VF. There are basically two main hypotheses who propose a mechanism for understanding VF.

The first hypothesis is the *spiral breakup hypothesis*. The claim of this theory is that VF occurs due to instability and subsequent breakup of rotor(s) in the ventricles. In Fig. 1.10 we already showed how a spiral could be initiated in the ventricles or atria. The spiral breakup hypothesis postulates that these spiral waves can breakup into a multispiral disordered state, even in homogeneous tissue. In its original form, the spiral breakup hypothesis stated that spiral breakup arises if the maximal slope of the APD restitution curve (APD in function of the diastolic interval (DI)) exceeds one. Because of this, APD alternans (the alternation of long and short action potentials) occur, leading to spiral breakup [93, 46, 98, 62, 63, 19]. Experimental evidence for this hypothesis came from [72, 114, 36]. Although, it has become clear that also other factors play an important role in determining if a spiral breaks up or not. For instance, it was shown both in experiments [36] and in simulation studies [112] that spiral stability not only depends on whether the slope of the restitution curve exceeds one, but also on the range of diastolic intervals for which this is the case. Also several other factors have been shown to influence the stability of a spiral wave<sup>4</sup>. In Fig. 1.11 we show the breakup of a spiral wave caused by a steep APD restitution curve, simulated using an anatomical model of the human ventricles.

On the other hand, another school of thought believes that long lasting, stable, rotors may be the driving force behind VF. In 1995 it was shown by Gray et al. [44], in a combined simulation and experimental study, that even a single drifting rotor could produce an ECG that is indistinguishable from VF in the rabbit heart. However, it has been shown in other

<sup>4</sup>For a more complete overview, we refer to [134] or **chapter 5**

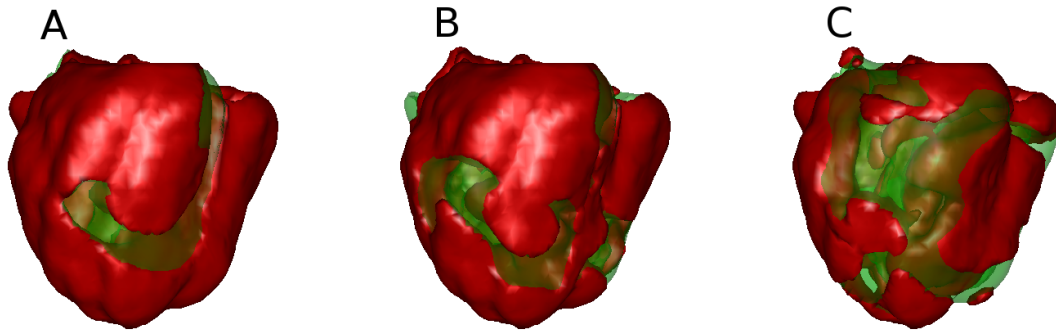


**Figure 1.11: Spiral breakup as a mechanism for VF.** In A, B and C, the red color indicates the excitation wave. A: Initial spiral wave. B: Occurrence of the first wave break due to dynamical instabilities. C: Spiral wave fragmentation. Simulations were performed in an anatomical TP06 model of the human ventricles.

hearts that the spatiotemporal organization during VF is more complex than this. This has led to propose that fibrillatory conduction, in which reentrant circuits drive VF, is the leading mechanism causing VF. Evidence for this came from experiments performed in the guinea pig heart by Samie et al. [118] and in the rabbit heart by Chen et al. [15] and Wu et al. [153]. Although, despite extensive search, these mother rotors have not been observed in larger animal hearts (pigs, dogs) with a size comparable to that of the human heart [115, 57, 55, 64]. However, it has been argued that the hearts of these larger animals do not provide the best model for the human heart. This because the effective size (i.e. the ratio of the size of the tissue to the wavelength of reentry) of dogs and pigs differ substantially from that of humans [97]. Moreover, it was argued that the effective size of the rabbit heart is close to that of humans, making these hearts a better model for the human heart. Also experimental [90, 82] and simulation [66] studies have provided evidence that mother rotors can drive VF in the human heart.

Summarizing, we can conclude that both in the ventricles as in the atria the mechanism behind fibrillation is not completely understood, although there is general consensus on several points. One of them is that heterogeneity of cardiac tissue plays a major role both for the initiation of spiral waves as for the development of tachycardia into fibrillation. This is important to keep in mind, as the study of (ionic) heterogeneities on spiral and scroll wave dynamics is one of the main subjects of this thesis. However, we note that, in the ventricles, we mentioned that tachycardia could also develop into fibrillation in homogeneous tissue due to spiral breakup. Finally, ventricular tachycardia and fibrillation can also be caused by focal triggered activity, especially in the heart of patients with cardiomyopathies [17, 107]. These non-reentrant types of ventricular tachycardia and fibrillation will not be studied in this thesis.

### 3 Modeling in cardiac electrophysiology

#### 3.1 The need for modeling in cardiac electrophysiology

From the previous section it should be clear that the use of models in cardiac electrophysiology has been very helpful to gain insight in the processes which both initiate and maintain cardiac arrhythmias. For instance, initiation of spiral waves due to interaction of a wave with an excitable [73] or an inexcitable obstacle [101, 3] was first described using models of excitable media. Also the aforementioned multiple wavelet [87] and spiral breakup hypothesis [98, 62, 63, 19] for fibrillation were formulated based on modeling studies.

A main reason why modeling of cardiac excitation is very valuable is that the tools available for measuring excitation in the heart are still somewhat limited. The major limitation of the present-day technologies is that they are not able to record the 3D propagation in the heart with sufficient temporal and spatial resolution to give reliable information about the mechanisms of the arrhythmias. Of course, the most recent developed methods in this field, such as optical imaging using voltage-sensitive fluorescent dyes [28, 74] are of great importance, but they are only able to map electrical activation on the surface of the heart or on a wedge. Therefore, to gain a better insight into arrhythmias, (whole) heart modeling is of paramount importance.

Another reason to use models, are practical and ethical limitations to experimental research, which do not apply to modeling studies. *In vivo*, experimental research on human heart is limited to noninvasive measurements (ECG, body surface mappings) and low risk invasive measurements (catheter and multi-electrode mapping) on the heart of people undergoing cardiac surgery. *In vitro* it is limited to the few explanted hearts available for research. Recently, however the amount of data available for human hearts has increased exponentially. *The human heart physiology program* at Washington University in St. Louis, for instance already performed *in vitro* experiments on more than 200 failing and non failing human hearts. In this thesis we used this new available data to set up new models both in cardiac tissue and in the whole heart. It is clear that this unique data opens up a large window of possibilities for modelers. Also, as we mentioned in the previous sections, a lot of research is being performed on *in vivo* and *in vitro* hearts of guinea pigs, rabbits, dogs, pigs,... We already noted that the rabbit heart is considered as a good model for the human heart. Thus, although one should be cautious in extending the conclusions of these studies to the human heart, these animal studies are very valuable.

#### 3.2 Model formalism

The first models to study the excitable behavior of the heart, were so called cellular automata (CA) models. These models were the first to study reentry [148] and fibrillation [87]. In CA models, cells have a discrete state (resting, excited, refractory), and a set of rules describe state transitions depending on the current state of the cell and its neighbors. However these models are not accurate enough to precisely describe properties such as action potential duration, conduction velocity restitution properties or wave front curvature effects. To study the excitable behavior in more detail, partial differential equations (PDE) are used.

As we already explained in 1.2, the excitation process of a cardiac cell is governed by the flux of ions (predominantly  $Na^+$ ,  $K^+$ ,  $Ca^{2+}$  and  $Cl^-$ ) through channels in the cell membrane, which leads to a change in transmembrane potential. This cell membrane can be seen, in

electrical terms, as a capacitor, whereby voltage is changed by the ionic currents across the membrane. This leads to the following equation [65]:

$$C_m \frac{dV_m}{dt} = -I_{\text{ion}}(V_m, g_i), \quad (1.2)$$

where  $C_m$  is the membrane capacitance,  $V_m$  is the transmembrane voltage and  $I_{\text{ion}}$  is the sum of the ionic transmembrane currents describing the excitable behavior of the cell. In addition to Eq. (1.2) there are one or more equations for  $g_i$  needed to describe the dynamics of the transmembrane current. Integration of these equations gives us the time course of an individual cardiac cell.

In 1.2, we made clear that an excitation wave propagates through cardiac tissue because the individual cells are coupled via gap junctions. To model this, we need to modify Eq. (1.2) in order to incorporate the current flow between electrically coupled cardiac cells. In this thesis, we will use the following standard monodomain model for cardiac tissue [65]<sup>5</sup>:

$$C_m \frac{\partial V_m}{\partial t} = \frac{\partial}{\partial x_i} \left( D_{ij} \frac{\partial V_m}{\partial x_j} \right) - I_{\text{ion}}(V_m, g_i), \quad (1.3)$$

where  $D_{ij}$  is a diffusion matrix describing the conductivity of the tissue;  $i, j = 1 \dots n$ , where  $n = 1$  in 1D, 2 in 2D...

### 3.3 From phenomological to ionic models

For modeling the ionic currents across the membrane  $I_{\text{ion}}$  there are basically two approaches. One possible approach is to use phenomological two variable FitzHugh-Nagumo type models [33, 34]. In such models, one variable describes the transmembrane current and the other the recovery processes of the cell. By fitting the parameters of these models, they can reproduce some important measurable characteristics of cardiac tissue, such as the general shape of the action potential, action potential duration restitution and the effects of tissue anisotropy and heterogeneity [70, 5, 31, 137]. These models are extensively used, especially due to their computational efficiency. However, they lack the level of detail to investigate matters such as the effects of mutations and drugs on ionic currents and action potential shape; they do not describe intercellular calcium handling. To describe these complex processes, ionic models are used.

In ionic models, a set of equations is used to describe the dynamic behavior of each individual ionic current. These equations are based on experimental data of voltage and time dynamics of these currents using voltage clamp techniques. In 1953 Hodgkin and Huxley were the first to successfully apply this approach to describe the nerve action potential of the squid giant axon [53]. Some years later they received the Nobel Prize in Physiology or Medicine for this work. Noble extended this work to describe the cardiac action potential [91]. Driven by the discovery of new ionic currents and properties of intracellular calcium dynamics, different models of increasing complexity were developed, both for animals as for human cardiac cells. We mention the Luo-Rudy phase 1 [78] and phase 2 [79] models for guinea pig ventricular cells, the Noble guinea pig ventricular cell model [92] and the Priebe-Beuckelmann model for human ventricular cells [109]. For a more complete overview of different ionic cardiac models

---

<sup>5</sup>We note that such a monodomain model is a reduction of the bidomain model. The monodomain model assumes that the intra- and extracellular domains have equal anisotropy ratios (i.e. that the conductivity in the extracellular space is proportional to the intracellular conductivity).

we refer to [18]. Recent ionic models for cardiac tissue include around 60-100 variables to model the details of ionic channel dynamics identified in cardiac cells. One of these models is the TP06 model for human ventricular cells developed by ten Tusscher et al. [136, 139]. This is the model which we will use in this thesis. It describes the dynamics of the following currents:

$$I_{ion} = I_{Na} + I_{to} + I_{Kr} + I_{Ks} + I_{CaL} + I_{K1} + I_{NaCa} + I_{NaK} + I_{pCa} + I_{pK} + I_{Ca,b} + I_{Na,b} , \quad (1.4)$$

where  $I_{Na}$  denotes the fast sodium current;  $I_{to}$  the transient outward current,  $I_{Kr}$  the slow rectifier current;  $I_{Ks}$  the slow delayed rectifier current;  $I_{CaL}$  the L-type calcium current;  $I_{K1}$  the inward rectifier current;  $I_{NaCa}$  the sodium/calcium exchanger current;  $I_{NaK}$  the sodium/potassium pump current;  $I_{pCa}$  and  $I_{pK}$  the plateau calcium and potassium currents;  $I_{Ca,b}$  and  $I_{Na,b}$  the background currents.

## 4 Thesis outline

The main topic of this thesis is the effect of heterogeneities on electrical waves of excitation in the human heart, studied using mathematical models. In particular, in a major part of this thesis, we will study action potential duration (APD) heterogeneity of cardiac tissue, and its role in formation and influence on dynamics of spiral waves.

In **chapter 2**, we study effects from cell coupling on APD heterogeneity in human cardiac tissue. It is known that the extent of heterogeneity at tissue and single cell level can differ substantially, and it is important to know the relation between them, for instance to model these type of heterogeneities, as we do in **chapter 3 and 4**. We show that the effect of cell coupling on APD heterogeneity can be described mathematically using a Gaussian Green's function approach. We solve both the forward problem (determining effects of tissue heterogeneity from cell heterogeneity) and the inverse problem (determining cell properties from tissue level measurements). The solution of the forward and inverse problem is illustrated on several examples of 1D and 2D systems. With the APD distribution in the 2D examples, based on typical spatial distribution of APD as measured in human heart preparations.

In **chapter 3**, we numerically model APD heterogeneity of realistic size and value in a model for human cardiac tissue, and study formation and dynamics of spiral waves around such heterogeneity. We show that spiral waves can be formed under high frequency pacing of such a heterogeneous medium, and moreover, we find that the only sustained pattern obtained, is a single spiral wave anchored around the heterogeneity. Next, we study the effect of the extent of heterogeneity on the dynamics of such an anchored spiral wave. We find, for certain heterogeneity size, an abrupt regional increase in the period of excitation occurring as a bifurcation. We study factors determining spatial distribution of excitation periods of anchored spiral waves, and discuss consequences of such dynamics for cardiac arrhythmias.

In **chapter 4**, we study the effect of small size ionic heterogeneities, similar to those measured experimentally, on dynamics of spiral waves. This study is performed both in 2D and in an anatomical model of the human ventricles. We show that these heterogeneities can not only anchor, as we show in **chapter 3**, but can also attract spirals rotating at a substantial distance from the heterogeneity. This attraction distance depends on the extent of the heterogeneities and can be as large as 5-6 cm in realistic conditions. So from this,

## CHAPTER 1. INTRODUCTION

---

we can conclude that small size ionic heterogeneities can be preferred localization points for spirals, and discuss their possible mechanism and value for applications.

In **chapter 5**, we study dynamical heterogeneities in homogeneous tissue created due to APD-restitution effects. In particular, we show that a region of initial wave block results in dynamical Wenckebach ‘blocks’ which grow in space and in some cases can result in the formation of new spirals, or the removal of existing spirals. We explain why such behavior can be considered as an ultimate alternans instability or a global alternans instability (GAI). We start this chapter by studying this instability in 1D, and illustrate the growth of this region, find the velocity at which this region grows and the dependency on the forcing period. We use the results obtained in **chapter 2** to propose a semi-analytical theory, and demonstrate that it can describe the observed behavior with a high accuracy. Then we show that in 2D this region extends itself in a similar way, and that it can result in the creation of new spirals, and the eventual removal of spirals from the tissue. This result is very important in the light of the results obtained in **chapter 3 and 4**, where we found that small size ionic heterogeneities can create spirals, but only after they had grown in space. In **chapter 5** we illustrate that the possible mechanism of this growth of the heterogeneity is GAI.

Then, in **chapter 6**, we explain the need for a database where data of experiments on human hearts, as we used in previous chapters to build our models, can be stored. We’ve set up a prototype of such a database using the content management system Drupal, and in **chapter 6** we show how the general structure looks like, and how users can both upload and download data from the database. We also expand on possible future directions which would make it possible for such a database to bridge the gap between experimentalist and modelers.

Finally, in **chapter 7** we end this thesis with a summarizing discussion in which we discuss the major findings found in this thesis.



---

# 2

## APD heterogeneity of cardiac tissue can be evaluated from cell properties using Gaussian Green's function approach

### Abstract

---

Action potential duration (APD) heterogeneity of cardiac tissue is one of the most important factors underlying initiation of deadly cardiac arrhythmias. In many cases such heterogeneity can be measured at tissue level only, while it originates from differences between the individual cardiac cells. The extent of heterogeneity at tissue and single cell level can differ substantially and in many cases it is important to know the relation between them. Here we study effects from cell coupling on APD heterogeneity in cardiac tissue in numerical simulations using the ionic TP06 model for human cardiac tissue. We show that the effect of cell coupling on APD heterogeneity can be described mathematically using a Gaussian Green's function approach. This relates the problem of electrotonic interactions to a wide range of classical problems in physics, chemistry and biology, for which robust methods exist. We show that, both for determining effects of tissue heterogeneity from cell heterogeneity (forward problem) as well as for determining cell properties from tissue level measurements (inverse problem), this approach is promising. We illustrate the solution of the forward and inverse problem on several examples of 1D and 2D systems.

### 1 Introduction

---

Cardiac contraction is initiated by electrical waves of excitation propagating through cardiac tissue. Abnormal wave propagation may result in cardiac arrhythmias. Sudden cardiac death due to cardiac arrhythmias is among the most common causes of death in the industrialized world [159]. One of the leading causes for the onset of cardiac arrhythmias is the heterogeneity of cardiac tissue [87, 73, 69].

Wave propagation in the heart is a result of successive excitation of individual cardiac cells, which are electrically coupled to each other by gap junctions. Such electrical connectivity of the cells not only enables wave propagation, but also affects properties of the individual cells. Fig. 2.1A, with a maximal APD difference of 40 ms and size at 50% heterogeneity of 5 on 6 mm, shows a typical spatial action potential duration (APD) distribution similar to these measured in human heart preparations [40]. If we use these measured values as APD values at cell level, we can fit the parameters of a cell model to reproduce such APD at a given location. If we then connect these cells into the tissue model, we obtain the APD

## CHAPTER 2. APD HETEROGENEITY OF CARDIAC TISSUE CAN BE EVALUATED FROM CELL PROPERTIES USING GAUSSIAN GREEN'S FUNCTION APPROACH

distribution as shown in Fig. 2.1B. We see that the shape and magnitude of the heterogeneity is substantially changed due to coupling between the cells (Fig. 2.1B): the amplitude of the heterogeneity in Fig. 2.1B is almost twice as small as the one in Fig. 2.1A. Alternatively, if one uses a patch clamp procedure and measures properties of various types of uncoupled cardiac cells, it is not clear which heterogeneity will be produced by these cells if they are coupled to tissue. Therefore, the question how to recover real heterogeneity from tissue level experiments and how heterogeneity at cell level manifests itself at tissue level is very important both for theoretical and experimental work.

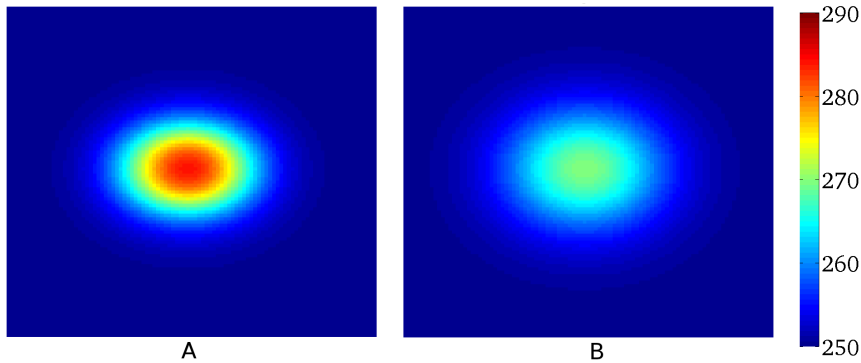


**Figure 2.1: Effect of cell coupling on APD distribution simulated in a human cardiac tissue model.** A: APD distribution in cardiac tissue simulated numerically in a human cardiac tissue model (2.1) after simultaneous excitation of all cells (this to avoid effects resulting from wave propagation [119]). B: APD distribution after input of the measured data (shown in A) into the tissue model. Comparing A and B thus illustrates the effect of cell coupling in a human cardiac tissue model. Heterogeneity is created by changing  $G_{Ks}$ . Total size of the medium is  $25 \text{ mm} \times 25 \text{ mm}$ . Colormap shows APD in ms.

These modulations of APD heterogeneity due to cell-to-cell coupling are called electrotonic effects. In this chapter we show that such electrotonic effects on APD heterogeneity can be characterized by a linear approach using Gaussian functions fits. In particular, we show that APD at tissue level can be found by a convolution of APD distribution at cell level with a bell-shaped Gaussian function (forward problem). Convolutions involving Gaussian functions are among the most studied in mathematics, and applied to various physical, chemical and biological phenomena. Using this formalism, we are able to solve not only the forward problem (i.e. to find APD at tissue level from known APDs of individual cardiac cells), but also start developing an approach to solve the inverse problem (namely to find properties of individual cells from measurements at the tissue level). We illustrate it on several examples.

## 2 Materials and Methods

*Model* - In this chapter we consider a monodomain description of cardiac tissue [65] which has the following form:

$$C_m \frac{\partial V_m}{\partial t} = \frac{\partial}{\partial x_i} \left( D_{ij} \frac{\partial V_m}{\partial x_j} \right) - I_{\text{ion}} , \quad (2.1)$$

where  $D_{ij}$  is a diffusion matrix accounting for anisotropy of cardiac tissue,  $i, j = 1 \dots n$ , where  $n = 1$  in 1D, 2 in 2D...,  $C_m$  is membrane capacitance,  $V_m$  is transmembrane voltage,  $t$  is time and  $I_{\text{ion}}$  is the sum of ionic transmembrane currents describing the excitable behavior of individual ventricular cells. To represent human ventricular electrophysiological properties, we used the ionic TP06 model [136, 139]. This model provides a detailed description of voltage, ionic currents, and intracellular ion concentrations for human ventricular cells. A complete list of all equations can be found in [136, 139]. We used the default parameter settings from [139] for epicardial cells. All parameter changes made to obtain tissue heterogeneity are detailed in the text.

*Numerical methods* - For 1D and 2D computations, the forward Euler method was applied to integrate Eq.(2.1). A space step of  $\Delta x = 0.25$  mm and a time step of  $\Delta t = 0.02$  ms were used. To integrate the Hodgkin-Huxley-type equations for the gating variables of the various time-dependent currents ( $m$ ,  $h$  and  $j$  for  $I_{\text{Na}}$ ;  $r$  and  $s$  for  $I_{\text{to}}$ ;  $x_{r1}$  and  $x_{r2}$  for  $I_{\text{Kr}}$ ;  $x_s$  for  $I_{\text{Ks}}$ ;  $d$ ,  $f$ ,  $f_2$  and  $f_{\text{CaS}}$  for  $I_{\text{CaL}}$ ), the Rush and Larsen scheme [117] was used.

*Heterogeneity* - To study heterogeneity, we change the parameters  $G_{\text{Ks}}$ ,  $G_{\text{Kr}}$  and  $G_{\text{CaL}}$  from their default values 0.392 nS/pF, 0.153 nS/pF and  $3.98 \times 10^{-5}$  cm/(ms  $\cdot$   $\mu$ F) for epicardial cells in [139]. Unless otherwise stated, APD is measured at 80% repolarization level.

*Inverse problem* - The inverse problem in 1D was solved using Tikhonov's regularization method. In 2D, the inverse problem was solved using the Tikhonov image deblurring fast fourier transform algorithm. To implement this in 1D and 2D we used two Matlab packages developed by Per Christian Hansen [48, 49].

## 3 Results

---

### 3.1 1D step-wise heterogeneity

To establish a proper description of the heterogeneity, we first considered the simplest type of heterogeneity: a stepwise heterogeneity in a cable (see Fig. 2.2A).

We excited all points of the cable simultaneously and calculated the spatial APD distribution. Fig. 2.2A shows that, due to electrotonic effects, the stepwise heterogeneity becomes spatially distributed with a characteristic space constant ( $A_3$ ) of around 3.5 mm. After trying several types of sigmoidal functions, we found that an almost perfect fit of spatial APD distribution can be obtained using the error function, which is the antiderivative of the Gaussian function. Indeed, if we use for the stepwise heterogeneity in Fig. 2.2A:

$$\overline{\text{APD}}(x) = A_1 + A_2 \text{erf} \left( (x - \alpha_0 - A_0) \frac{1}{A_3} \right), \quad (2.2)$$

with  $A_0 = 0.631$  mm,  $A_1 = 308.624$  ms,  $A_2 = 21.3745$  ms,  $A_3 = 3.497$  mm and the location of the heterogeneity  $\alpha_0 = 24.875$  mm, then the exact solution (red line in Fig. 2.2A) and the fit (blue line) are almost indistinguishable from each other with a relative error less than 0.4 %.

Note that the parameters  $A_1$  and  $A_2$  in Eq.(2.2) are obviously connected to the APD in the uncoupled system (APD0) from Fig. 2.2A as  $A_1 = \frac{\text{APD0}_1 + \text{APD0}_2}{2}$  and  $A_2 = \frac{\Delta \text{APD0}}{2}$  with  $\Delta \text{APD0} = \text{APD0}_2 - \text{APD0}_1$ . The parameter  $A_3$  gives the spatial distribution, and in our case is 3.497 mm; the parameter  $A_0$  indicates some additional shift, which in our case is 0.631 mm.

By varying  $\Delta \text{APD0}$ , we studied how the parameters  $A_0$  and  $A_3$  of our fit depend on the degree of heterogeneity. We found that parameter  $A_3$  showed only minimal dependency on

## CHAPTER 2. APD HETEROGENEITY OF CARDIAC TISSUE CAN BE EVALUATED FROM CELL PROPERTIES USING GAUSSIAN GREEN'S FUNCTION APPROACH

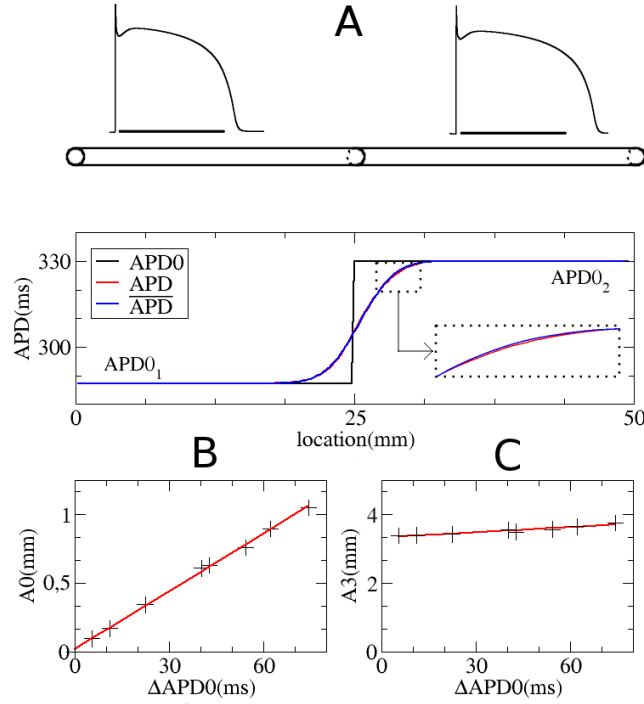


**Figure 2.2: Electrotonic effect for a stepwise heterogeneity in a cable.** A: Spatial distribution of APD in a fiber with stepwise heterogeneity. Computations using TP06 model in a fiber of 50 mm long. The upper panel shows action potential shapes in the uncoupled system. The black line under both action potentials represents a time interval of 300 ms. The bottom panel shows APD distribution: black APD in the uncoupled system, red APD in the coupled system and blue the APD obtained via Eq.(2.2). B: Plot of  $\Delta\text{APD}0$  versus  $A_0$ . C: Plot of  $\Delta\text{APD}0$  versus  $A_3$ . B and C: best linear fit through these points are shown in red.  $G_{Ks}$  in the left part of the fiber was 0.392 nS/pF. Other degrees of heterogeneity are obtained by changing  $G_{Ks}$ . In general, for a heterogeneity of 10 ms it was necessary to change  $G_{Ks}$  by 0.073 nS/pF.

$\Delta\text{APD}0$ . Indeed, in Fig. 2.2C we see that by changing  $\Delta\text{APD}0$  13.3 fold,  $A_3$  changes just by 10.8 %. Furthermore, if we put  $A_0 = 0$ , in Eq.(2.2), our curve is shifted to the left, and gives us a maximal error of around 2ms. However, for small values of  $\Delta\text{APD}0$ , which will be the most important for us in the future  $A_0$  is small. For example, for  $\Delta\text{APD}0 = 10$  ms,  $A_0$  is of the order of 0.15 mm, which is approximately 20 fold less than the characteristic space constant  $A_3$ . Therefore, we can conclude that with a high degree of accuracy we can assume that the parameters  $A_3$  and  $A_0$  do not depend on  $\Delta\text{APD}0$ .

In Fig. 2.2 we studied a heterogeneity obtained by changing the  $I_{Ks}$  current. Besides  $I_{Ks}$ , other ionic currents such as  $I_{Kr}$  and  $I_{CaL}$  have important influence on APD. To find possible effect of other ionic currents on the electrotonic interaction we study a stepwise heterogeneity as in Fig. 2.2A, but with a heterogeneity now obtained by changing  $G_{Kr}$ , respectively  $G_{CaL}$  (Fig. 2.3). We see that the electrotonic effect in our model does not depend on ionic current used to induce tissue heterogeneity. In particular, in all cases the fit of Eq.(2.2) works good and we have  $A_3 = 3$  mm, for  $G_{Kr}$  induced heterogeneity, and  $A_3 = 3.5$  mm for  $G_{CaL}$  or  $G_{Ks}$  induced heterogeneity. Furthermore, we find that the parameter  $A_0$  is also small. For  $G_{Ks}$ ,

$G_{Kr}$  and  $G_{CaL}$ , we find for  $A_0$  respectively 0.4, 0.5 and 0.2 mm.

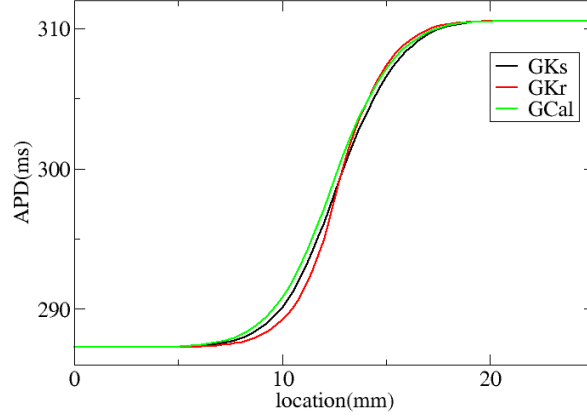


**Figure 2.3: Electrotonic interaction for different parameters.** In black, red and green, heterogeneity was created by changing, respectively,  $G_{Ks}$ ,  $G_{Kr}$  and  $G_{CaL}$ . In the left part of the fiber  $G_{Ks}=0.392$  nS/pF;  $G_{Kr}=0.153$  nS/pF and  $G_{CaL}=3.98 \times 10^{-5}$  cm/(ms ·  $\mu$ F). For a heterogeneity of 10 ms it was necessary to change  $G_{Kr}$  and  $G_{CaL}$  with respectively 0.048 nS/pF and  $7.4 \times 10^{-6}$  cm/(ms ·  $\mu$ F).

Overall we can conclude that our problem of dependency of  $APD(x)$  on  $\Delta APD_0$  can thus with high accuracy be considered as linear. This allows us to formulate an approach for finding  $APD(x)$  not only for a stepwise heterogeneity, but for a heterogeneity of any sharp  $APD_0(x)$ .

### 3.2 The forward problem

Thus, as for a linear problem, any heaviside-like heterogeneity will generate an APD distribution given by Eq.(2.2), this yields that the expected  $\overline{APD}(x)$  will be given by:

$$\overline{APD}(x) = \frac{1}{2} \int_{-\infty}^{+\infty} \operatorname{erf} \left( (x - \alpha) \frac{1}{A_3} \right) \frac{dAPD_0(\alpha)}{d\alpha} d\alpha . \quad (2.3)$$

Integrating by parts yields

$$\overline{APD}(x) = \frac{1}{A_3 \sqrt{\pi}} \int_{-\infty}^{+\infty} APD_0(\alpha) e^{-\left( (x - \alpha) \frac{1}{A_3} \right)^2} d\alpha . \quad (2.4)$$

The observed distribution  $APD(x)$  can thus be found as a convolution of  $APD_0$  with a Gaussian function.

Let us extend this formula to  $n$  dimensions and to the general anisotropic case, as in Eq.(2.1). First, note that if we consider a 1D system with a constant diffusion coefficient  $D$ , then due to spatial scaling,  $A_3^2$  is proportional to  $D$  and based on our simulation we can write for an arbitrary  $D$  that  $A_3^2 = kD$ , where  $k \approx 204$  ms. Similar considerations for a 2D case with the fibers directed along the  $x$  axis and diffusivities in the  $x$  and  $y$  directions given by  $D_f$  and  $D_t$  yield a Gaussian kernel  $\exp \left( -\frac{(x-\alpha)^2}{kD_f} - \frac{(y-\beta)^2}{kD_t} \right)$ . Note, as in this case  $D_{ij} = \operatorname{diag}(D_f, D_t)$ ,

## CHAPTER 2. APD HETEROGENEITY OF CARDIAC TISSUE CAN BE EVALUATED FROM CELL PROPERTIES USING GAUSSIAN GREEN'S FUNCTION APPROACH

this expression can be rewritten as  $\exp\left(- (x_i - \alpha_i) D_{ij}^{-1} (x_j - \alpha_j) \frac{1}{k}\right)$ , where  $D_{ij}^{-1}$  is the inverse of  $D_{ij}$ . For an arbitrary fiber orientation, we can proceed to a local coordinate system aligned with the fibers, in which, as in the previous case, the diffusion tensor will be diagonal. Direct calculation shows that the general case will simply result in transformation of a diagonal matrix to a general non-diagonal matrix  $D_{ij}^{-1}$ , which is the inverse of the diffusivity matrix  $D_{ij}$  from Eq.(2.1), but the form of the expression will be unchanged. Thus, in  $n$  dimensions, in presence of anisotropy given by a constant matrix  $D_{ij}$  slowly varying in space, formula (2.4) will be given by

$$\overline{\text{APD}}(\bar{x}) = \frac{1}{(k\pi)^{\frac{n}{2}}} \int_{-\infty}^{+\infty} \frac{\text{APD0}(\bar{\alpha})}{\sqrt{\det D_{ij}(\bar{x})}} e^{-((x_i - \alpha_i) D_{ij}^{-1}(\bar{x}) (x_j - \alpha_j) \frac{1}{k})} d\bar{\alpha}, \quad (2.5)$$

with  $\bar{x} = (x_1, x_2, \dots, x_n)$ ,  $\bar{\alpha} = (\alpha_1, \alpha_2, \dots, \alpha_n)$ . Note that, although this formula is formally valid only for a matrix  $D_{ij}$  which is constant in space, it is reasonable to assume that it will be also valid for fibers for which the orientation changes slowly in space, as the Gaussian function in Eq.(2.5) is exponentially localized in space. Possible extensions of this formula to a general curved space will be studied in future work.

We first test our method by considering gradients in APD with different steepness obtained by changing  $G_{Ks}$  (Fig. 2.4),  $G_{Kr}$  (Fig. 2.5) and  $G_{CaL}$  (Fig. 2.6). We use Eq.(2.4) to predict APD duration in the coupled system and observe that our method works good for the heterogeneities induced by  $G_{Ks}$  and  $G_{CaL}$ . For the heterogeneity induced by  $G_{Kr}$  (Fig. 2.5), we see some deviations from the predicted values, especially for steep heterogeneities. However, we see that in all situations our method predicts the maximal value of APD in the coupled system, which is important for characterization of the extent of heterogeneity. We also did two simulations for an asymmetric heterogeneity (see Fig. 2.7). We see that our method also works good in that case.

Next, we test our method for a more complex 1D heterogeneous APD0 distribution (Fig. 2.8A). Heterogeneity is, in this case, created by changing  $G_{Ks}$ . We see that Eq.(2.4), with  $A_3 = 3.5$  mm gives a good prediction for the observed APD distribution, with a maximal error of 3 ms. To quantify how well our approach predicts the electrotonic effect, we compared the measured electrotonic effect ( $\|\text{APD} - \text{APD0}\|_2$ , using the L2 norm) with the predicted electrotonic effect ( $\|\overline{\text{APD}} - \text{APD0}\|_2$ ) as  $E_{\text{fwd}} = \frac{\|\text{APD} - \text{APD0}\|_2}{\|\overline{\text{APD}} - \text{APD0}\|_2} - 1$ . For Fig. 2.8A, we obtained  $E_{\text{fwd}} = 0.5\%$ .

We have also checked if our method works for the electrotonic effects if APD is measured at 50% repolarization level ( $\text{APD}_{50}$ ). As electrotonic effects depend on the level at which we perform a measurement [119], we recalculated  $A_3$  for this case, which was found to be  $A_3 \approx 3$  mm. We performed the same simulations as those in Fig. 2.8A for  $\text{APD}_{50}$ . We see (Fig. 2.9A) that Eq.(2.4), gives a good prediction for the observed  $\text{APD}_{50}$  distribution, with a maximal error of 3 ms and  $E_{\text{fwd}} = 0.45\%$ .

We performed the same analysis in 2D for a diffusivity matrix  $D_{ij}(\bar{x})$  which changes slowly in space using Eq.(2.5). For this, we supposed that the fibers lay along parabolas  $y = B(x - x_0)^2 + y_0$ , with  $x_0 = 25/2$  mm, varying  $y_0$  and a fixed shape parameter  $B = 0.04$  1/mm. This gives us the local fiber direction

$$\vec{e}_f = \frac{\vec{e}_x + 2B(x - x_0)\vec{e}_y}{\sqrt{1 + 4B^2(x - x_0)^2}}. \quad (2.6)$$

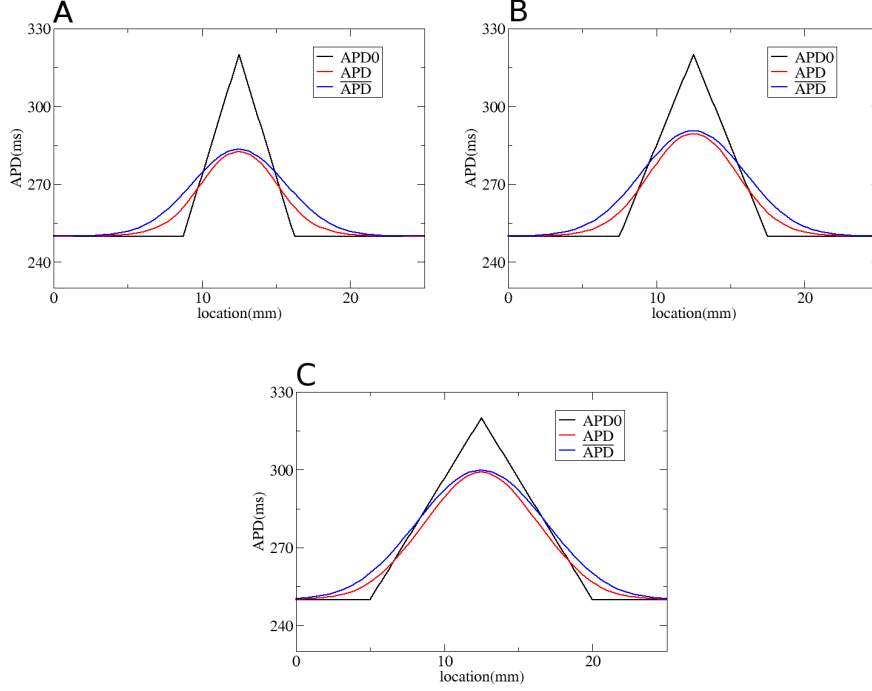


**Figure 2.4: Solution of the forward problem for heterogeneity created by changing  $G_{Ks}$ .**

In A, B and C: in black APD0, in red APD, and in blue the predicted APD via Eq.(2.4) with  $A_3 = 3.5$  mm and  $A_0 = 0$  mm. Parameters of the model in A are:  $G_{Ks}(x)=0.72$  nS/pF if  $x < 9$  mm;  $G_{Ks}(x) = \frac{0.22-0.72}{3.5}(x-9) + 0.72$  nS/pF if  $9 \text{ mm} \leq x < 12.5$  mm;  $G_{Ks}(x) = \frac{0.72-0.22}{3.5}(x-16) + 0.72$  nS/pF if  $12.5 \text{ mm} \leq x < 16$  mm;  $G_{Ks}(x)=0.72$  nS/pF if  $16 \text{ mm} \leq x$ . In B:  $G_{Ks}(x)=0.72$  nS/pF if  $x < 7.5$  mm;  $G_{Ks}(x) = \frac{0.22-0.72}{5}(x-7.5) + 0.72$  nS/pF if  $7.5 \text{ mm} \leq x < 12.5$  mm ;  $G_{Ks}(x) = \frac{0.72-0.22}{5}(x-17.5) + 0.72$  nS/pF if  $12.5 \text{ mm} \leq x < 17.5$  mm;  $G_{Ks}(x)=0.72$  nS/pF if  $17.5 \text{ mm} \leq x$ . In C:  $G_{Ks}(x)=0.72$  nS/pF if  $x < 5$  mm;  $G_{Ks}(x) = \frac{0.22-0.72}{7.5}(x-5) + 0.72$  nS/pF if  $5 \text{ mm} \leq x < 12.5$  mm;  $G_{Ks}(x) = \frac{0.72-0.22}{7.5}(x-20) + 0.72$  nS/pF if  $12.5 \text{ mm} \leq x < 20$  mm;  $G_{Ks}(x)=0.72$  nS/pF if  $20 \text{ mm} \leq x$ .

Thus for the diffusivity matrix  $D_{ij} = (D_L - D_T)e_{f,i}e_{f,j} + D_T\delta_{ij}$ , we obtain

$$\begin{cases} D_{xx} = \frac{D_L - D_T}{1 + 4B^2(x-x_0)^2} + D_T, \\ D_{xy} = D_{yx} = \frac{(D_L - D_T)2B(x-x_0)}{1 + 4B^2(x-x_0)^2}, \\ D_{yy} = \frac{(D_L - D_T)4B^2(x-x_0)^2}{1 + 4B^2(x-x_0)^2} + D_T. \end{cases} \quad (2.7)$$

with in our case  $D_L = 0.128 \frac{\text{mm}^2}{\text{ms}}$ , and  $D_T = D_L/4$ . In Fig. 2.10A we show APD0, in Fig. 2.10B measured APD and in Fig. 2.10C the predicted values  $\overline{\text{APD}}$ . Here, we found a maximal error of 6 ms, and  $E_{\text{fwd}} = 0.6\%$ . We can thus conclude that our forward method for calculating APD by convoluting APD0 with a Gaussian function produces accurate results.

The proposed approach can also be used for finding analytical estimates of electrotonic effects. Let us apply it to estimate dependence of electrotonic effects on the size of heterogeneity. For this, consider a block of size  $d$  of tissue with a longer APD (Fig. 2.11A) and

## CHAPTER 2. APD HETEROGENEITY OF CARDIAC TISSUE CAN BE EVALUATED FROM CELL PROPERTIES USING GAUSSIAN GREEN'S FUNCTION APPROACH

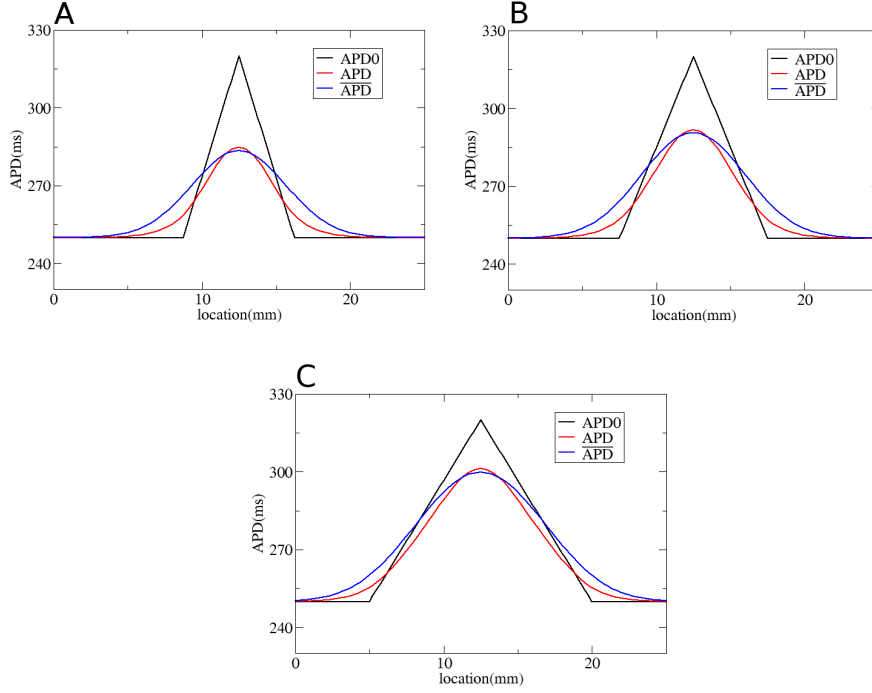


**Figure 2.5: Solution of the forward problem for heterogeneity created by changing  $G_{Kr}$ .** In A, B and C: in black APD0, in red APD, and in blue the predicted APD via Eq.(2.4) with  $A_3 = 3.5$  mm and  $A_0 = 0$  mm. Parameters of the model in A are:  $G_{Kr}(x)=0.35$  nS/pF if  $x < 9$  mm;  $G_{Kr}(x) = \frac{0.025-0.35}{3.5}(x-9) + 0.35$  nS/pF if  $9 \text{ mm} \leq x < 12.5$  mm;  $G_{Kr}(x) = \frac{0.35-0.025}{3.5}(x-16) + 0.35$  nS/pF if  $12.5 \text{ mm} \leq x < 16$  mm;  $G_{Kr}(x)=0.35$  nS/pF if  $16 \text{ mm} \leq x$ . In B:  $G_{Kr}(x)=0.35$  nS/pF if  $x < 7.5$  mm;  $G_{Kr}(x) = \frac{0.025-0.35}{5}(x-7.5) + 0.35$  nS/pF if  $7.5 \text{ mm} \leq x < 12.5$  mm;  $G_{Kr}(x) = \frac{0.35-0.025}{5}(x-17.5) + 0.35$  nS/pF if  $12.5 \text{ mm} \leq x < 17.5$  mm;  $G_{Kr}(x)=0.35$  nS/pF if  $17.5 \text{ mm} \leq x$ . In C:  $G_{Kr}(x)=0.35$  nS/pF if  $x < 5$  mm;  $G_{Kr}(x) = \frac{0.025-0.35}{7.5}(x-5) + 0.35$  nS/pF if  $5 \text{ mm} \leq x < 12.5$  mm;  $G_{Kr}(x) = \frac{0.35-0.025}{7.5}(x-20) + 0.35$  nS/pF if  $12.5 \text{ mm} \leq x < 20$  mm;  $G_{Kr}(x) = 0.35$  nS/pF if  $20 \text{ mm} \leq x$ .

compare maximum of APD in coupled system relative to the maximum in the uncoupled system. For such step-wise distribution, the APD0 integral (2.3) can be evaluated explicitly, yielding for the maximal value of APD:

$$\text{APD}_{\max} = \text{APD}_{\min} + \Delta\text{APD}_0 \text{erf}\left(\frac{d}{2A_3}\right), \quad (2.8)$$

or thus

$$\frac{\Delta\text{APD}}{\Delta\text{APD}_0} = \text{erf}\left(\frac{d}{2A_3}\right). \quad (2.9)$$

This curve is plotted in red in Fig. 2.11B. We also plot the values we obtained via simulations. We see a good correspondence of numerical and analytical estimates. The correspondence is perfect for a small and large thickness of the heterogeneity, although in the intermediate



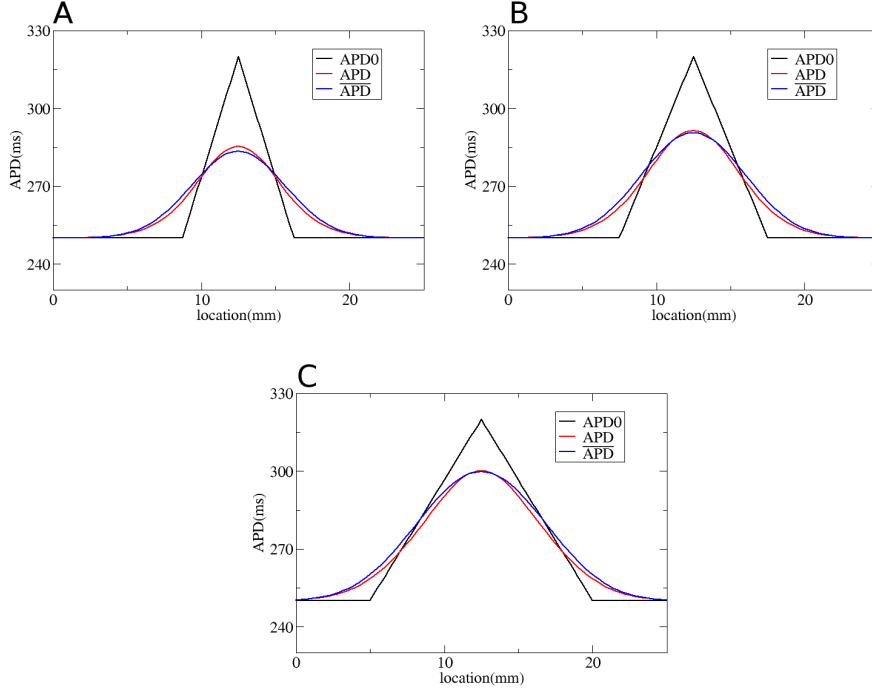


**Figure 2.6: Solution of the forward problem for heterogeneity created by changing  $G_{CaL}$ .** In A, B and C: in black APD0, in red APD, and in blue the predicted APD via Eq.(2.4) with  $A_3 = 3.5$  mm and  $A_0 = 0$  mm. Parameters of the model in A are:  $G_{CaL}(x) = 2.2 \times 10^{-5}$  cm/(ms  $\cdot$   $\mu$ F) if  $x < 9$  mm;  $G_{CaL}(x) = \frac{7.1 \times 10^{-5} - 2.2 \times 10^{-5}}{3.5}(x - 9) + 2.2 \times 10^{-5}$  cm/(ms  $\cdot$   $\mu$ F) if  $9$  mm  $\leq x < 12.5$  mm;  $G_{CaL}(x) = \frac{2.2 \times 10^{-5} - 7.1 \times 10^{-5}}{3.5}(x - 16) + 2.2 \times 10^{-5}$  cm/(ms  $\cdot$   $\mu$ F) if  $12.5$  mm  $\leq x < 16$  mm;  $G_{CaL}(x) = 2.2 \times 10^{-5}$  cm/(ms  $\cdot$   $\mu$ F) if  $16$  mm  $\leq x$ . In B:  $G_{CaL}(x) = 2.2 \times 10^{-5}$  cm/(ms  $\cdot$   $\mu$ F) if  $x < 7.5$  mm;  $G_{CaL}(x) = \frac{7.1 \times 10^{-5} - 2.2 \times 10^{-5}}{5}(x - 7.5) + 2.2 \times 10^{-5}$  cm/(ms  $\cdot$   $\mu$ F) if  $7.5$  mm  $\leq x < 12.5$  mm;  $G_{CaL}(x) = \frac{2.2 \times 10^{-5} - 7.1 \times 10^{-5}}{5}(x - 17.5) + 2.2 \times 10^{-5}$  cm/(ms  $\cdot$   $\mu$ F) if  $12.5$  mm  $\leq x < 17.5$  mm;  $G_{CaL}(x) = 2.2 \times 10^{-5}$  cm/(ms  $\cdot$   $\mu$ F) if  $17.5$  mm  $\leq x$ . In C:  $G_{CaL}(x) = 2.2 \times 10^{-5}$  cm/(ms  $\cdot$   $\mu$ F) if  $x < 5$  mm;  $G_{CaL}(x) = \frac{7.1 \times 10^{-5} - 2.2 \times 10^{-5}}{7.5}(x - 5) + 2.2 \times 10^{-5}$  cm/(ms  $\cdot$   $\mu$ F) if  $5$  mm  $\leq x < 12.5$  mm;  $G_{CaL}(x) = \frac{2.2 \times 10^{-5} - 7.1 \times 10^{-5}}{7.5}(x - 20) + 2.2 \times 10^{-5}$  cm/(ms  $\cdot$   $\mu$ F) if  $12.5$  mm  $\leq x < 20$  mm;  $G_{CaL}(x) = 2.2 \times 10^{-5}$  cm/(ms  $\cdot$   $\mu$ F) if  $20$  mm  $\leq x$ .

range, we have some deviations. We also see that the electrotonic effects are substantially affected by heterogeneity size. Indeed, we see that if the heterogeneity is 1-2mm, the value of the heterogeneity measured in tissue experiments will differ from the real heterogeneity 2-5 fold.

### 3.3 The inverse problem

Because the forward problem can be written in the standard form Eq.(2.4) and Eq.(2.5), it can also be used to solve the inverse problem, i.e. predict APD0 from a given APD. Standard approaches to solve inverse problems of this type use regularization methods [143].

## CHAPTER 2. APD HETEROGENEITY OF CARDIAC TISSUE CAN BE EVALUATED FROM CELL PROPERTIES USING GAUSSIAN GREEN'S FUNCTION APPROACH

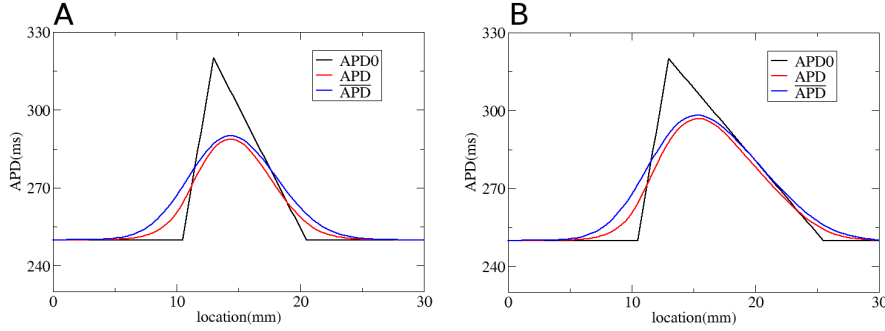


**Figure 2.7: Solution of the forward problem for an asymmetric heterogeneity created by changing  $G_{Ks}$ .** In A and B: in black APD0, in red APD, and in blue the predicted APD via Eq.(2.4) with  $A_3 = 3.5$  mm and  $A_0 = 0$  mm. Parameters of the model in A are:  $G_{Ks}(x)=0.72$  nS/pF if  $x < 10.5$  mm;  $G_{Ks}(x) = \frac{0.22-0.72}{2.5}(x - 10.5) + 0.72$  nS/pF if  $10.5$  mm  $\leq x < 13$  mm;  $G_{Ks}(x) = \frac{0.72-0.22}{7.5}(x - 20.5) + 0.72$  nS/pF if  $13$  mm  $\leq x < 20.5$  mm;  $G_{Ks}(x)=0.72$  nS/pF if  $20.5$  mm  $\leq x$ . In B:  $G_{Ks}(x)=0.72$  nS/pF if  $x < 10.5$  mm;  $G_{Ks}(x) = \frac{0.22-0.72}{2.5}(x - 10.5) + 0.72$  nS/pF if  $10.5$  mm  $\leq x < 13$  mm;  $G_{Ks}(x) = \frac{0.72-0.22}{12.5}(x - 25.5) + 0.72$  nS/pF if  $13$  mm  $\leq x < 25.5$  mm;  $G_{Ks}(x)=0.72$  nS/pF if  $25.5$  mm  $\leq x$ .

Here, we will use the most common and well-known form of regularization, namely Tikhonov regularization [48]. The regularized solution via Tikhonov regularization is given by

$$x_\lambda = \min\{\|Ax - b\|_2^2 + \lambda^2\|x\|_2^2\} . \quad (2.10)$$

With  $A$  the Gaussian kernel,  $b$  the APD distribution in the coupled system and  $x$  the unknown APD distribution in the uncoupled system. Thus,  $Ax$  indicates the solution of the forward problem. The amount of regularization is controlled by the regularization parameter  $\lambda$ , which depends on the problem itself. Larger values of  $\lambda$  produce increasingly smoother solutions, while for small  $\lambda$  values the inverse solution is less stable. We note that properly choosing  $\lambda$  is a common problem of all inverse problems. There is basically only one established approach, called the Morozov discrepancy principle [143]; however, it does not always produce a suitable value for  $\lambda$ . In the present work, we manually adapted  $\lambda$  until the solution to the inverse problem appeared as regular. Our criterion for this was: a small oscillatory component.

To solve the inverse problem in 1D via Tikhonov regularization, we used the algorithms available at [48]. As for the forward problem, we first consider simple gradients in Fig. 2.12, 2.13 and 2.14. Heterogeneities are the same as in Fig. 2.4, 2.5 and 2.6, and thus obtained by changing, respectively,  $G_{Ks}$ ,  $G_{Kr}$  and  $G_{CaL}$ . We see that for intermediate and shallow heterogeneities, we can reconstruct APD0 with reasonably high accuracy (Fig. 2.12B, C; 2.13B, C and 2.14B, C) especially the maximal value of APD0. We see that in all solutions, there is an oscillatory component present which increases with the increase of steepness of the gradient. This causes substantial errors for the steepest heterogeneity (Fig. 2.12A, Fig. 2.13A and Fig. 2.14A). We also applied our method for the two asymmetric heterogeneities as in Fig. 2.7. In Fig. 2.15, we see that we can reconstruct APD0 in both cases. Again, we observe an oscillatory component, especially for the steep part of the heterogeneity.

Now we illustrate our method on a more complex APD0 distribution. We consider the

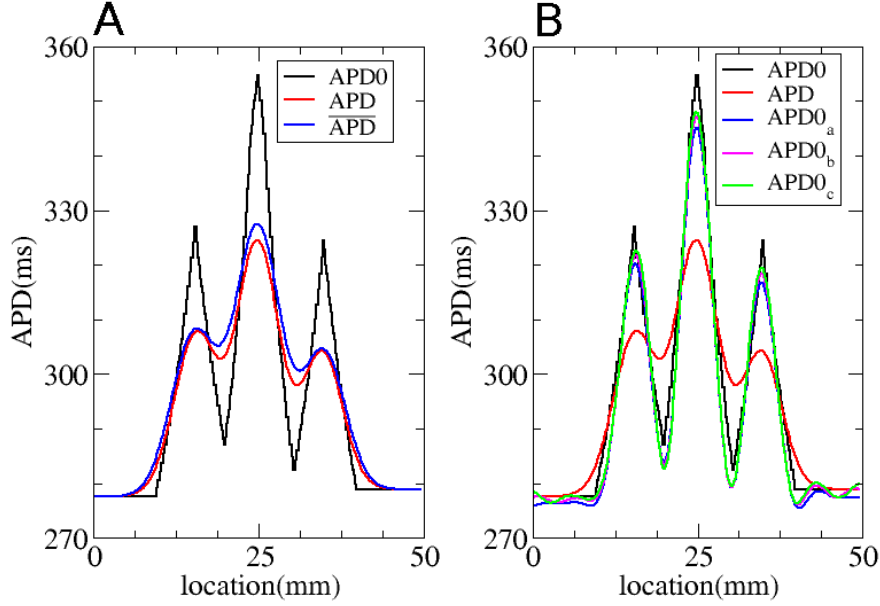


**Figure 2.8: Solution of the forward and inverse problem in 1D.** A: The solution of the forward problem in 1D. In black the APD in the uncoupled system, in red APD in the coupled system and in blue the APD obtained via Eq.(2.4) with  $A_3 = 3.5$  mm and  $A_0 = 0$  mm. B: The solution of the inverse problem in 1D. Black represents APD0 and red APD for the coupled system. APD0<sub>a</sub> (blue), APD0<sub>b</sub> (pink) and APD0<sub>c</sub> (green) display the predicted APD0 values for regularization parameter  $\lambda$  equal to 0.07, 0.05 or 0.036.

same APD0 distribution as in Fig. 2.8A. In Fig. 2.8B, we reconstruct the initial APD0 distribution (black), based on the measured APD distribution (Fig. 2.8B, red). Three reconstructions are shown, for various values of the Tikhonov parameter  $\lambda$ . The maximal absolute errors for APD0<sub>a</sub>, APD0<sub>b</sub>, APD0<sub>c</sub> are respectively 8 ms, 7 ms and 6 ms. In the same way as for the forward problem, we can quantify how well our approach reproduces the electrotonic effects by calculating  $E_{\text{inv}} = \frac{\|\text{APD0} - \text{APD}\|_2}{\|\text{APD0}_a - \text{APD}\|_2} - 1 = 4.4\%$ . For APD0<sub>b</sub>, APD0<sub>c</sub>, we find respectively 8.8% and 10.4%. Thus, we observe that this method works well and that we can recover the APD0 distribution in the uncoupled system.

Fig. 2.9B illustrates that the method also works good for APD<sub>50</sub>. We see that the predicted APD0 (green) is close to the initial APD0 distribution. The maximal absolute error is 5 ms and  $E_{\text{inv}} = 8.3\%$ , which is close to that for the APD distribution measured at 80% repolarization level.

To solve the inverse problem in 2D via Tikhonov regularization, we used the algorithms from [49]. To test our method in 2D, we used the dataset from Fig. 2.1A, and quantified the real heterogeneity via the solution of the inverse problem. We obtain the solution shown in Fig. 2.16A. In Fig. 2.16B we plot the exact APD0 distribution used in our model to obtain Fig. 2.1A. In this way, we see that our inverse solution properly recovers the underlying heterogeneity. As in 1D, we calculate  $E_{\text{inv}} = \frac{\|\text{APD0} - \text{APD}\|_2}{\|\text{APD0}_{\text{pred}} - \text{APD}\|_2} - 1 = 13\%$ . In particular, the most important parameter: the maximal value of APD0 in the inverse solution is 355

## CHAPTER 2. APD HETEROGENEITY OF CARDIAC TISSUE CAN BE EVALUATED FROM CELL PROPERTIES USING GAUSSIAN GREEN'S FUNCTION APPROACH

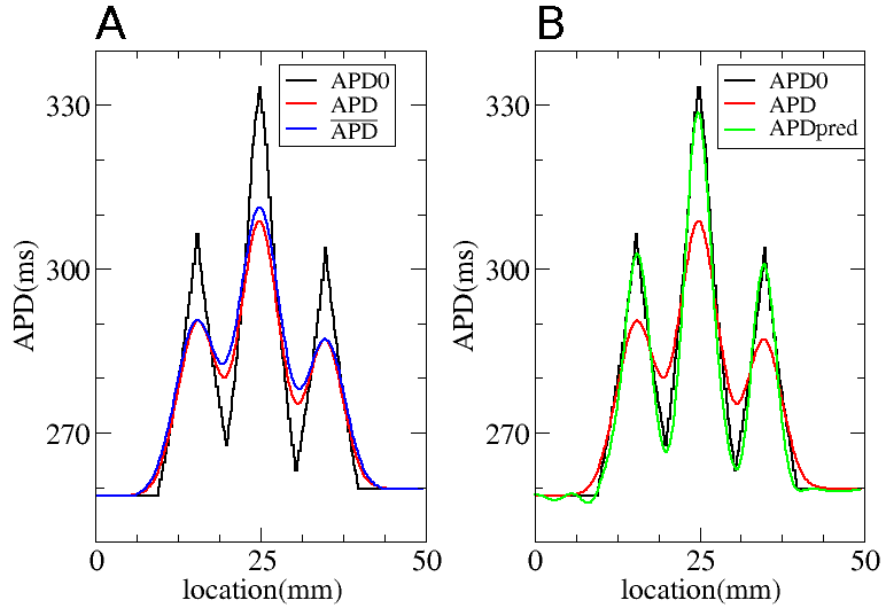


**Figure 2.9: Solution of the forward and inverse problem in 1D with APD measured at 50%.** A: The solution of the forward problem in 1D. In black the APD in the uncoupled system, in red APD in the coupled system and in blue the APD obtained via Eq.(2.4) with  $A_3 = 3$  mm and  $A_0 = 0$  mm. B: The solution of the inverse problem in 1D. Black represents APD0 and red APD for the coupled system. Green shows the predicted APD0 for regularization parameter  $\lambda$  equal to 0.036.

ms, while the exact value is 360 ms. The characteristic width at 50% of heterogeneity in the inverse solution is 2 mm in the vertical and 3 mm in the horizontal direction, while the exact values are 2 mm and 3.25 mm. However, we also see that, as in 1D, the inverse solution has a damped oscillatory component in certain directions, with amplitude up to 20 ms. This component is absent in the original APD0 distribution. Note, however, that we applied the simplest method for solution of the inverse problem here, so it can certainly be improved. For, the inverse problem given by Eq.(2.5) is one of the most studied inverse problems in applied mathematics. Thus it should be possible to suppress the oscillatory component by choosing a proper formulation, which we intend to do in the future.

## 4 Discussion

In this chapter we have shown that the electrotonic effects in heterogeneous cardiac tissue can with good accuracy be treated using a linear Green's function approach. Interestingly, a good approximation for the Green's function is given by a Gaussian kernel. This relates our problem to one of the most studied classical problems in science and engineering arising from the diffusion equation, such as mass and heat transfer, image processing, light scattering etc.

We have shown that even the most simple and straightforward approaches for the forward and inverse problems produce promising results, which opens possibilities for the application

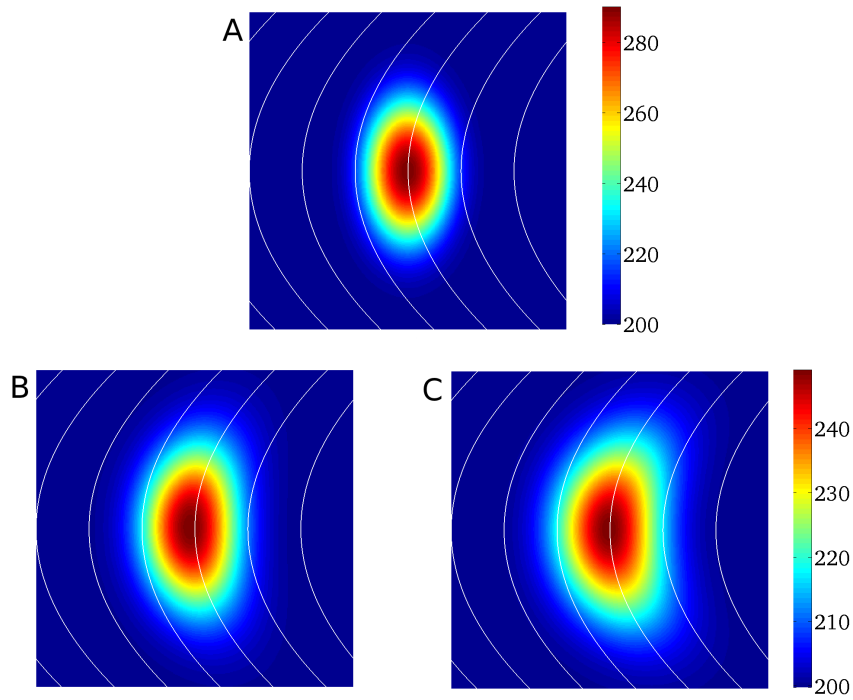


**Figure 2.10: Solution of the forward problem in 2D for a curved space.** A: APD0 distribution. B: APD distribution after input of APD0 in a human cardiac tissue model. C: Predicted APD distribution obtained using formula (2.5) from main text. Fiber direction is drawn in white lines.

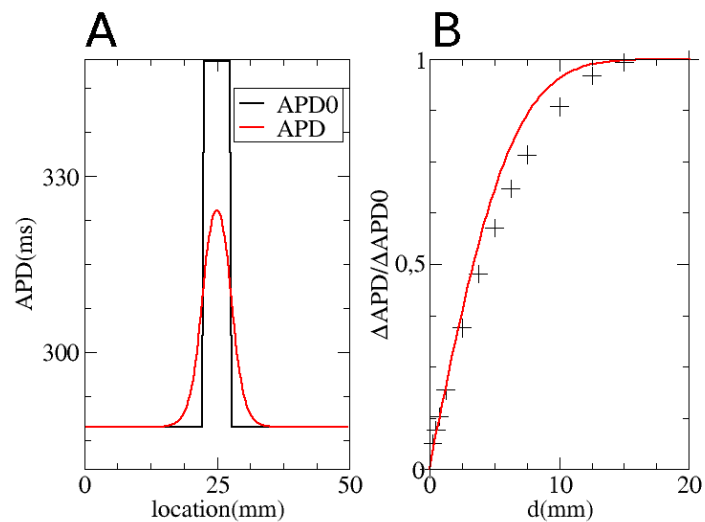


**Figure 2.11: Analytical estimate of electrotonic effect.** A: In black APD0, in red APD. B: In red Eq.(2.9). The '+'s are the values obtained via simulations.

## CHAPTER 2. APD HETEROGENEITY OF CARDIAC TISSUE CAN BE EVALUATED FROM CELL PROPERTIES USING GAUSSIAN GREEN'S FUNCTION APPROACH

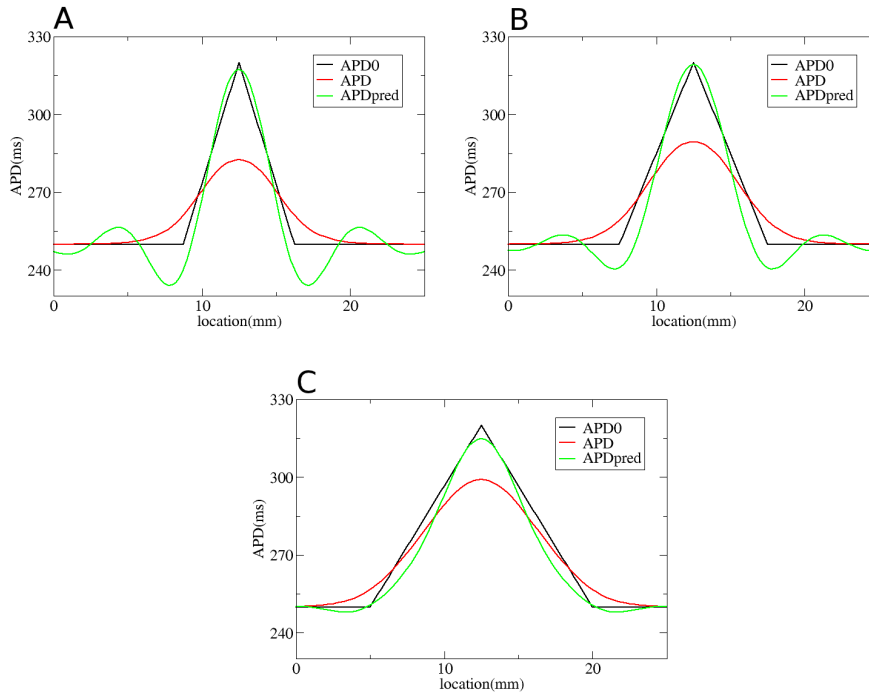


**Figure 2.12: Solution of the inverse problem for heterogeneity created by changing  $G_{Ks}$ .** In A, B and C: in black APD0, in red APD, and in green the predicted APD0 via Tikhonov regularization. Parameters of the model for A, B and C are the same as in Fig. 2.4. Regularization parameter is 0.05.

of this approach to computational studies as well as to experimental research. Regarding the forward problem, we showed that our method works good, and that, even for steep gradients, we can predict the maximal value of APD in the coupled system, which is important for characterization of the extent of heterogeneity. Our solution of the inverse problem is also promising for non steep gradients. However, for steep gradients we have an additional oscillatory component outside the heterogeneity which does not allow us to determinate the maximal amplitude with sufficient degree of certainty. This is a well known feature of the inverse solutions. The solution may certainly be improved by using, for example, different norms of Tikhonov regularization etc. This subject requires additional specific investigation and the development of non-standard software, which is outside the scope of this manuscript.

Application of the approach to computational studies for both forward and inverse problems is straightforward. To accomplish this, one just needs to determine the parameter  $A_3$  for the Green's function, which can easily be done by direct numerical computations similar to those shown in Fig. 2.2.

Applying the approach to experimental studies is more difficult and several important issues still need to be investigated. The most important of them is to determine the space constant of the Green's function. The best approach here would be direct measurement of spatial distribution of repolarization in tissues with known heterogeneity. This heterogeneity might be static or dynamic (e.g. by local injection of currents into cardiac cells). Also,

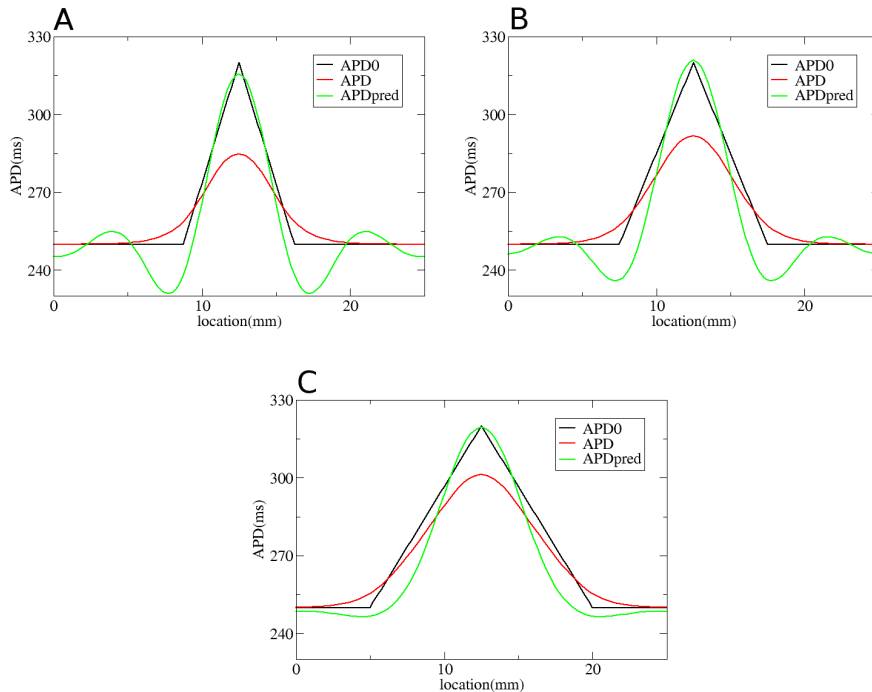


**Figure 2.13: Solution of the inverse problem for heterogeneity created by changing  $G_{Kr}$ .** In A, B and C: in black APD0, in red APD and in green the predicted APD0 via Tikhonov regularization. Parameters of the model for A, B and C are the same as in Fig. 2.5. Regularization parameter is 0.09.

computational [119] and recent experimental data [144] show that the extent of electrotonic effects depends on the shape of the action potential. It would thus be interesting to investigate the possibility to determine the space constant of the Green's function from measured action potential shapes.

As in [119], we studied electrotonic effects by simultaneous stimulation of all cells. In such an approach, effects arising from wave propagation are absent. However, this stimulation protocol is difficult to realize in experiments. To account for this shortcoming we compared several typical APD distributions obtained by this protocol with those resulting from wave propagation. In Fig. 2.17A and B we compare the simultaneous stimulation (black line) and stimulation by wave propagating from the left, respectively right, boundary (red line). Fig. 2.18A and B shows the APD profile for the same heterogeneity as shown in Fig. 2.1A, but obtained by wave propagating from the left, respectively right, boundary. In both cases the changes due to the different stimulation protocol are less than 1% and thus comparable with errors of the method. This causes the results obtained here to be also valid in the case where the APD heterogeneity measured from the propagating waves is used.

In this chapter, we used a monodomain description of cardiac tissue, see Eq.(2.1). Another widely used model for cardiac tissue is a bidomain model [52]. Note, however, that in 1D, the bidomain and monodomain approaches coincide. Therefore, all our 1D results for the forward and inverse problem will be valid for the bidomain case as well. In 2D, effects on non-equal

**CHAPTER 2. APD HETEROGENEITY OF CARDIAC TISSUE CAN BE EVALUATED FROM CELL PROPERTIES USING GAUSSIAN GREEN'S FUNCTION APPROACH**

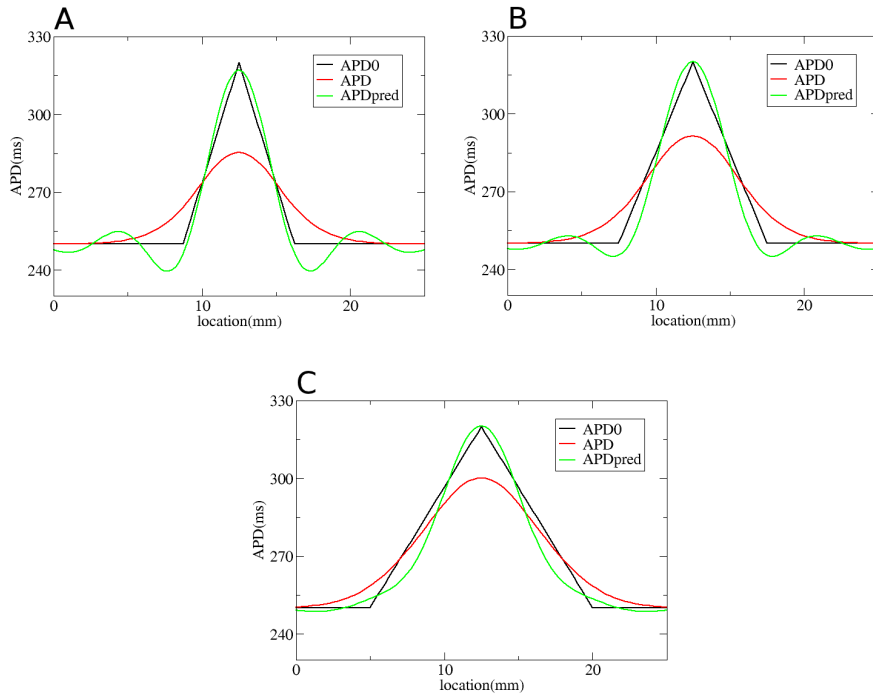


**Figure 2.14: Solution of the inverse problem for heterogeneity created by changing  $G_{CaL}$ .** In A, B and C: in black APD0, in red APD and in green the predicted APD0 via Tikhonov regularization. Parameters of the model for A, B and C are the same as in Fig. 2.6. Regularization parameter is 0.05.

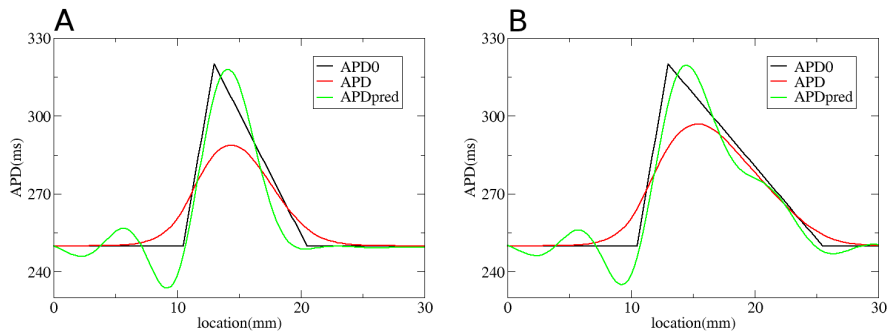


**Figure 2.15: Solution of the inverse problem for an asymmetric heterogeneity created by changing  $G_{Ks}$ .** In A and B: in black APD0, in red APD and in green the predicted APD0 via Tikhonov regularization. Parameters of the model for A, B and C are the same as in Fig. 2.7. Regularization parameter is 0.05.

anisotropy ratio, although essential for defibrillation problems, normally have a small effect on normal wave propagation [108]. Therefore, we expect little effect of using bidomain equations on our approach. However, it would be interesting to study it in the future.



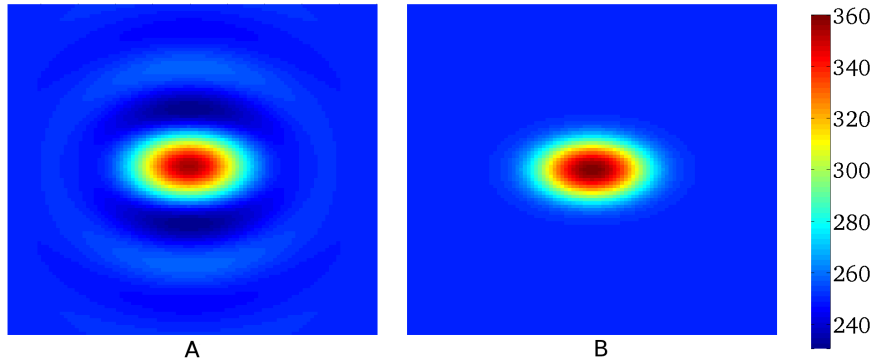


**Figure 2.16: Solution of the inverse problem in 2D.** A: The predicted APD0 values for a measured APD distribution given by Fig. 2.1A. Regularization parameter  $\lambda$  is 0.025. B: The exact solution.

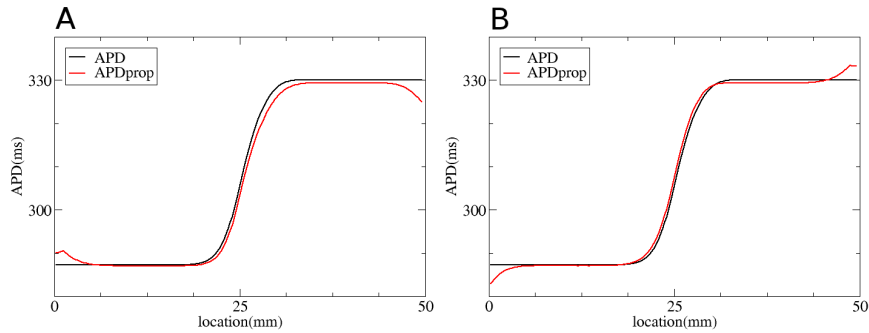


**Figure 2.17: Effect of wave propagation in 1D.** A: In black APD distribution obtained via simultaneous stimulation of all cells. In red the APD distribution obtained by wave propagating from the left boundary. B: Same as A, but now in red the APD distribution obtained by wave propagating from the right boundary.

The fact that the error function almost perfectly fits the APD profiles found, indicates that electrotonic effects are closely related to processes described by the diffusion equation. It would be interesting to investigate this similarity using analytical approaches applied to Eq.(2.1).

## CHAPTER 2. APD HETEROGENEITY OF CARDIAC TISSUE CAN BE EVALUATED FROM CELL PROPERTIES USING GAUSSIAN GREEN'S FUNCTION APPROACH

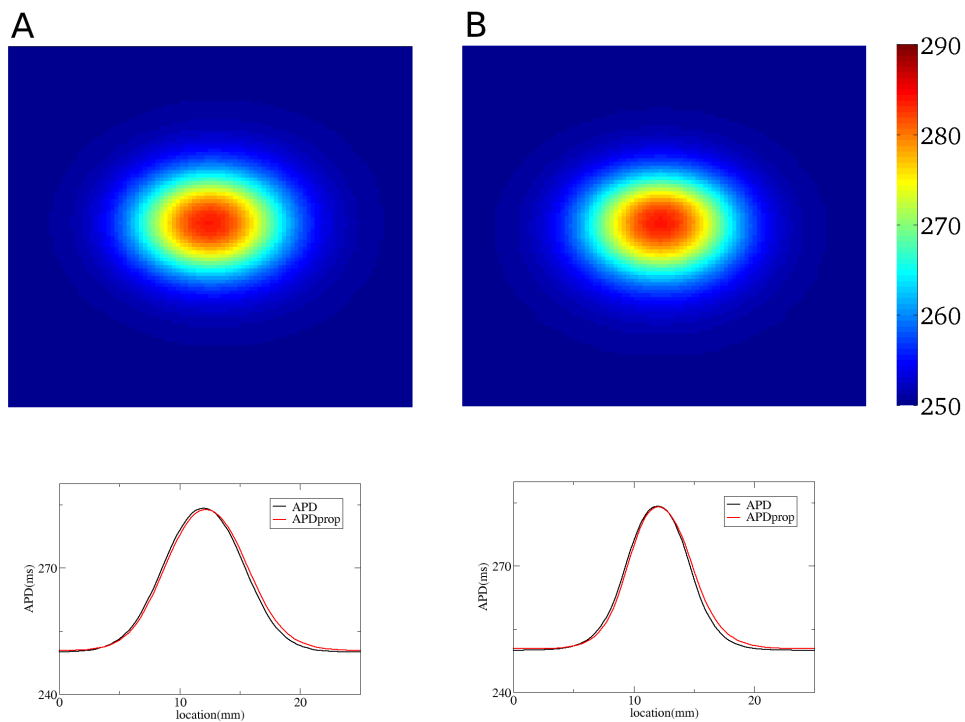


**Figure 2.18: Effect of wave propagation in 2D.** A: Upper panel: APD distribution obtained by wave propagating from the left boundary. Lower panel: APD distribution along the horizontal line through the center. In black for simultaneous stimulation of all cells as in Fig. 2.1A. In red for stimulation from the left boundary. B: Upper panel: APD distribution obtained by wave propagating from the upper boundary. Lower panel: APD distribution along the vertical line through the center. In black for simultaneous stimulation of all cells. In red for stimulation from the upper boundary.

---

# 3

## Initiation and dynamics of a spiral wave around an ionic heterogeneity in a model for human cardiac tissue

### Abstract

---

In relation to cardiac arrhythmias, heterogeneity of cardiac tissue is one of the most important factors underlying the onset of spiral waves and determining their type. In this chapter, we numerically model heterogeneity of realistic size and value and study formation and dynamics of spiral waves around such heterogeneity. We find that the only sustained pattern obtained, is a single spiral wave anchored around the heterogeneity. Dynamics of an anchored spiral wave depend on the extent of heterogeneity, and for certain heterogeneity size, we find abrupt regional increase in the period of excitation occurring as a bifurcation. We study factors determining spatial distribution of excitation periods of anchored spiral waves, and discuss consequences of such dynamics for cardiac arrhythmias and possibilities for experimental tests of our predictions.

### 1 Introduction

---

Contraction of the heart is initiated by the propagation of electrical waves of excitation. Electrical waves propagating through the heart belong to a large class of nonlinear waves which are widely studied theoretically in reaction-diffusion systems. One of the most important phenomena in such systems is the existence of vortices in the form of spiral waves of excitation. Spiral waves were found in a variety of nonlinear excitable media. In physicochemical systems, they have been observed in oscillating reactions [150, 158] and heterogeneous catalysis [59, 3]. Biological examples of such media include spiral waves of cAMP during morphogenesis of *Dictyostelium discoideum amoebae* [38, 129], spiral waves of spreading depression in retina and in cortical tissue [42], calcium waves in *Xenopus oocytes* [76, 27] and spiral waves in cardiac tissue [6, 21, 22]. In the heart, spiral waves underlie life threatening cardiac arrhythmias.

One of the most important scientific questions for applications is to understand the mechanisms of initiation of spiral waves, i.e. of cardiac arrhythmias. Another important question is to find factors underlying their dynamics, as they are directly related to the type of cardiac arrhythmia [44, 45]. It turns out that heterogeneity of cardiac tissue is important in the answer to both questions.

It was shown that heterogeneity substantially affects the dynamics of spiral waves. For example, spiral waves can drift because of heterogeneity [29, 1, 44, 45, 138]. Such drift can

## CHAPTER 3. INITIATION AND DYNAMICS OF A SPIRAL WAVE AROUND AN IONIC HETEROGENEITY IN A MODEL FOR HUMAN CARDIAC TISSUE

---

explain the onset of arrhythmia with periodically varying electrocardiogram (ECG), called torsades de pointes [1, 2], or an arrhythmia with nonperiodic ECG: a polymorphic ventricular tachycardia [44, 45].

Regarding the onset of spiral waves, it was shown that wave propagation at heterogeneities can be temporarily blocked [73, 69], and that such a pattern can evolve into spiral waves. The process of wave blocks and spiral wave formation in the presence of heterogeneity was studied in various modeling studies [102, 110, 111, 4, 67, 66]. These studies showed that in order to be able to generate a 2D spiral wave, the heterogeneity should have a substantial size, comparable to the wavelength of the spiral wave [102].

Most of the listed studies were performed using generic models of cardiac tissue and by using generic types of heterogeneity, as data on real heterogeneities, for example in the human heart, were not available. Recently, measurements of heterogeneity in the human heart were performed [40]. Interestingly, in many cases the size of the heterogeneity was small. The possibility of formation of spirals, and the dynamics of spiral waves around such heterogeneities was not addressed, even at the generic level.

The aim of this chapter is to study effects of heterogeneity of realistic size and value on the onset of spiral waves using the TP06 model [139] for human cardiac cells. We also study dynamics of spirals waves around such heterogeneities. In particular, we model heterogeneity similar to that measured by Glukhov in [40]. We apply high frequency forcing and study if spiral waves can be formed in such situation. We find that formation of spiral waves is possible. However, in all cases the created spiral wave will be anchored around the heterogeneity. Further, we study dynamics of such anchored spiral waves and factors determining its dynamics by varying the size and value of the heterogeneity. We discuss possible mechanisms of such dynamics and its importance for applications.

## 2 Materials and methods

---

*Model* - As in previous chapter, we used the ionic TP06 model for human ventricular tissue [136, 139]. We refer to the materials and methods section of **chapter 2** for more details. Again, we used the default parameter settings from [139] for epicardial cells. All parameter changes made to obtain tissue heterogeneity are detailed in the text.

*Numerical methods* - For 1D and 2D computations, the forward Euler method was applied to integrate Eq. (2.1). A space step of  $\Delta x = 0.2$  mm and a time step of  $\Delta t = 0.02$  ms were used. To integrate the Hodgkin-Huxley-type equations for the gating variables of the various time-dependent currents ( $m$ ,  $h$  and  $j$  for  $I_{Na}$ ;  $r$  and  $s$  for  $I_{to}$ ;  $x_{r1}$  and  $x_{r2}$  for  $I_{Kr}$ ;  $x_s$  for  $I_{Ks}$ ;  $d$ ,  $f$ ,  $f_2$  and  $f_{Cass}$  for  $I_{CaL}$ ), the Rush and Larsen scheme [117] was used.

*Anisotropy* - In most of our simulations, the fibers are directed along the x-axis. In few simulations we study effect of rotational anisotropy, in that case the diffusion matrix is given by

$$\begin{cases} D_{xx} = D_L \cos^2 \theta + D_T \sin^2 \theta , \\ D_{xy} = D_{yx} = 0 , \\ D_{yy} = D_T , \end{cases} \quad (3.1)$$

with  $\theta(y) = \frac{y}{d}(\theta_2 - \theta_1) + \theta_1$ . Here  $d$  is the distance between epicardium and endocardium,  $\theta_1 = -60^\circ$ ,  $\theta_2 = 60^\circ$ ,  $D_L = 0.128 \frac{\text{mm}^2}{\text{ms}}$  and  $D_T = D_L/4$ .

*Heterogeneity* - To study heterogeneity, we change the ionic conductances  $G_{Ks}$ ,  $G_{Kr}$  and  $G_{CaL}$

from their default values 0.392 nS/pF, 0.153 nS/pF and  $3.980 \times 10^{-5} \frac{\text{cm}}{\text{ms}\mu\text{F}}$  for epicardial cells in [139]. Typical profile of heterogeneity is shown in Fig. 3.1. Spiral wave dynamics for homogeneous cardiac tissue is shown in Fig. 3.2A. We see that it has a circular core and shows stationary rotation. Fig. 3.2B shows dynamic APD restitution curve for the homogeneous tissue (red) and inside the heterogeneous tissue configuration used as a baseline model (black). We see that inside the heterogeneity the restitution curve has more shallow slope (maximal slope of 0.9 for the black line compared to 1.1 for the red line).

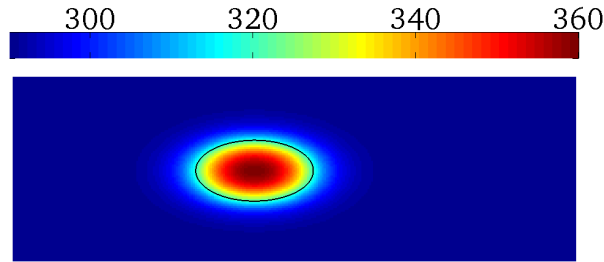


**Figure 3.1: APD distribution in cardiac tissue simulated numerically in TP06 model [136, 139].** Total size of the medium is 60 mm  $\times$  20 mm. Colormap shows APD in ms. Max. APD=359.5 ms, min. APD=290 ms. Size at 50% heterogeneity is 11.2 mm on 5.6 mm. Which is comparable to heterogeneity measured in the human heart [40]. In black, we show the size of the heterogeneity.

*Pacing protocol* - External pacing was performed by applying a current of 15  $\mu\text{A}/\text{mm}^2$  for 1 ms for cells located in a rectangular region of 60 mm  $\times$  1 mm at the bottom of the medium (e.g. see Fig. 3.3A).

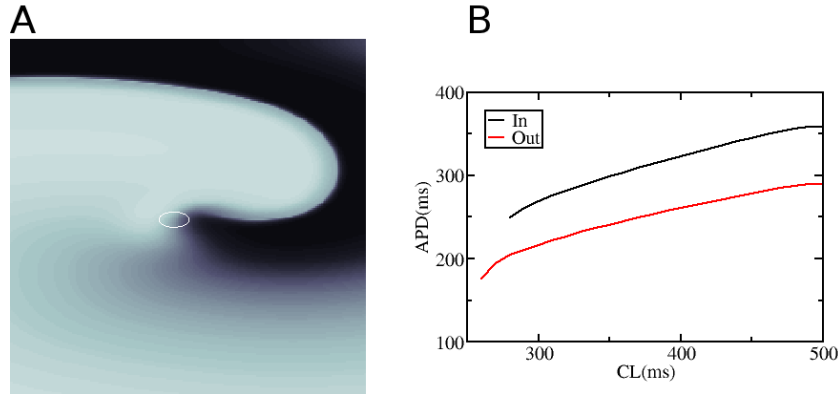
*Electrocardiogram* - To calculate the ECG, we used the formula for the potential from [1]:  $\Phi = \sum \partial V / \partial x_i \partial / \partial x_i (\frac{1}{R})$ , where  $\sum$  denotes the summation over all points of the numerical grid,  $i=1,2$  is the index for the coordinate axes and  $R$  is the distance from a lead to the point of the heart where  $\partial V / \partial x_i$  is evaluated.

### 3 Results

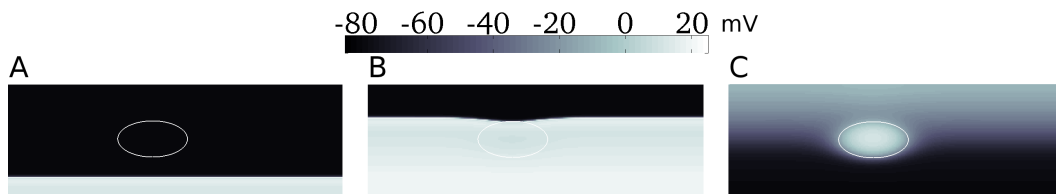
#### 3.1 Baseline model

Fig. 3.1 shows our baseline tissue configuration. It is qualitatively similar to heterogeneity of the human ventricular tissue measured in [40]. In particular, the maximal and minimal values of APD are approximately the same and the size at 50 % heterogeneity in both cases is around 10 mm  $\times$  6 mm. The exact underlying reason of the APD difference in [40] was not studied. However, as for the case of other APD heterogeneities between cardiac cells studied experimentally in [127, 128] it can be achieved by changing  $I_{K_r}$  and  $I_{K_s}$  conductances. In our case we did it by setting  $G_{K_s} = 0.3751$  nS/pF,  $G_{K_r} = 0.1532$  nS/pF outside the heterogeneity and  $G_{K_s} = 0$  nS/pF,  $G_{K_r} = 0.0948$  nS/pF inside the heterogeneity. These values were initially estimated using an approach we developed earlier [25].

In the first series of simulations, we studied behavior of waves around the heterogeneity at high frequency pacing. We paced the medium from below with increasingly smaller pacing periods. We started with a pacing period  $T = 400$  ms. After 10 stimuli, this pacing rate was decreased with 10 ms, and so on. We observed the following changes in the wave patterns



**Figure 3.2: Spiral wave and restitution curve in human cardiac tissue.** A: A spiral wave in homogeneous epicardial tissue. White lines shows the tip trajectory. Total size of the medium is  $40 \text{ mm} \times 40 \text{ mm}$ . B: Dynamic APD restitution curve. In black the restitution curve for a cell located at the centre of the heterogeneity shown in Fig. 3.1. In red (grey) the restitution curve for a cell located outside the heterogeneity.



**Figure 3.3: Wave propagation at pacing rate  $T = 380 \text{ ms}$ .** White line shows size of the heterogeneity. Time interval between A and B is  $40 \text{ ms}$ , between B and C it is  $240 \text{ ms}$ .

(we also refer to supplemental Movie S1, available via the online version of [24]).

For relatively slow pacing rate (period  $T > 290 \text{ ms}$ ), the effect of heterogeneity on wavefront is small (Fig. 3.3A and Fig. 3.3B) and its only influence is longer repolarization time (Fig. 3.3C).

For pacing periods in the interval  $T < 290 \text{ ms}$ , we see the formation of two breaks (Fig. 3.4A) which penetrate into the heterogeneity from above (Fig. 3.4B and Fig. 3.4C) as in classical mechanisms for spiral wave initiation [73, 102]. However, the size of the heterogeneity is too small, and there is not enough room for the onset of spiral waves via this mechanism. If the pacing period becomes faster than  $270 \text{ ms}$ , the wave cannot penetrate the heterogeneity. So we get a classical Wenckebach 1:2-block at the heterogeneity (see Fig. 3.5). Again, no

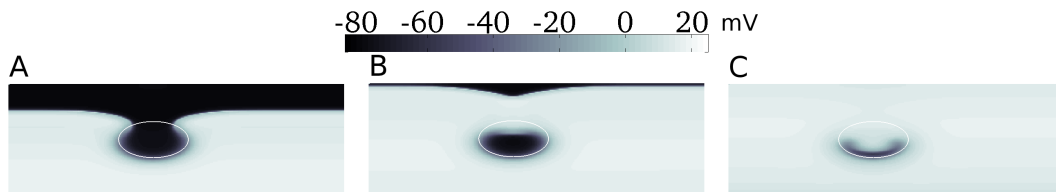


**Figure 3.4: Wave propagation at pacing rate  $T = 280 \text{ ms}$ .** A: Formation of two breaks at pacing rate  $T = 280 \text{ ms}$ . B and C: The breaks enter the heterogeneity from above. Time interval between the frames is  $20 \text{ ms}$ .

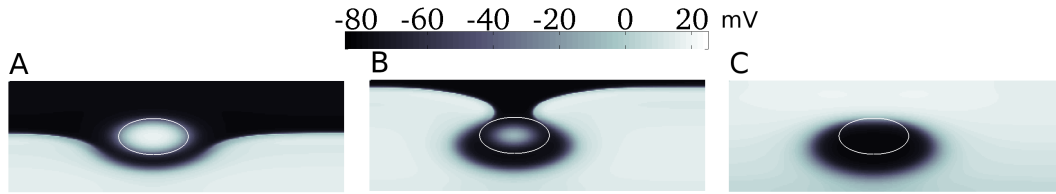


**Figure 3.5:** Wave propagation for pacing rate  $T = 260$  ms: the breaks cannot penetrate the heterogeneity. We get a classical Wenckebach 1:2-block at the heterogeneity. Time interval between the frames is 40 ms.

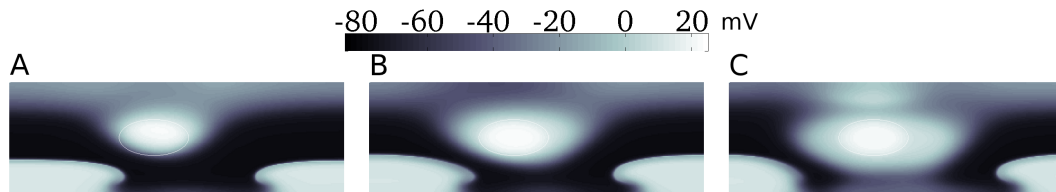


**Figure 3.6:** Wave propagation at pacing rate  $T = 240$  ms (A) and  $T = 230$  (B) and (C). Time interval between A and B is 480 ms; between B and C 460 ms.

spirals are formed. Thus we conclude that due to small size of the heterogeneity, we do not observe spiral wave formation at the heterogeneity via a classical mechanism as in [73].

However, if we further increase the frequency of stimulation, we find that the effect of heterogeneity on waves spreads to the boundary of the medium (Fig. 3.6). In particular, at some stage, stimulation of the medium produces a wave consisting of two disjoint wavebreaks (Fig. 3.6A). Further increase in frequency of stimulation increases the gap between the wavebreaks (Fig. 3.6C). Because the heterogeneity was not centrally located, such increasing gap eventually results in the disappearance of the left break. Interaction of the right break with the heterogeneity eventually leads to a clockwise rotating spiral wave (Fig. 3.7C). After this, the picture becomes self-reproducing: a rotating wave interacts with external forcing and reproduces itself after each next stimulation. If we stop external stimulation at this stage, we get a single spiral wave rotating around and anchored to the heterogeneity. We note that the direction of rotation of the spiral wave is not necessarily the same as for Fig. 3.7C, see also section 3.4. It depends on the interaction of the right break with the heterogeneity, on the moment of time when we stop external forcing and on the recovery pattern of the tissue around the heterogeneity .

We performed several simulations following this protocol and we always found, after we

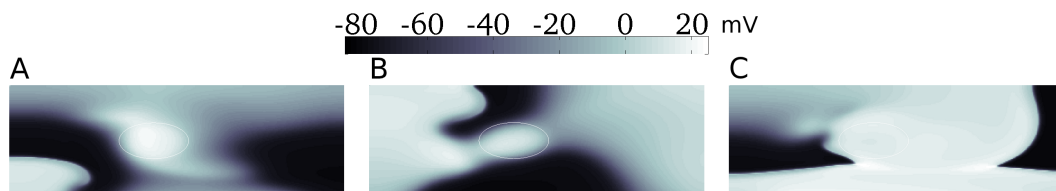


**Figure 3.7:** Wave propagation at pacing rate  $T = 220$  ms. A: Single break formation; B and C: Formation of a single spiral wave rotating around and anchored to the heterogeneity. Time interval between A and B is 320 ms; 120 ms between B and C.

### CHAPTER 3. INITIATION AND DYNAMICS OF A SPIRAL WAVE AROUND AN IONIC HETEROGENEITY IN A MODEL FOR HUMAN CARDIAC TISSUE

---

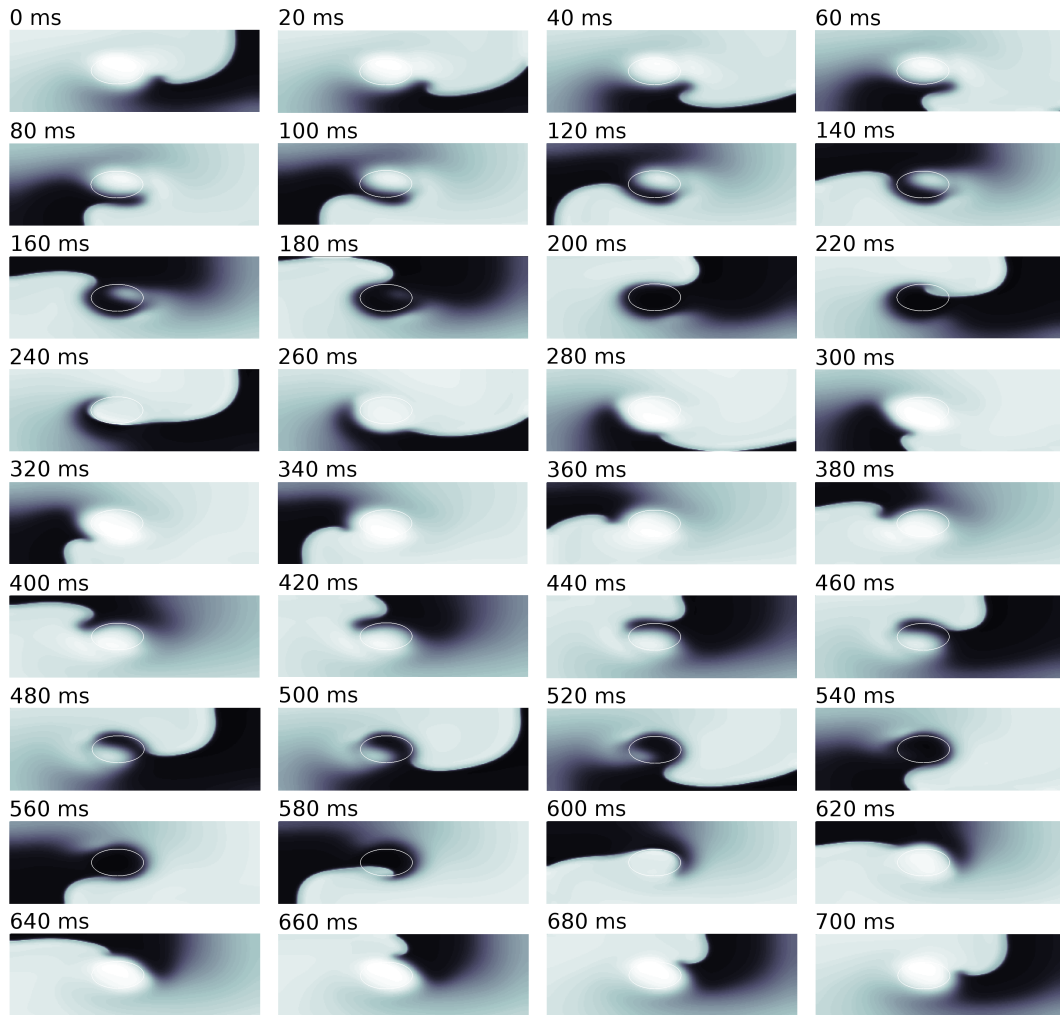
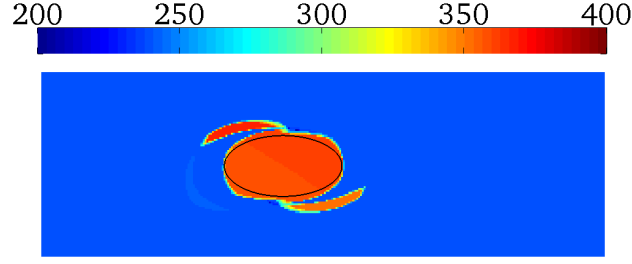


**Figure 3.8: Rotation of spiral wave anchored around heterogeneity of Fig. 3.1.** Figures show wave pattern at 20 ms intervals. White line shows size of the heterogeneity.

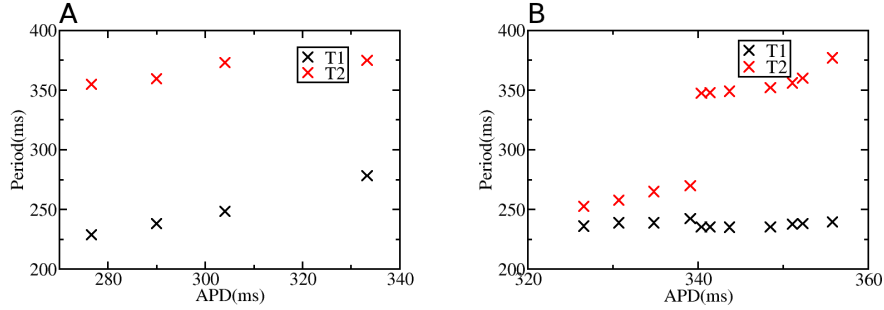
stopped the stimulation, either disappearance of spiral waves or a single spiral wave rotating around the heterogeneity. We conclude that at heterogeneities similar to those measured by Glukhov in [40], a spiral source can be generated and these spiral sources will be anchored to these heterogeneities. Our next step is to study the dynamics of such anchored excitation source.

Fig. 3.8 shows typical dynamics for a spiral wave rotating around the heterogeneity. The first figure (time=0 ms) shows such phase of rotation when the heterogeneity is in the refractory state. The spiral rotates around it as around an inexcitable obstacle (0-200 ms). However, after some time, the refractory state at the heterogeneity ends and it becomes excitable again. Now the spiral can enter this region (around time=220 ms). Subsequently, the wave will exit the heterogeneity and will join with the wavefront of the spiral wave (time=260 ms). After this, the process is repeated.





**Figure 3.9: Period of excitation of the medium for spiral wave dynamics shown in Fig. 3.8.** Figure shows average value of period in each point over 15 excitations. Period inside the heterogeneity ( $T_2$ ) is approximately 360 ms. Period in the other part of the medium ( $T_1$ ) is around 240 ms.



**Figure 3.10: Period of excitation versus APD.** A:  $T_1$  and  $T_2$  versus APD outside the heterogeneity: we alter  $G_{Ks}$  and  $G_{Kr}$  outside the heterogeneity. B:  $T_1$  and  $T_2$  versus the maximal value of APD inside the heterogeneity: we alter  $G_{Ks}$  and  $G_{Kr}$  inside the heterogeneity.

### 3.2 Periods

Let us characterize the process of rotation of a spiral wave in these conditions, i.e. for an anchored spiral wave around a heterogeneity, as in Fig. 3.8. In Fig. 3.9 we show the period of excitation in each point of the medium.

We see two distinct values for the period:  $T_2=360$  ms at/around the heterogeneity and  $T_1=240$  ms in other parts of the tissue. We also see that the longer period region mainly coincides with the heterogeneity. Let us study the factors which determine these two values of the period.

We first change  $G_{Ks}$  and  $G_{Kr}$  outside the heterogeneity, keeping the same values inside it. As in the previous case, we generated a spiral wave rotating and anchored around the heterogeneity and found period of excitation in the medium. Fig. 3.10A shows the values of the period inside ( $T_2$ ) and outside ( $T_1$ ) the heterogeneity vs APD outside the heterogeneity. We observe a gradual increase of  $T_1$  with increase of APD. We also see a slight increase of the period inside the heterogeneity. This is due to effect of the surrounding tissue on the heterogeneity properties: value of APD inside heterogeneity slightly increases when APD outside is increased, because of electronic effects [119].

We also altered  $G_{Ks}$  and  $G_{Kr}$  inside the heterogeneity, keeping the same values outside. The results are shown in Fig. 3.10B and 3.11. We see that the period outside the heterogeneity ( $T_1$ ) is almost unchanged. The period inside the heterogeneity ( $T_2$ ) is severely affected by

CHAPTER 3. INITIATION AND DYNAMICS OF A SPIRAL WAVE AROUND AN IONIC HETEROGENEITY IN A MODEL FOR HUMAN CARDIAC TISSUE

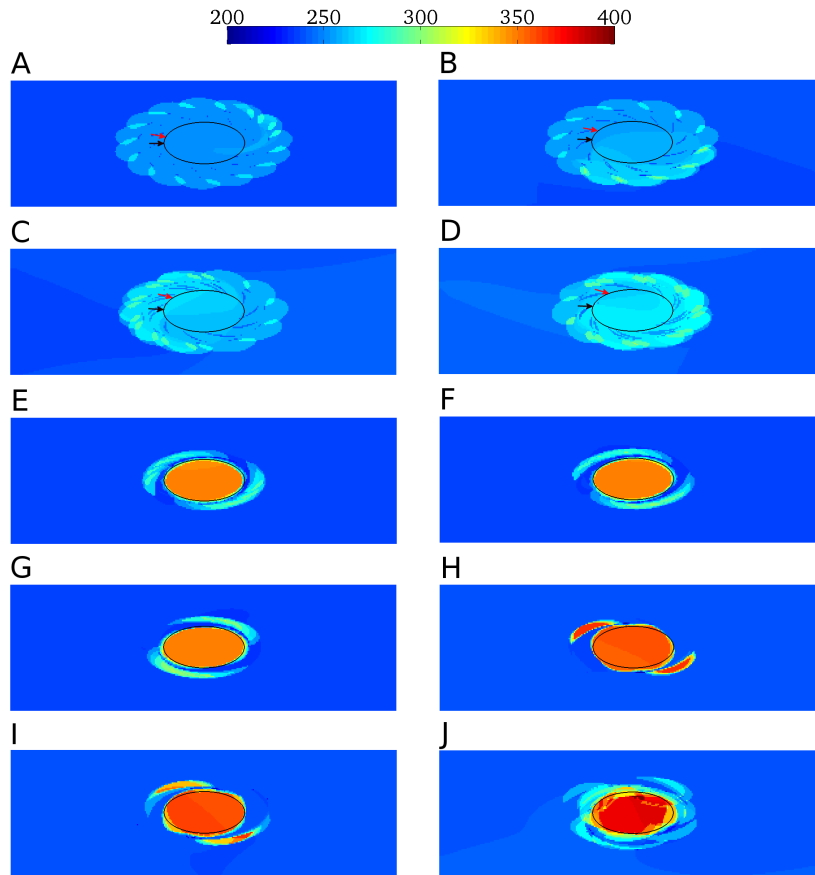


**Figure 3.11: Period of excitation of the medium for spiral wave dynamics anchored around a heterogeneity with different maximal APD values.** The ionic properties of the cells inside the heterogeneity were changed, resulting in different maximal APD values. The size of the heterogeneity is kept constant and the same as in Fig. 3.1. Total size of the medium is  $60 \text{ mm} \times 20 \text{ mm}$ . Outside the heterogeneity we have in all cases:  $G_{Ks} = 0.3751 \text{ nS/pF}$ ,  $G_{Kr} = 0.1532 \text{ nS/pF}$ . Parameter values inside the heterogeneity were in A:  $G_{Ks} = 0.1226 \text{ nS/pF}$ ,  $G_{Kr} = 0.1532 \text{ nS/pF}$ . B:  $G_{Ks} = 0.0981 \text{ nS/pF}$ ,  $G_{Kr} = 0.1532 \text{ nS/pF}$ . C:  $G_{Ks} = 0.0736 \text{ nS/pF}$ ,  $G_{Kr} = 0.1532 \text{ nS/pF}$ . D:  $G_{Ks} = 0.049 \text{ nS/pF}$ ,  $G_{Kr} = 0.1532 \text{ nS/pF}$ . E:  $G_{Ks} = 0.0421 \text{ nS/pF}$ ,  $G_{Kr} = 0.1532 \text{ nS/pF}$ . F:  $G_{Ks} = 0.0368 \text{ nS/pF}$ ,  $G_{Kr} = 0.1532 \text{ nS/pF}$ . G:  $G_{Ks} = 0.0245 \text{ nS/pF}$ ,  $G_{Kr} = 0.1532 \text{ nS/pF}$ . H:  $G_{Ks} = 0 \text{ nS/pF}$ ,  $G_{Kr} = 0.1149 \text{ nS/pF}$ . I:  $G_{Ks} = 0 \text{ nS/pF}$ ,  $G_{Kr} = 0.0948 \text{ nS/pF}$ . J:  $G_{Ks} = 0 \text{ nS/pF}$ ,  $G_{Kr} = 0.0479 \text{ nS/pF}$ .

this change. For a small  $\Delta\text{APD}$  (Fig. 3.11A-D), we do not observe two clear distinct values of the period. Spatially in this case, we have a large region around the heterogeneity with slightly increased period. For large heterogeneity,  $\text{APD}_{\text{max}} > 340$  (Fig. 3.11E-J), we have a typical two-period distribution similar to that of Fig. 3.9. We also observe a clear bifurcation: an abrupt change in  $T_2$  around  $\text{APD}_{\text{max}} \approx 340$  (Fig. 3.10B).

### 3.3 Period increase bifurcation

Bifurcation in the period of excitation obviously results in a change of the wave propagation pattern. If we consider two successive points where the spiral wave tip enters the heterogeneity, we observe the following dynamics before and after the period jump. For smaller heterogeneity (Fig. 3.11A), the wave tip makes a rotation of about 380 degrees before entering the heterogeneity again. To show it in Fig. 3.11A-D, we marked by black and red arrows the entry points of the wave into the heterogeneity for two successive rotations (first black, then red). For larger heterogeneity the rotation is about 390 degrees (Fig. 3.11B). Thus rotation angle increases when we increase heterogeneity. However, at the bifurcation point, it approaches 400 degrees and then it jumps to about 540 degrees, which results in an abrupt period increase.

We also found that this bifurcation only occurs in a limited range of size of the heterogeneity. Fig. 3.12 shows results similar as to Fig. 3.10B, but now with different sizes of the heterogeneity: we increased the size respectively 1.2, 1.5, 1.7 and 2 times. We see that in Fig. 3.12A, B and C, we have qualitatively the same bifurcation as in Fig. 3.10B. However, the location of the bifurcation on the APD axis slightly increases with the size of the heterogeneity. The amplitude of the jump first also slightly increases (Fig. 3.10B, Fig. 3.12A, B), then decreases (Fig. 3.12C) and finally the bifurcation disappears (Fig. 3.12D).

Note that this bifurcation in period has a substantial effect on overall dynamics of the system. Fig. 3.13 shows how it is manifested on the ECG. We see that even tiny changes in the extent of the heterogeneity results in ECGs of very different type: ECG with gradual amplitude variation as in Fig. 3.13A, which is reminiscent of torsades de points (before the bifurcation point) and ECG with large beat-to-beat variations in amplitude (after the bifurcation), see Fig. 3.13C. We also see substantial shift in the secondary peaks in the Fourier transforms of ECG before and after the bifurcation, which indicates the recorded change in  $T_2$ .

### 3.4 Modifications of baseline model

So far, we have studied the process of spiral wave onset and period increase bifurcation for one particular shape of heterogeneity, anisotropy and parameter set. Here we extend our study to additional configurations.

In Fig. 3.1, heterogeneity in APD was created by changing  $G_{K_s}$  and  $G_{K_r}$  conductances. A similar heterogeneity can be created by changing other parameter values. For instance, another current which has a substantial effect on APD is  $I_{CaL}$ . We have checked if our results also hold for heterogeneity created by changing  $G_{CaL}$  instead of  $G_{K_r}$ . In particular, we studied a heterogeneity of the same elliptical shape as in our baseline model and used inside the value  $G_{CaL} = 6.766 \times 10^{-5} \frac{\text{cm}}{\text{ms}\mu\text{F}}$  (an increase by a factor 1.7) and  $G_{K_s} = 0$  nS/pF. Outside the heterogeneity, we used the same parameter values as in our baseline model. This results in a difference between maximal and minimal APD of 62 ms, which is comparable to the

## CHAPTER 3. INITIATION AND DYNAMICS OF A SPIRAL WAVE AROUND AN IONIC HETEROGENEITY IN A MODEL FOR HUMAN CARDIAC TISSUE

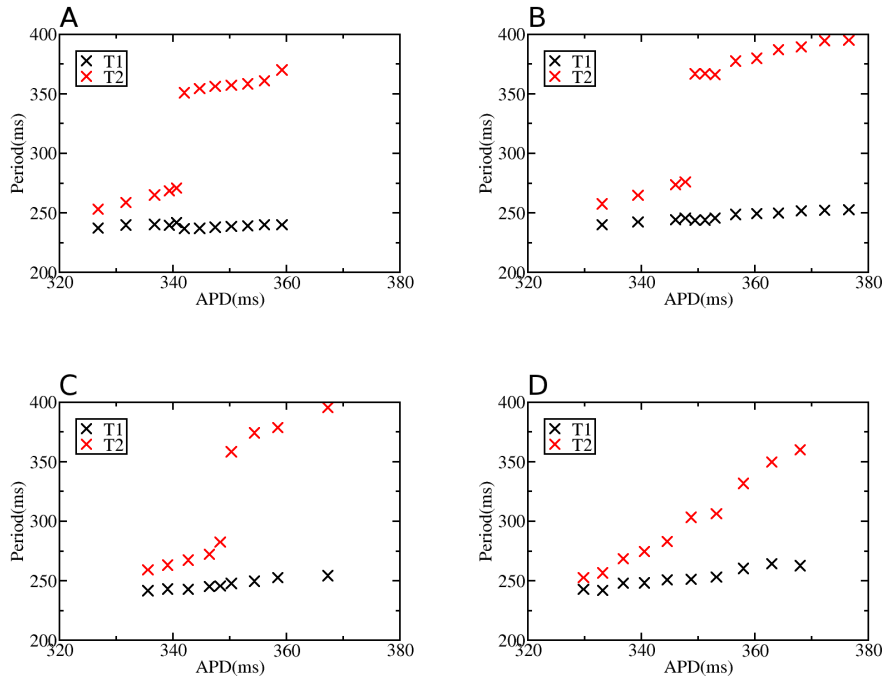


**Figure 3.12:**  $T_1$  and  $T_2$  versus the maximal value of APD inside the heterogeneity for different sizes of the heterogeneity. In A: the axes of the heterogeneity are 1.2 times larger than in the basic model. B, C, and D: axes are 1.5, 1.7 and 2 times larger.

heterogeneity shown in Fig. 3.1.

We performed the same simulations as we did for our baseline model. First, we studied behavior of waves around the heterogeneity at high frequency pacing. The results are shown in the supplemental Movie S2 (see online version of [24]) and in Fig. 3.14 (upper panel). In Fig. 3.14A, we see the formation of wavebreaks which cannot penetrate the heterogeneity, as in Fig. 3.5. Again, if we further increase pacing rate, we observe that the size of the heterogeneity increases: the effect of heterogeneity spreads to the boundary of the medium (see Fig. 3.14B). Similar to Fig. 3.7 it results in complex patterns of excitation, and eventually in the formation of a single clockwise rotating spiral wave anchored to the heterogeneity (see Fig. 3.14C and D).

Next, we did the same analysis of the period of excitation for the spiral wave anchored to the heterogeneity, as for the baseline model. We found similar results: two distinct values of period for different parts of the tissue ( $T_2 \approx 370$  ms inside the heterogeneity,  $T_1 \approx 240$  ms outside the heterogeneity). We also studied if we have a similar bifurcation as for the baseline model. For that, we varied  $G_{Ks}$  inside the heterogeneity, and measured the period of excitation. The results are shown in Fig. 3.15A. We observe a clear bifurcation, similar to that of Fig. 3.10B.

In the second series of simulations, we changed the shape of the heterogeneity from an ellipse to a circle which has approximately the same area. We used the same parameter values inside and outside the heterogeneity as for the baseline model, resulting in the same difference between maximal and minimal APD as in Fig. 3.1. We also studied behavior under high frequency pacing: see supplemental Movie S3 and Fig. 3.14 (middle panel). Again, we

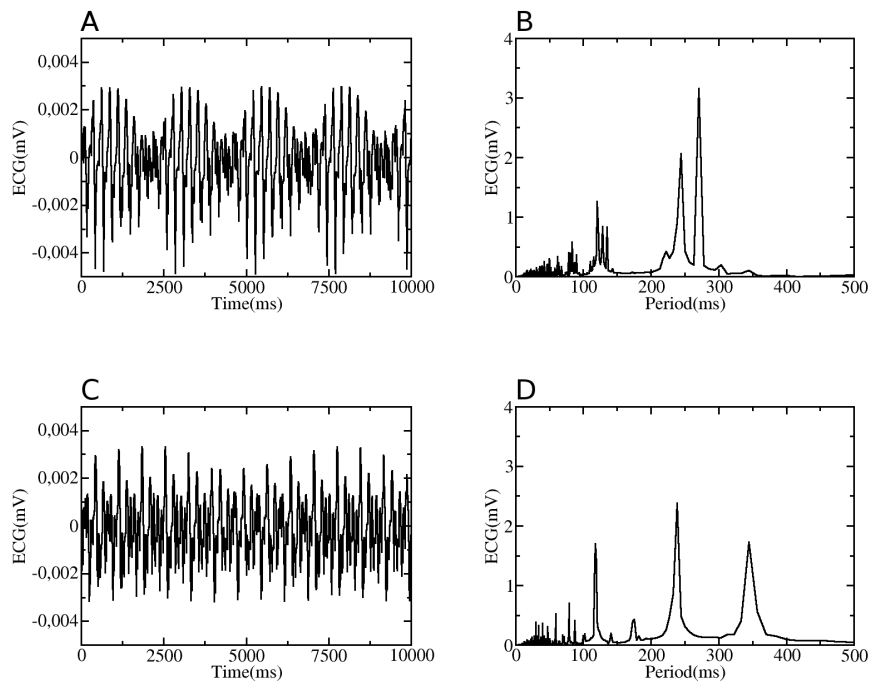


**Figure 3.13: ECG and corresponding Fourier-transform.** A: ECG for the heterogeneity as in Fig. 3.11D. B: Fourier-transform of this ECG profile. We see two dominant periods corresponding to  $T_1$  and  $T_2$ . C and D: ECG and Fourier-transform for heterogeneity as in Fig. 3.11E. Again, we find the two dominant periods  $T_1$  and  $T_2$ . ECG calculations are based on the infinite medium potential approximation as described in the materials and methods section.

### CHAPTER 3. INITIATION AND DYNAMICS OF A SPIRAL WAVE AROUND AN IONIC HETEROGENEITY IN A MODEL FOR HUMAN CARDIAC TISSUE

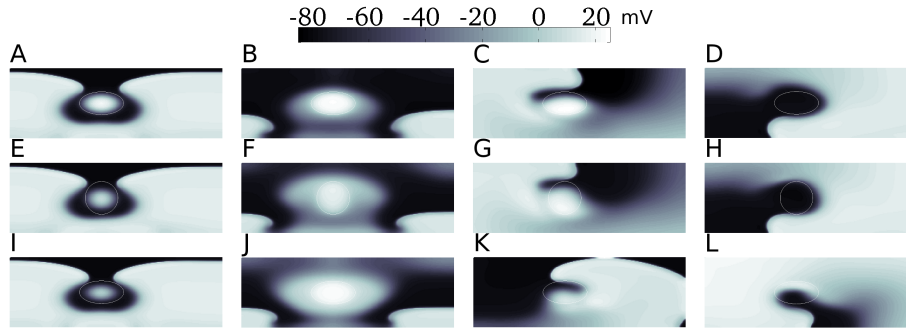


**Figure 3.14: Spiral wave initiation under high frequency pacing.** Upper panel: heterogeneity is created by changing  $G_{CaL} = 6.766 \times 10^{-5} \frac{\text{cm}}{\text{ms}\mu\text{F}}$  and  $G_{Ks} = 0 \text{ nS/pF}$ . A: Formation of wavebreaks ( $T = 260 \text{ ms}$ ). B: Wavebreak dynamics under higher pacing rate ( $T = 250 \text{ ms}$ ). C and D: formation of a single spiral wave rotating around and anchored to the heterogeneity. Middle panel: simulations for a circular heterogeneity with radius 4.5 mm. Parameter values inside and outside the heterogeneity are the same as for the baseline model. E:  $T = 260 \text{ ms}$ , F:  $T = 240 \text{ ms}$ . G and H: spiral wave anchored to the heterogeneity. Lower panel: similar simulations for model with rotational anisotropy (details are in the text). Parameter values inside and outside the heterogeneity are the same as for the baseline model. I:  $T = 260 \text{ ms}$ , J:  $T = 240 \text{ ms}$ . K and L: spiral wave anchored to the heterogeneity.

get the formation of a single clockwise rotating anchored spiral, created as a result of similar processes (compare Fig. 3.14A-D with Fig. 3.14E-H).

We found similar results for period of excitation: two clear distinct values ( $T_2 \approx 360 \text{ ms}$  and  $T_1 \approx 240 \text{ ms}$ ) for other parts of the tissue. We also varied  $G_{Ks}$  and  $G_{Kr}$  inside the heterogeneity (Fig. 3.15B). Again, we observe two regimes indicating the bifurcation.

Finally we studied the possible effect of rotational anisotropy on our results. This because the measurements of heterogeneity in [40] were performed in a transmural wedge of the left ventricular free wall. It is known that the direction of the fibers is not constant along a transmural wedge: the fibers rotate counterclockwise from endocardium to epicardium. At the endocardium the angle between the fibers and the  $x - y$  plane is around  $-60^\circ$ ; at the epicardium it is around  $60^\circ$  [132]. Therefore, we studied if such fiber rotation might have an effect on our results. We refer to the method section for the diffusivity matrix under rotational anisotropy. The distance  $d$  between epicardium and endocardium was in our case 20 mm. Again, we performed the same simulations as in previous situations. We used the same elliptical shape of the heterogeneity as in our baseline model, and the same parameter values inside and outside the heterogeneity, as in Fig. 3.1. This results in a difference between maximal and minimal APD of 62 ms. We refer to the supplemental Movie S4 and lower panel of Fig. 3.14 for the results under high frequency pacing. We observe similar behavior as in our other situations. However, the direction of the resulting spiral wave is now opposite to previous simulations.

For the period of excitation we also find two clear distinct values ( $T_2 \approx 360 \text{ ms}$  and  $T_1 \approx 240 \text{ ms}$ ) for different parts of the tissue. By changing  $G_{Ks}$  and  $G_{Kr}$  inside the heterogeneity, we find a similar bifurcation pattern as in Fig. 3.10B (see Fig. 3.15C).

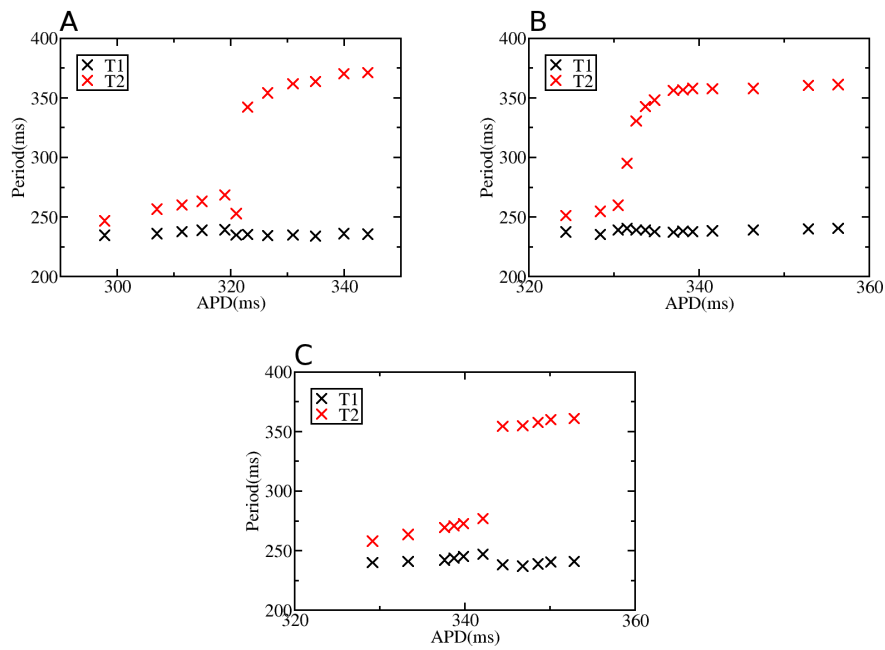


**Figure 3.15:**  $T_1$  and  $T_2$  versus the maximal value of APD inside the heterogeneity. A: Simulations in which APD inside the heterogeneity was changed by changing  $G_{Ks}$  at  $G_{CaL} = 6.766 \times 10^{-5} \frac{\text{cm}}{\text{ms}\mu\text{F}}$ ; B and C: Same simulations as for the baseline model in Fig. 3.10B, but now with a circular shape of the heterogeneity, respectively rotational anisotropy.

### 4 Discussion

---

In this chapter, we study possible effects of small sized heterogeneities, similar to those found in human cardiac tissue, on initiation of spiral waves and their dynamics. We found that new spiral waves can be formed even on a small heterogeneity with a size around 1 cm. However, initiation of these new sources involves not only break formation as in classical mechanisms [73, 102], but also interaction of wavebreaks with other upcoming waves, which eventually results in the formation of a single spiral wave anchored around the heterogeneity.

Previous studies, of the TP06 model [139], show that slopes of the restitution curves, corresponding to parameter values used here, do not result in the onset of dynamical instabilities leading to breakup. We have also performed a simulation in a medium without heterogeneity and did not observe any dynamical instabilities there.

In our simulations spirals are initiated by the complex interaction between the wavebreaks and the heterogeneity. In particular, the heterogeneity in our simulations was not located in the centre of the tissue. This breaks the symmetry of our model. Because of a successive increase in distance between the generated wavebreaks, one of the wavebreaks eventually disappears at the boundary, leading to the formation of a spiral wave. Thus, formation of a single spiral wave here does depend on initial asymmetry, which however is likely to be present in any realistic setup.

We studied the dynamics of these anchored spiral waves. We found that in such systems we have two distinct values of the period of excitation: one inside and one outside the heterogeneity. We show that each of these periods is mainly determined by properties of cardiac tissue at the corresponding region: an increase of the refractory period results in an increase of the period. The ratio of these periods is not given by an integer number. At first glance, this contradicts the classic view of excitation of heterogeneity by Wenckebach [147], who showed that at fast pacing rate, block of excitation at the heterogeneity results in an integer ratio in period of excitation inside and outside of the heterogeneity. Note, however, that in our case the wave enters the heterogeneity at different places, which results in the existence of non-integer ratio's of periods of excitation. A similar effect in 3D was found in [100], where it was shown that in a 3D heterogeneous medium, the ratio is not given by an integer number.

We found that the increase in period inside the heterogeneity, when we increase the extent of heterogeneity, is not gradual: we find a bifurcation point. At this bifurcation point, the period suddenly increases around 1.3 times.

The mechanism of this bifurcation is still under investigation. It is not trivial and involves interplay of several factors, such as heterogeneity size, heterogeneity value and relation of the refractory periods and the rotation time of the wave around the heterogeneity. In a very simplified way, the jump in period can be explained in the following way. The heterogeneity can be excited when the refractory period inside the heterogeneity ends. However, the refractory period depends on the history of wave propagation through the heterogeneity, as is schematically shown in Fig. 3.16A.

If the wave enters the heterogeneity at point X, its front will have successive positions marked as line 1, 2 and 3. Wave propagation will thus have an effect on the spatial distribution of the recovery time. Indeed, the refractory period will first end at point X, and then at lines 1, 2 and 3. This is because points at line 1 were excited later than at point X and thus will recover at a later time. Let us now consider rotation of a wave around such heterogeneity and assume that the tip of the spiral wave first enters the heterogeneity at point X. It will follow the boundary of the heterogeneity as shown by a red arrow in Fig. 3.16B and the wave will



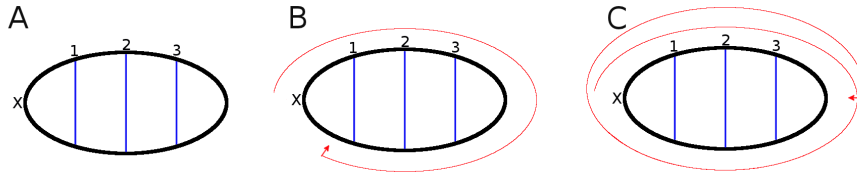


**Figure 3.16: Schematic explanation of mechanism behind the bifurcation.** A: Wave propagation through the heterogeneity after it enters it at point X. B: Rotation of a wave tip around the heterogeneity. The wave follows the boundary of the heterogeneity along the red arrow. The wave enters the heterogeneity again in the region around point X. C: Same as B, but now in the case of longer refractory period inside the heterogeneity. The wave enters the heterogeneity after making an extra half rotation in comparison to B, because of increased heterogeneity.

be able to enter again when the tissue at the tip location is recovered. For a heterogeneity with a longer refractory period this will take a longer time. The tip will thus make a rotation over an increasingly larger angle, as we saw in Fig. 3.11, which results in a gradual increase of the period  $T_2$ . However, if the value of the refractory period at the heterogeneity grows, the wave, even after coming back to the region around point X, will not be able to enter the heterogeneity, as the tissue is still not recovered there. In that case, the tip has to travel further to line 1. However, at line 1 the tissue will recover later than at point X and the wave will not be able to enter the heterogeneity there as well. The reason for this is, as discussed above, that the wave tip propagates along the same trajectory as the wave which made the heterogeneity refractory at the previous excitation. This effect will disappear after making an additional half rotation (see Fig. 3.16C).

Such simple schematic consideration can explain the onset of bifurcation in Fig. 3.10B, and even predict that after the bifurcation the tip of the spiral has to make 1.5 rotation around the heterogeneity before entering it. However, this consideration is, in many aspects, oversimplified: it does not take into account about many other important effects, for example the possible difference in velocity of the wave inside the heterogeneity and the wave tip outside the heterogeneity. It also does not consider the effects of wavefront curvature etc. As a result, in reality the wave can make a rotation slightly more than 360 degrees (the bifurcation occurs at a rotation angle of around 400 degrees). Also, the jump is slightly less than 1.5 rotation (in reality it is 1.44). Finally, such simple consideration cannot explain the disappearance of the bifurcation for larger sizes of the heterogeneity as shown in Fig. 3.12D. For a heterogeneity of larger size, the pattern of rotation of the wave around the heterogeneity changes: instead of rotating around it, the wave tip periodically propagates through the heterogeneous region and is not anchored to it anymore, as we saw in Fig. 3.8.

We checked that our results on the dynamics of a spiral wave around a heterogeneity are general, and also hold for heterogeneities of different size, shape and induced by modification of different parameters of our model. Our results are also valid for tissue with rotational anisotropy.

Experimental studies which are somewhat similar to situations studied in this chapter were performed in [13]. In that paper, the authors studied wave dynamics in the presence of a heterogeneity of  $0.8 \text{ cm} \times 0.8 \text{ cm}$  in a rabbit heart. After giving several premature stimuli, they observed that wavebreaks were formed at the place where the heterogeneity was located. After further pacing, they observed the formation of two counterrotating waves of which

### CHAPTER 3. INITIATION AND DYNAMICS OF A SPIRAL WAVE AROUND AN IONIC HETEROGENEITY IN A MODEL FOR HUMAN CARDIAC TISSUE

---

only one survives resulting in a single spiral wave rotating around the heterogeneity, as in our study. Unfortunately, the authors did not measure spatial distribution of period of excitation. However, dynamics look close to what we observed, as the authors saw breakthrough in the heterogeneity, as well as the rotation of a spiral wave around it.

Compared to other modeling studies [1, 102, 2], the main effects of heterogeneity on spiral wave dynamics in our study, is its anchoring effect and not drift along the heterogeneity boundary. We also get a torsades de pointes like ECG and an ECG reminiscent of polymorphic tachycardia. However, in our case it is a result of a different frequency of excitation of tissue inside and outside the heterogeneity and not a result of shift of the excitation source in space.

Note that anchoring of spiral waves in 2D and scroll waves in 3D was the subject of intensive study [22, 142, 152, 81, 156, 131]. However, in all these cases the spiral waves were anchored around inexcitable regions in 2D or 3D. Here we show that a heterogeneity which is excitable can also anchor spirals. Compared to anchoring around an inexcitable obstacle, anchoring here results in more complex dynamics because of a direct influence of the heterogeneity on wave rotation.

Dynamics of waves in the presence of large non-conducting and ionic heterogeneities was studied in [124]. It was shown that dynamics of waves, including anchoring, is dependent on the location of the heterogeneity in the tissue.

Finding the bifurcation described in this chapter in an experimental study might not be easy, as it requires a gradual change of the extent of heterogeneity, which is difficult to obtain in experiments at the whole organ level. However, it might be possible to use cell cultures of neonatal rat ventricular myocytes, such as in [12, 14], where heterogeneities of various form and size can be created. Further gradual changing of the extent of the heterogeneity can be achieved by application of drugs changing the refractory period of cardiac tissue.

---

# 4

## Small size ionic heterogeneities in the human heart can attract spiral waves

### Abstract

---

Spiral waves occurring in the heart underlie the mechanisms of cardiac arrhythmias. Answering the question whether or not the location of spirals is related to local properties of cardiac tissue has important practical applications. This is because ablation of spirals has been shown to be an effective way to fight cardiac arrhythmias. In this study, we investigate, *in silico*, the dynamics of spiral waves in 2D and in an anatomical model of human ventricles using a TNNP model for ventricular cells. We study the effect of small size ionic heterogeneities, similar to those measured experimentally. It is shown that such heterogeneities can not only anchor, but can also attract spiral waves rotating at a substantial distance from the heterogeneity. This attraction distance depends on the extent of the heterogeneities and can be as large as 5-6 cm in realistic conditions. We conclude that small size ionic heterogeneities can be preferred localization points for spirals, and discuss their possible mechanism and value for applications.

### 1 Introduction

---

Sudden cardiac death is the largest cause of mortality in the industrialized world, accounting for more than 400000 deaths per year in the United States alone [41]. In most of the cases it occurs as a result of cardiac arrhythmias. Therefore, it is important to study the mechanism of initiation of cardiac arrhythmias, factors affecting arrhythmia initiation and dynamics, and to find new ways to manage them. These phenomena are studied using a wide variety of methods, including experimental and clinical research as well as computer modeling.

One of the most important mechanisms of arrhythmias are reentrant sources of excitation, which may form spiral waves. Spiral waves were first predicted in modeling studies [121], and then discovered experimentally [6, 22]. Recently, they have attracted a lot of attention, as clinical studies by the group of Narayan showed that identification and ablation of these spirals can result in termination or slowing of atrial fibrillation (AF) [88, 89]. Similar research is being done in the ventricles [51]. Thus, factors which determine the formation of spiral waves and the possible position of spirals in the heart are of great practical interest. Therefore, it is of paramount importance to know whether the final position of the spiral wave is affected by specific local properties (substrate) of cardiac tissue.

From a general point of view, prevalence of a spiral at a specific position can be the result of the formation of a spiral at a given place, or it can be due to some process which brings

## CHAPTER 4. SMALL SIZE IONIC HETEROGENEITIES IN THE HUMAN HEART CAN ATTRACT SPIRAL WAVES

---

the spiral wave from one location to another, and stabilizes it there. It is well known that a spiral can be locally stabilized due to anchoring to an inexcitable obstacle [104, 22, 103, 133], i.e. process when a spiral wave attaches to the boundary of such an obstacle. Later, it was shown that spirals can anchor to other types of heterogeneities: ionic heterogeneities [123, 122], blood vessels [140], pectinate [152] and papillary muscles [68]. And in [13, 155] it was shown that spirals can be anchored to regions of prolonged APD (created through regional cooling) in the rabbit heart. Due to subsequent collision with the boundaries a spiral wave could also be eliminated [155].

In this chapter, we investigate *in silico* the possibility for anchoring of a spiral wave at ionic heterogeneities of realistic size and shape, similar to those measured in the ventricles of the human heart [40]. We show that such small size ionic heterogeneities with prolonged APD can anchor a spiral wave locally. Moreover, we find that these heterogeneities can also attract spirals from a substantial distance (up to 5-6 cm), while inexcitable obstacles do not show this property. We confirm this result both in simple geometries and in an anatomical model of the human ventricles. In addition, we discuss the mechanism of this attraction and its potential usage for removing spiral waves from the heart.

## 2 Materials and methods

---

*Model* - As in the previous chapters, we used the ionic TP06 model for human cardiac tissue [136, 139]. We refer to the materials and methods section of **chapter 2** for more details. Again, we used the default parameter settings from [139] for epicardial cells. All parameter changes made to obtain tissue heterogeneity are enlisted in the text.

*Numerical methods* - The diffusion tensor is given by

$$D_{ij} = (D_L - D_T)\tau_i\tau_j + D_T\delta_{ij} , \quad (4.1)$$

with  $\delta_{ij}$  the Kronecker delta and  $\tau_i$  a normalized vector oriented along the fibers.

For 2D computations, the fibers are directed along the x-axis ( $\bar{\tau} = (1, 0)$ ),  $D_L = 0.128 \text{ mm}^2/\text{ms}$ , and  $D_T = D_L/4$ .

For 3D whole heart simulations, we used an anatomical model of the human ventricles. For a more detailed description, we refer to [135]. This model takes anisotropy into account by reconstructing the fiber direction field described in [54]. We assume that the diffusion coefficient across the fibers  $D_T$  is 4 times less than the diffusion coefficient along the fibers  $D_L$ , which is set to  $0.154 \text{ mm}^2/\text{ms}$ .

To solve the differential equations we used a finite difference approach. For 2D simulations, we used a rectangular mesh of about half a million points, and for 3D simulations one million points. To approximate the diffusion term, we used a stencil of 5 grid points for 2D and 17 points for 3D. We used an explicit first order Euler method to solve the discretized system, which for 2D tissue is:

$$\frac{\tilde{V}_{ij} - V_{ij}}{\Delta t} = \frac{1}{\Delta x^2} \sum_{i'j'} w_{i'j'}^{ij} V_{i+i',j+j'} - I_{\text{ion}}(V_{ij}, \dots) , \quad (4.2)$$

where the time step is  $\Delta t = 0.02 \text{ ms}$ ,  $\Delta x$  is the space step, and  $w_{i'j'}^{ij}$  are the weights corresponding to the diffusion tensor at location  $i, j$ . The space step is  $0.2 \text{ mm}$  for 2D simulations, and  $0.5 \text{ mm}$  for 3D simulations. To integrate the Hodgkin-Huxley-type equations for the gating

variables of the various time-dependent currents ( $m$ ,  $h$  and  $j$  for  $I_{Na}$ ;  $r$  and  $s$  for  $I_{to}$ ;  $x_{r1}$  and  $x_{r2}$  for  $I_{Kr}$ ;  $x_s$  for  $I_{Ks}$ ;  $d$ ,  $f$ ,  $f_2$  and  $f_{Cass}$  for  $I_{CaL}$ ), the Rush and Larsen scheme [117] was used. *Heterogeneity* - To study heterogeneity, we changed the parameters  $G_{Ks}$  and  $G_{Kr}$  from their default values 0.3923 nS/pF and 0.153 nS/pF for epicardial cells in [139]. For example, to raise the action potential duration (APD) by 10 ms in single cell, it is necessary to decrease  $G_{Ks}$  by 0.073 nS/pF and  $G_{Kr}$  by 0.048 nS/pF. The APD is measured at 80% repolarization level.

For our 2D simulations, we used four tissue configurations as shown in Fig. 4.1. Fig. 4.1A is the same heterogeneity as modeled in the baseline model of [24]. It is qualitatively similar to heterogeneity of the human ventricular tissue measured in [40]. In particular, the maximal and minimal values of APD are approximately the same and the size at 50 % heterogeneity (for  $APD = (\text{minimal APD} + \text{maximal APD})/2$ ) in both cases is around 1 cm by 0.6 cm. This APD distribution is the distribution at tissue level when paced at a frequency of 500 ms, which matches the APD distribution of the experimental preparations in [40] when paced at the same frequency. Note that sizes for heterogeneities presented in [40] are the sizes of regions isolated from the neighbors by a local APD gradient of 15 ms/mm. This algorithm results in much smaller heterogeneity sizes by choosing the regions which are much closer to the maximal APD values. In our research we estimate the size at 50 % heterogeneity, because this, in our view, describes the heterogeneity better than a max APD region. The exact underlying reason of the APD difference in [40] was not studied. However, as for the case of other APD heterogeneities between cardiac cells studied experimentally in [127, 128] it can be achieved by changing the  $I_{Kr}$  and  $I_{Ks}$  conductances. In our case we did it by setting  $G_{Kr}=0.1532$  nS/pF,  $G_{Ks}=0.3923$  nS/pF outside the heterogeneity, and  $G_{Kr}=0.0948$  nS/pF,  $G_{Ks}=0.0$  nS/pF inside the heterogeneity. These values were initially estimated using an approach we developed earlier [25]. In Fig. 4.1B, C and D we take the same values for  $G_{Kr}$  and  $G_{Ks}$  outside the heterogeneity as in Fig. 4.1A, but different values for  $G_{Kr}$  and  $G_{Ks}$  inside the heterogeneity. This results in heterogeneities with different maximal APD value. Due to electrotonic effects, the size at 50% heterogeneity remains the same. The latter probably reflects the fact that in that parameter range, electrotonic coupling is linear with respect to the amplitude of the heterogeneity.

In Fig. 4.2A, B, C and D, we present the action potential (AP) both in the center of the heterogeneities ( $AP_i$ ) shown in resp. Fig. 4.1A, B, C and D, as at a location outside these heterogeneities ( $AP_o$ ). We see that in our case prolongation of APD inside the heterogeneity is caused by the prolongation of phase 2 of the action potential which occurs as a result of the decrease of  $G_{Ks}$  and  $G_{Kr}$ .

To set up the heterogeneity in the whole heart, we used the following method. We first took an intersection of the ventricles, parallel to the vertical axis (see section (1), demonstrated in Fig. 4.9B and C). Next, we set up a region, with the shape of an ellipse in this plane. We labeled the points inside this ellipse with the number  $H_0 = H(0) = 10$  and then let it diffuse for 300 steps in the isotropic version of our whole heart model, using  $\frac{\partial H}{\partial a} = \nabla^2 H$  with  $\Delta a = 0.00008$ , and  $\Delta x = 0.5$  mm. As a final step, all points for which  $H(\bar{x}) > 0.05$ , we defined as being part of the heterogeneity. Unless stated otherwise, we use, in all the whole heart models which contain a heterogeneity, the same initial ellipse as a starting configuration for our diffusion based algorithm, with a major axis of 6.5 mm and a minor axis of 2.5 mm, but each time located at a different position in section (1).

## CHAPTER 4. SMALL SIZE IONIC HETEROGENEITIES IN THE HUMAN HEART CAN ATTRACT SPIRAL WAVES

---

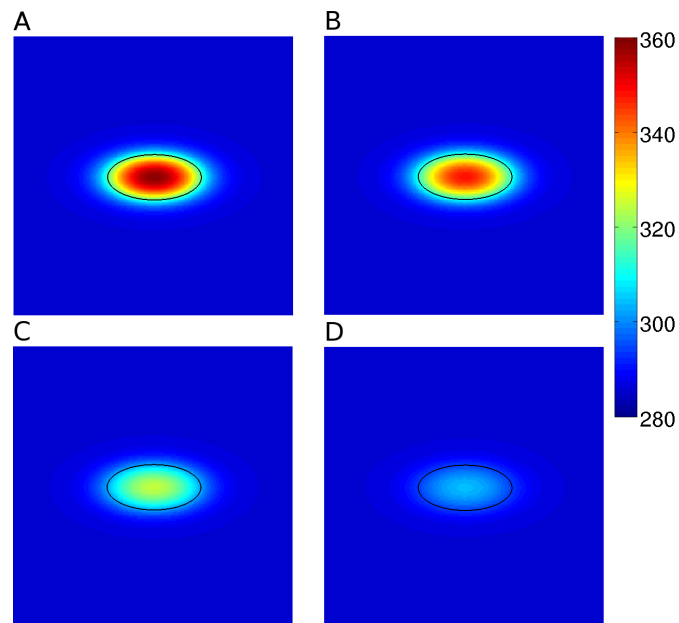


**Figure 4.1:** A, B, C and D shows the APD distribution in cardiac tissue simulated numerically in a human cardiac tissue model. The total size of the medium is  $4 \text{ cm} \times 4 \text{ cm}$ . In black we show the size of the heterogeneity, which is the same for the four tissue configurations. The colormap shows the APD in ms. In all four cases we set  $G_{K_r}=0.1532 \text{ nS/pF}$  and  $G_{K_s}=0.3923 \text{ nS/pF}$  outside the heterogeneity, resulting in a min. APD=286 ms. In A we set  $G_{K_r}=0.0948 \text{ nS/pF}$ ,  $G_{K_s}=0.0 \text{ nS/pF}$  inside the heterogeneity, which results in a max. APD=358.5 ms. In B we set  $G_{K_r}=0.1532 \text{ nS/pF}$  and  $G_{K_s}=0.0 \text{ nS/pF}$  inside the heterogeneity, which gives a max. APD=348.2 ms. In C we set  $G_{K_r}=0.1532 \text{ nS/pF}$  and  $G_{K_s}=0.1295 \text{ nS/pF}$  inside the heterogeneity, which gives a max. APD=324.5 ms. In D we set  $G_{K_r}=0.1532 \text{ nS/pF}$  and  $G_{K_s}=0.2589 \text{ nS/pF}$  inside the heterogeneity, which gives a max. APD=304.2 ms. In all cases, this results in a size at 50% heterogeneity of  $1.2 \text{ cm}$  by  $0.56 \text{ cm}$ . This is comparable to heterogeneity measured in the human heart [40].

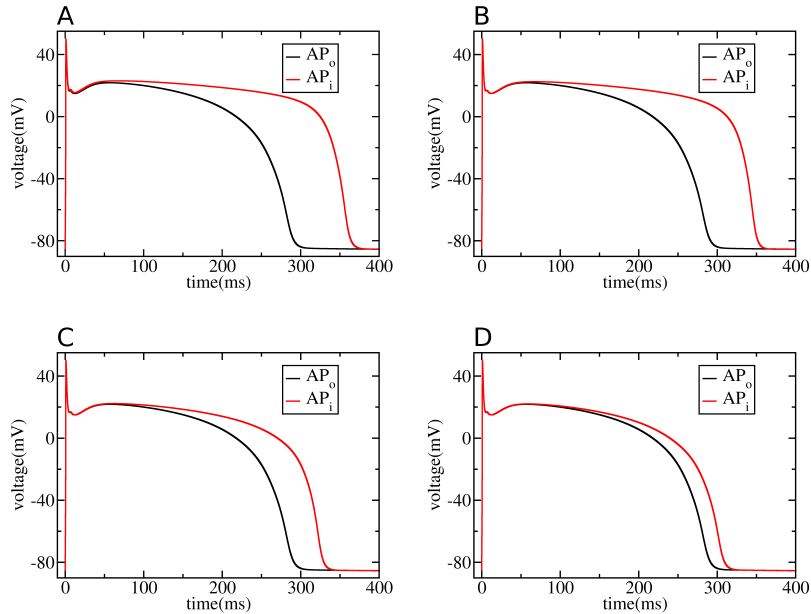


**Figure 4.2: AP inside and outside the heterogeneity.** Figure shows AP shape at the center of the heterogeneities ( $AP_i$ , red lines) and outside the heterogeneities ( $AP_o$ , black lines) for the heterogeneities shown in Fig. 4.1. Parameter values for the subfigures A, B, C and D correspond to those of Fig. 4.1.

### 3 Results

#### 3.1 Ionic heterogeneities as attractors of spiral waves in 2D cardiac tissue

As an initial step, we generate a heterogeneity which has size and value similar to that reported in experimental work by Glukhov [40]. We study its effect on a spiral wave, which is originally located at some distance from the heterogeneity (for more details, we refer to the materials and methods section and to Fig. 4.1A). Fig. 4.3 shows typical dynamics of a spiral wave in a 2D medium with such a heterogeneity. In particular, we initiate a spiral rotating in the center of the medium and position the ionic heterogeneity at a distance of 4.1 cm from the center (the distance along the x-axis to the center is the same as the distance along the y-axis). We then simulate for 10 s, and investigate the influence of the ionic heterogeneity on spiral wave dynamics (we also refer to supplemental Movie S1, available via the online version of [26]). At first, the effect of the heterogeneity on the spiral wave rotation is small. We see that the spiral rotates at its initial position. At the heterogeneity, we see the formation of two breaks which cannot penetrate into the heterogeneity and we get a classical Wenckebach 1:2 block (see Fig. 4.3, from 0 s to 1 s). However, for the next rotation, the gap between the wavebreaks at the heterogeneity has become large enough, and we observe formation of a figure-of-eight reentry pattern (time=1.36 s). The waves generated by it propagate through the heterogeneity and interact with the wave generated during the following rotation of the original spiral (time=1.4 s). As a result of this interaction, the figure-of-eight reentry disappears. However, it reappears at the next rotations with the wavebreaks at larger distance (time=5.3 s) and new reentry patterns now affect spiral wave rotation in a

## CHAPTER 4. SMALL SIZE IONIC HETEROGENEITIES IN THE HUMAN HEART CAN ATTRACT SPIRAL WAVES

larger region (time=5.41 s). This effect spreads and newly formed reentrant patterns approach the center of the spiral (time=5.46 s, time=6.85 s, time=6.94 s). Their interaction with a spiral tip eventually moves the core of the spiral to another location closer to the heterogeneity (time=7 s, time=7.18 s, time=7.24 s). This process is repeated again (time=7.3 s, time=7.42 s, time=7.49 s, time=7.57 s, time=7.79 s) and again (time=8.34, time=8.41 s, time=8.45 s), and after this complex interaction, the spiral tip touches the heterogeneity and eventually anchors at it (time=8.62 s).

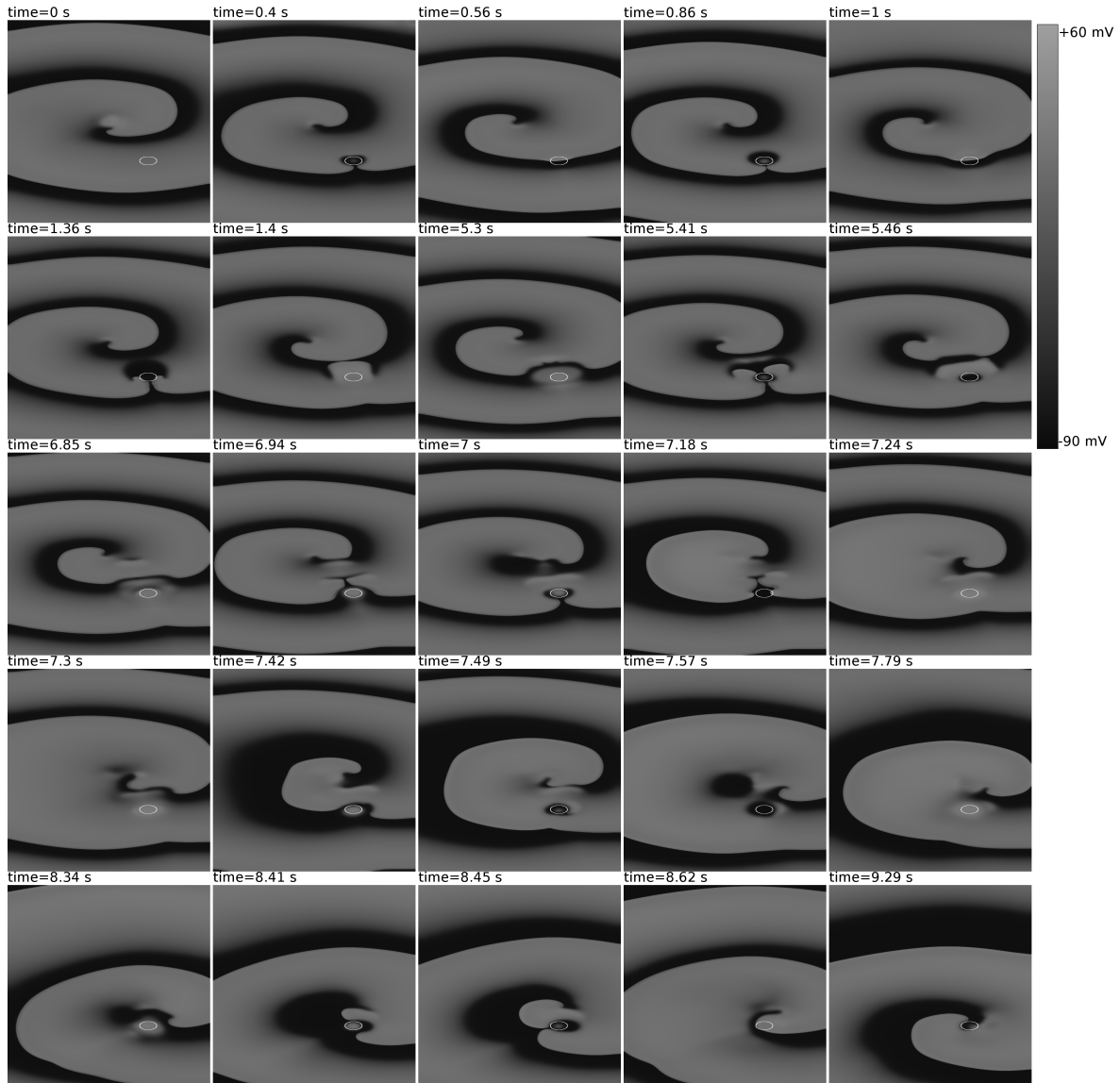


**Figure 4.3: Ionic heterogeneity attracts a spiral wave.** The ionic heterogeneity is taken from Fig. 4.1A and is located at a distance of 4.1 cm from the center of the tissue. The white line shows the size of the heterogeneity. Initially, the spiral rotates at the center of the tissue (time=0 s). At time=8.62 s, the spiral wave anchors to the heterogeneity. The subfigures show the intermediate wave patterns. More explanation can be found in the text. The total size of the medium is 15 cm by 15 cm.



We performed analogous simulations as described in Fig. 4.3, where we vary the location of the heterogeneity. We always start from a spiral wave located at the center of the medium and investigate if the spiral will anchor around the heterogeneity after 10 s. The results are shown in Fig. 4.4A. Here, position (0,0) is located at the center of the medium. We then move the heterogeneity along the x-axis (i.e. along the fibers), along the y-axis and along the first bisector. The dots in Fig. 4.4A show the location of the heterogeneity for a certain tissue configuration. Black dots indicate an anchored spiral wave after 10 s, while no anchoring occurred after 10 s for the red dots. We find that if we move the heterogeneity along the fibers, it can attract spirals rotating within 6 cm or less, while perpendicular to the fibers this distance decreases to approximately 4 cm. Along the first bisector it is around 5 cm. In all cases the process leading to the attraction and anchoring of the spiral wave at the heterogeneity is similar to that of Fig. 4.3 (or supplementary Movie S1). We refer to supplemental Movies S2 and S3 where we show the process of attraction of a spiral when the spiral is initially at a distance of 5.3 cm along the fibers and, resp., 3.7 cm across the fibers from the heterogeneity. In both cases we see that at first wavebreaks are generated at the heterogeneity. After a few rotations, the distance between these newly formed wavebreaks increases and we observe the formation of a reentry pattern at the heterogeneity which start to affect spiral wave rotation. In the same way as in Fig. 4.3, a complex interaction between newly generated spirals and the tip of the original spiral wave, shifts the spiral to a position closer to the heterogeneity. This process is repeated, until the spiral eventually anchors at the heterogeneity. The process of attraction is thus not a continuous process in which the spiral slowly drifts towards the heterogeneity, but a stepwise process with a fluctuating component in which the spiral is shifted due to a complex interaction with newly generated spirals, after which we normally observe a phase during which the spiral stabilizes for a few rotations. After that, the process of interaction between the spiral and newly generated spirals is repeated, until the spiral is anchored to the heterogeneity.

Next, we study the influence of the degree of heterogeneity on the attraction and anchoring of a spiral wave. We performed simulations similar to those of Fig. 4.3, while changing the APD distribution. This is done according to Fig. 4.1A-D, and presented resp. in Fig. 4.4A-D. In Fig. 4.4A-D (and resp. Fig. 4.1A-D), the degree of heterogeneity is decreased to a  $\Delta\text{APD}$  (= maximal APD - minimal APD) of resp. 72.5 ms (A), 62.2 ms (B), 38.5 ms (C) and 18.2 ms (D). Note that the spatial size of the heterogeneity is kept constant. We find that the distance for which the heterogeneity attracts the spiral wave decreases if the degree of heterogeneity is decreased. Indeed, the distance along the fibers, for which it is possible to attract spirals, decreases from 6 cm to 4.5 cm, 3 cm and 1.2 cm resp. (see Fig. 4.4A-D). In all cases the mechanism of attraction is similar to that described above. Note, that in Fig. 4.4B and C, there are few points with no anchoring inside the anchoring zone: in B for a distance of 2.9 cm and 3.7 cm, and in C for a distance of 2.9 cm. If, however, we increase the simulation time, the spirals anchor at these points as well (the extra time needed to achieve anchoring at these points is 0.24 s, 2.4 s and 3.6 s, correspondingly).

To characterize a metric for the propensity for anchoring we have also studied the time it takes for a spiral to anchor around a heterogeneity versus the initial distance and positioning of the spiral wave, and extent of the heterogeneity (Fig. 4.5). In Fig. 4.5A the spiral is positioned at a certain distance from the heterogeneity along the fibers, in B perpendicular to the fibers and in C diagonal to the fibers. We present results for the three largest heterogeneities shown in Fig. 4.1 ( $\Delta\text{APD}=72.5$  ms in black,  $\Delta\text{APD}=62.2$  ms in red and  $\Delta\text{APD}=38.5$  ms in green). We see that for most of the cases, if the initial distance of the spiral wave to the heterogeneity

## CHAPTER 4. SMALL SIZE IONIC HETEROGENEITIES IN THE HUMAN HEART CAN ATTRACT SPIRAL WAVES

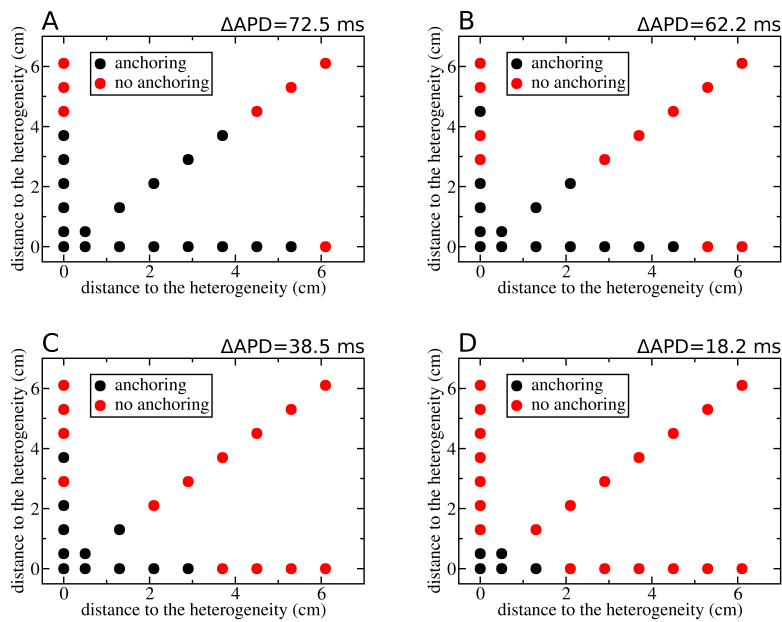


**Figure 4.4: Region of attraction of an ionic heterogeneity.** Figures A-D show final state of a spiral wave which is initially located at the center of the tissue (position (0,0)). Spirals attracted and anchored to the heterogeneity after 10 s are represented by black dots, not anchored states are represented by red dots. The horizontal resp. vertical axis shows the distance of the heterogeneity to the center along the x-axis resp. y-axis. Figures A-D present a different degree of heterogeneity, according to Fig. 4.1A-D, with a  $\Delta APD$  of 72.5 ms (A), 62.2 ms (B), 38.5 ms (C) and 18.2 ms (D). Simulations were performed in a tissue with a total size of 15 cm by 15 cm and a duration of 10 s.

is smaller, it takes less time for the spiral to anchor to the heterogeneity. The figure also reflects a fluctuating component of the process.

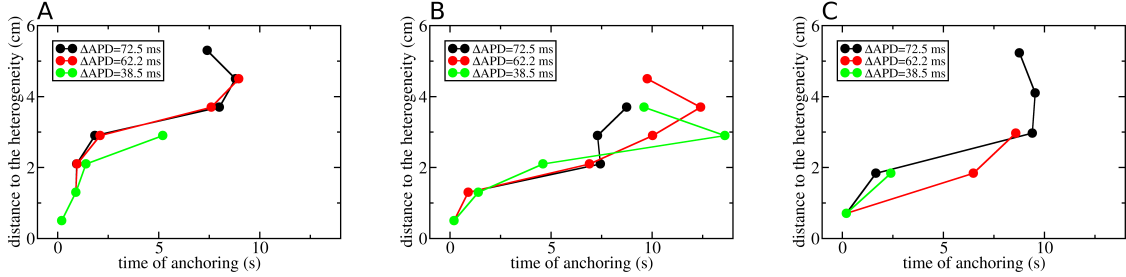


**Figure 4.5: Time needed to anchor versus the initial distance between the spiral wave and the heterogeneity.** In A for a heterogeneity positioned at a given distance along the fibers, in B perpendicular to the fibers and in C diagonal to the fibers. Black, red and green dots show the results for the heterogeneity as in Fig. 4.1A, B, and C respectively.

We also checked if our results are valid if we change the size of the heterogeneity, while keeping the ionic properties inside and outside the heterogeneity the same. For that we used the heterogeneity as shown in Fig. 4.1A ( $G_{K_r}=0.0948$  nS/pF and  $G_{K_s}=0.0$  nS/pF) and performed the same simulations as in Fig. 4.4 but now for a heterogeneity with a size which is 50% less resp. 50% more than the original size. We refer to Fig. 4.6. We find that both heterogeneities are able to attract spiral waves from a substantial distance. As expected, the region of attraction of the heterogeneity with a decreased size is smaller than that for an increased size.

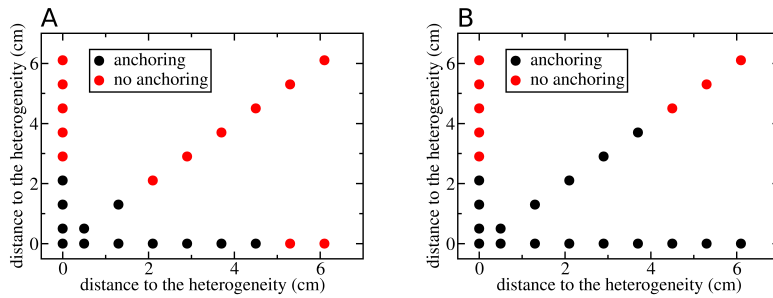


**Figure 4.6: Region of attraction of an ionic heterogeneity for different heterogeneity size.** Representation is the same as in Fig. 4.4. In A and B the size of the heterogeneity is decreased resp. increased by 50% compared to that of Fig. 4.4A while keeping the same ionic properties inside and outside the heterogeneity. In A this results in a max. APD of 343.3 ms and a size at 50% heterogeneity of 0.48 cm by 1.04 cm. For B this results in a max. APD of 376.7 ms and a size at 50% heterogeneity of 0.68 cm by 1.4 cm. Min. APD is not changed: 286 ms. Simulations were performed in a medium with a total size of 15 cm by 15 cm for 10 s.

In conclusion, we find that the ionic heterogeneities attract spiral waves from a substantial distance and that this distance is substantially affected by the degree of heterogeneity. We also find that if the heterogeneity is located at a larger distance from the spiral wave, it takes

## CHAPTER 4. SMALL SIZE IONIC HETEROGENEITIES IN THE HUMAN HEART CAN ATTRACT SPIRAL WAVES

longer for the spiral to anchor to the heterogeneity.

Both experimental [22, 104] and modeling studies [123] showed that spirals can anchor to inexcitable obstacles. Therefore, we compared our results on anchoring of spirals at ionic heterogeneities with the anchoring at inexcitable obstacles. We generate an inexcitable obstacle with the same size as the ionic heterogeneities shown in Fig. 4.1 and perform the same simulation as in Fig. 4.3. The results are shown in Fig. 4.7 and the supplemental Movie S4: we find that the effect of the obstacle on spiral wave dynamics is very small. The spiral remains rotating stationary at the center of the tissue and we do not see any wavebreak formation or other important effects.

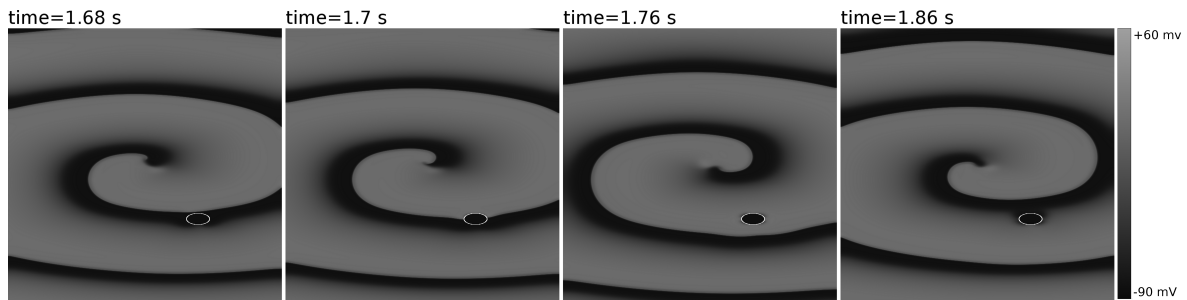


**Figure 4.7: Inexcitable obstacle does not attract the spirals wave.** The inexcitable obstacle is located at a distance of 4.1 cm from the center of the tissue. The white line shows the size of the obstacle. The effect of the obstacle on spiral wave dynamics is very small. The total size of the medium is 15 cm by 15 cm. In the text, we further elaborate on this result.

Next, we perform a similar series of simulations, where we start from a spiral rotating in the center of the tissue and position an obstacle at similar locations as we did for ionic heterogeneities (as in Fig. 4.4). We investigate whether the obstacle can attract and anchor spiral waves. From Fig. 4.8, we see that the inexcitable obstacle can only anchor spirals if it is located very close to it: along the fibers, the maximal distance for which it is possible to attract spirals is around 2 cm, while perpendicular to the fiber direction it is around 0.5 cm. We performed the same simulations (not shown) for an inexcitable obstacle with a size which is two times larger than the size of the obstacle used in Fig. 4.7 and obtained the same result: anchoring resp. no anchoring occurred for the same locations of this obstacle as for the original obstacle shown in Fig. 4.8.

Comparing Fig. 4.8 with Fig. 4.4, we find that ionic heterogeneities, having an APD difference which is large enough (in our case around 30 ms), can attract spirals rotating within larger distances than an inexcitable obstacle of the same size: ionic heterogeneities based on experimentally measured values can attract and anchor spirals rotating within 5-6 cm (see Fig. 4.4A), while for an inexcitable obstacle of the same size this distance is only around 1-2 cm.

### 3.2 Ionic heterogeneities as attractors of spiral waves in an anatomical model of the heart

We performed similar simulations in an anatomical model of human ventricles. We initiated a spiral wave in the left ventricle, containing an ionic heterogeneity as in Fig. 4.9. We refer

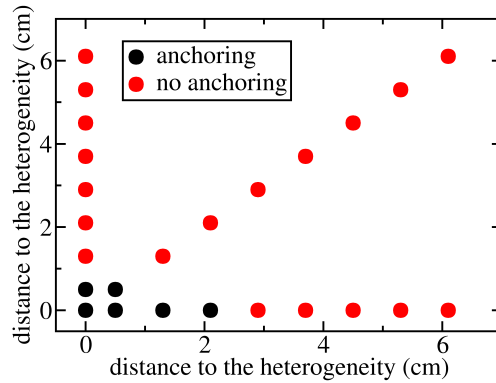


**Figure 4.8: Region of attraction of an inexcitable obstacle.** Representation is the same as in Fig. 4.4. Simulations were performed in a medium with a total size of 15 cm by 15 cm for 10 s.

to the materials and method section for more details on the heterogeneity. The size, maximal and minimal APD are again comparable to heterogeneities measured in ventricular tissue in [40] (see sections shown in Fig. 4.9C and D).

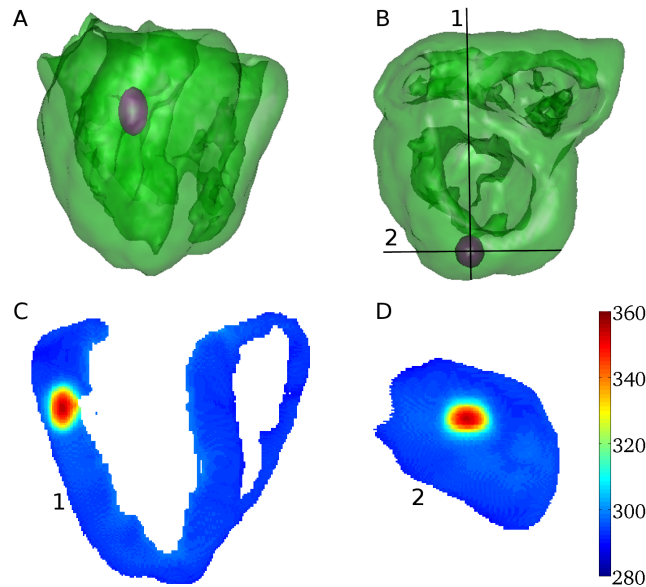


**Figure 4.9: An ionic heterogeneity in an anatomical model of the ventricles.** The heterogeneity is located in the free wall of the left ventricle (purple). Outside the heterogeneity, we set  $G_{Kr}=0.1532$  nS/pF and  $G_{Ks}=0.3923$  nS/pF, resulting in a minimal APD=286 ms; inside the heterogeneity, we set  $G_{Kr}=0.0$  nS/pF,  $G_{Ks}=0.0$  nS/pF, which results in a maximal APD=354 ms. The colormaps in C and D show APD distribution in ms for the two sections (1) and (2), through the middle of the heterogeneity, as illustrated in B. For C, the size at 50% heterogeneity is 0.85 cm by 1.2 cm, and for D: 1.2 cm by 0.8 cm.

In Fig. 4.10, we show the evolution of a spiral wave and the corresponding filament, both in a homogeneous anatomical model (left panel) and in the heterogeneous model of Fig. 4.9

## CHAPTER 4. SMALL SIZE IONIC HETEROGENEITIES IN THE HUMAN HEART CAN ATTRACT SPIRAL WAVES

(right panel). In both cases, we initiated a spiral at the same location, and followed its rotation for 10 s. In the homogeneous model, we see that the spiral wave remains rotating stationary at the place where it is initiated. In contrast, the spiral anchors around the heterogeneity in the heterogeneous model, and continues to rotate around it for the rest of the simulation (we also refer to the supplemental Movie S5). We see a slight shift of the filament if we compare the initial and final location (see Fig. 4.10G versus H) (as the heterogeneity is located close to the initial location of the spiral, the shift is rather small in this case).

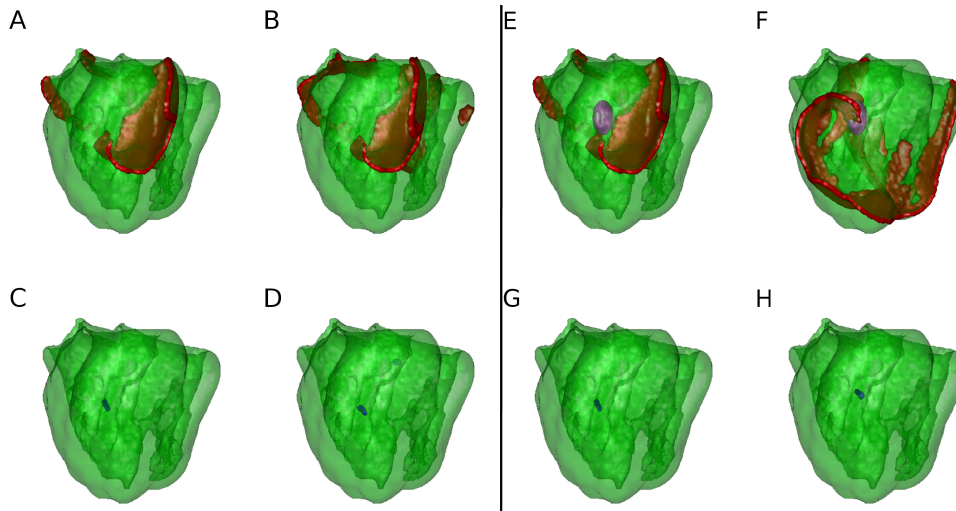


**Figure 4.10: Evolution of a spiral wave in a homogeneous (left panel) and heterogeneous (right panel) anatomical model of the ventricles.** The ionic heterogeneity is modeled according to Fig. 4.9. We show the initial position of the wavefront (A, E) and the corresponding filament (C, G). The position of the wavefront (B, F), resp. filament (D, H) after 10 s is also shown. In the homogeneous model, the spiral remains rotating stationary, while for the heterogeneous model, the spiral is attracted and eventually anchored to the heterogeneity.

Now, we move this heterogeneity to different locations, while keeping its size and magnitude constant, in the free wall of the left ventricle and investigate if the heterogeneity attracts the spiral waves from larger distances. In all cases the spiral has the same initial location as in Fig. 4.10.

Firstly, in Fig. 4.11, we show the results for two simulations with a heterogeneity located close to the apex. In both simulations, we see that the spiral wave is attracted and eventually anchored to the heterogeneity (see also supplemental Movie S6 and Movie S7 for the results illustrated in the upper resp. the lower panel). The dynamics of this attraction are similar to these in 2D cardiac tissue: at first, spiral wave rotation is not affected by the heterogeneity and we just observe wavebreaks at the heterogeneity; later, the effect of the heterogeneity on the waves spreads, and the gap between the wavebreaks increases; then the wavebreaks start to affect spiral wave rotation, and due to complex interaction, its tip moves towards the location of the heterogeneity, where it eventually anchors.

Secondly, in Fig. 4.12, we show the results for two similar simulations as in Fig. 4.11, but now with a heterogeneity located close to the base of the ventricles. In the upper panel, we see the same results as before: after some rotations, the spiral wave is anchored to the heterogeneity (we refer to supplemental Movie S8). However, in case of the lower panel of

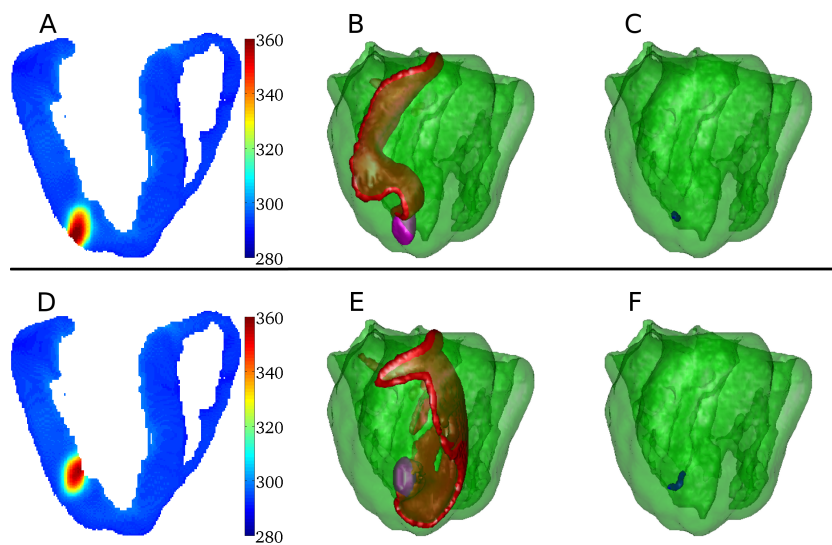


**Figure 4.11: Attraction and anchoring of a spiral wave by an ionic heterogeneity in an anatomical model of the ventricles.** The two models contain a heterogeneity (purple) of similar size as in Fig. 4.9, but now located close to the apex. The ionic properties inside and outside of the heterogeneity are the same as in Fig. 4.9, resulting in a minimal APD=286 ms and a maximal APD=360 ms and 359 ms for the upper resp. the lower panel. The colormaps in A and D shows the APD distribution in ms in section (1), (see Fig. 4.9B). We show the position of the wavefront (B, E) and the corresponding filament (C,F) after 10 s. In both models, the spiral is attracted and eventually anchored to the heterogeneity.

## CHAPTER 4. SMALL SIZE IONIC HETEROGENEITIES IN THE HUMAN HEART CAN ATTRACT SPIRAL WAVES

Fig. 4.12, after approximately 5 s the spiral disappears.

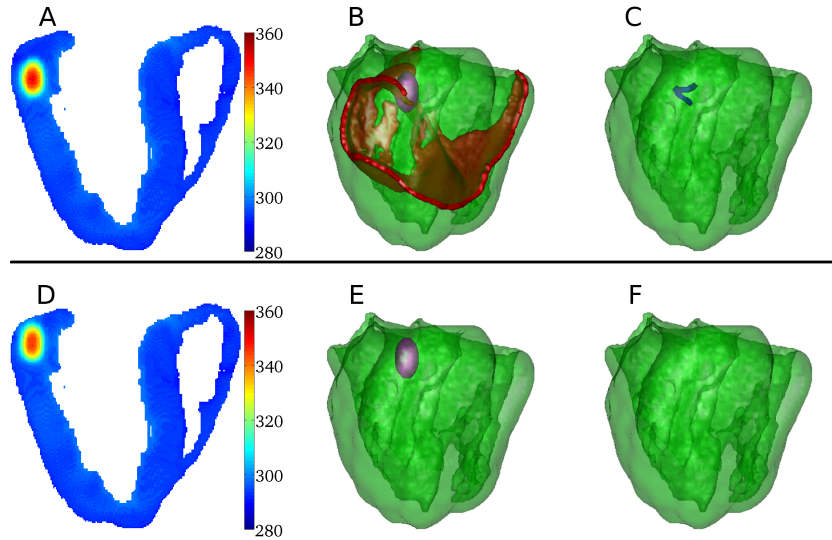


**Figure 4.12: Attraction, anchoring and removal of a spiral wave by an ionic heterogeneity in an anatomical model of the ventricles.** The two models contain a heterogeneity (purple) of similar size as in Fig. 4.9, but now located close to the base. The ionic properties inside and outside of the heterogeneity are the same as in Fig. 4.9, resulting in a minimal APD=286 ms and a maximal APD=353 ms and 352 ms for the upper resp. the lower panel. The colormaps in A and D shows the APD distribution in ms in section (1) (see Fig. 4.9B). We show the position of the wavefront (B) and the corresponding filament (C) after 10 s; and the result for wavefront (E), resp. filament (F) after 5.03 s. In the upper panel, the spiral wave is attracted and eventually anchored to the heterogeneity. In the lower panel, the spiral is attracted, anchored and eventually removed because of interaction with the heterogeneity and the boundary of the left ventricle.

We illustrate this process of removal of a spiral wave further in Fig. 4.13 and in the supplemental Movie S9. In Fig. 4.13, we see that, similar to previous simulations, the spiral is first attracted to the heterogeneity (from 0 s to 4.46 s), then, for one rotation (approximately from 4.54 s to 4.82 s), the spiral wave is anchored to the heterogeneity. However, subsequently, the tip of the spiral disappears at the top border of the left ventricle (around 4.82 s) and spiral wave rotation ends.

Thus we observe that if the heterogeneity is located close to the boundary of the ventricle, it can not only attract and anchor a spiral wave, but it can also eliminate it.

In the next series of simulations, we checked if our results also hold for heterogeneities of different sizes. For this, we changed the size of the ellipse used as a starting configuration for our diffusion based algorithm described in the materials and methods section. In particular we decreased (see Fig. 4.14), resp. increased (see Fig. 4.15) the size of this ellipse by 50%. The ionic properties inside and outside the heterogeneity were the same as previously. When positioned at the same location as the heterogeneity shown in Fig. 4.9, we obtained a maximal value of APD of 342 ms resp. 368 ms if we decrease resp. increase the size of the heterogeneity. Minimal APD is unchanged and is 286 ms.

We have tried the same initial locations of both the spiral and the heterogeneities used in Fig. 4.9, 4.11 and 4.12 and obtained the following results for smaller and larger hetero-



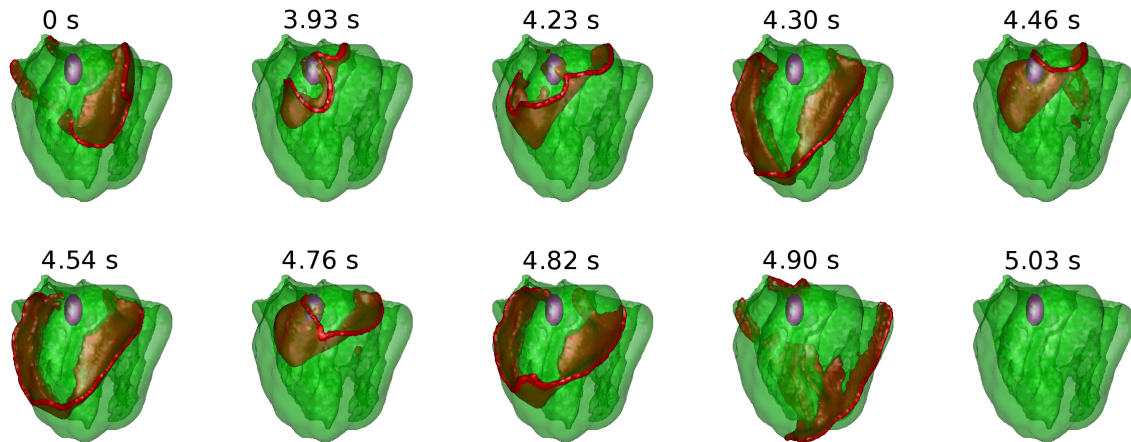


**Figure 4.13: Removal of a spiral wave due to interaction with an ionic heterogeneity.** An ionic heterogeneity, as in the right panel of Fig. 4.12, thus located close to the base of the ventricles, can attract, anchor and eventually remove a spiral wave.

genities. For the heterogeneity with decreased size at the location as in Fig. 4.9, we again observed attraction and anchoring of the spiral wave (results not shown). When we moved this heterogeneity to the apex, as in Fig. 4.11, we did not observe anchoring of the spiral around the heterogeneity after 10 s. However, after we shifted the heterogeneity approximately 9 mm closer to the initial position of the spiral wave (see Fig. 4.14A), we again find that the heterogeneity can anchor and attract the spiral after 10 s (see Fig. 4.14D). For heterogeneity locations close to the base, as in Fig. 4.12, we found that the heterogeneity attracted and anchored the spiral (see Fig. 4.14E). And if we move the heterogeneity even closer to the base (see Fig. 4.14C), we observed that the spiral wave, as in Fig. 4.12, was removed. However, to remove the spiral in that case we needed a simulation time of 12.8 s, i.e. longer than the 5.03 s needed for that in Fig. 4.12.

For larger sized heterogeneities, for all locations shown in Fig. 4.9, 4.11 and 4.12 we observed attraction and anchoring of the spiral wave, similar as for the heterogeneity of original size. The only difference was that for the location closest to base (see Fig. 4.15C), the removal of the spiral wave occurred after 13.4 s, compared to 5.03 s in Fig. 4.12.

From these simulations, we can conclude that our results on attraction, anchoring and removal of spiral waves also hold for heterogeneities of decreased and increased size. As in 2D, we observed that the region of attraction becomes smaller if the size of the heterogeneity is decreased.

## 4 Discussion

In this chapter, we study the effect of small size ionic heterogeneities on spiral wave rotation. These heterogeneities have a size and magnitude similar to these measured by Glukhov in [40].

We show that in 2D, these type of heterogeneities can attract and eventually anchor a spiral rotating within 6 cm along the fibers, 4 cm across the fibers and around 5 cm at 45

**CHAPTER 4. SMALL SIZE IONIC HETEROGENEITIES IN THE HUMAN HEART CAN ATTRACT SPIRAL WAVES**

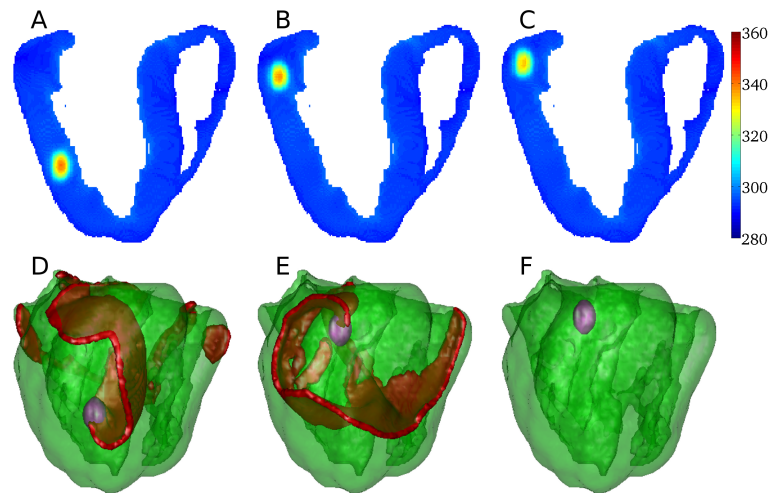


**Figure 4.14: Attraction, anchoring and removal of a spiral wave by an ionic heterogeneity of decreased size in an anatomical model of the ventricles** (see text for details). The ionic properties inside and outside the heterogeneity are the same as in Fig. 4.9, resulting in a minimal APD=286 ms and a maximal APD=342 ms. When positioned at the same location as the heterogeneity shown in Fig. 4.9, the size at 50% heterogeneity is 0.7 cm by 1 cm for section (1) and 1 cm by 0.8 cm for section (2). The colormaps in A, B and C show the APD distribution in ms in section (1). In D and E we show the corresponding position of the wavefront after 10 s; and in F after 12.8 s.

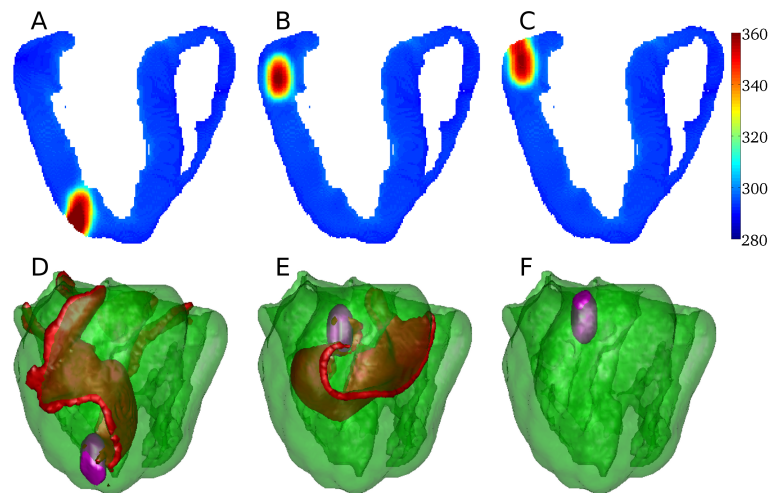


**Figure 4.15: Attraction, anchoring and removal of a spiral wave by an ionic heterogeneity of increased size in an anatomical model of the ventricles** (see text for details). The ionic properties inside and outside the heterogeneity are the same as in Fig. 4.9, resulting in a minimal APD=286 ms and a maximal APD=368 ms. When positioned at the same location as the heterogeneity shown in Fig. 4.9, the size at 50% heterogeneity is 0.85 cm by 1.55 cm for section (1) and 1.55 cm by 0.85 cm for section (2). The colormaps in A, B and C show the APD distribution in ms in section (1). In D and E we show the corresponding position of the wavefront after 10 s; and in F after 13.4 s.

degrees. In the whole heart, if the degree of heterogeneity was large enough, it was always anchored (or eventually removed). Thus, the basin of attraction of these ionic heterogeneities is very substantial in comparison to the typical size of the human heart, whose height is around 10 cm. We showed that this attraction over large distances is a property of ionic heterogeneities alone, i.e. it does not hold for non conducting heterogeneities.

In our anatomical model of the ventricles, we demonstrate that if the heterogeneity is located close to the base, it can not only attract and anchor a spiral wave, but can also remove it. This is an interesting result, as it suggests that some types of heterogeneities have an anti-arrhythmic effect. In [155] such regions of prolonged APD were already created in an experimental set-up through regional cooling, and they were indeed shown to be able to remove a spiral wave from the heart. It would be interesting to study this anti-arrhythmic effect when the heterogeneity is created in the same way as studied here, for example, by changing the local expression of genes responsible for the conductance of the  $I_{Ks}$  and  $I_{Kr}$  currents. Of course, this is a very controversial statement and it takes into account only one effect of heterogeneity: on attraction and anchoring of spiral waves. It does not consider its role in the formation of new spirals, for example.

The mechanism of attraction of spiral waves to heterogeneities can be attributed to a generic behavior of spirals in heterogeneous tissue. In [116, 102, 138] it was shown that spirals tend to drift to the regions of longer period of rotation. Longer period of rotation of a spiral is normally associated with a longer APD [100, 138]. Thus it is very natural to expect that in our simulations the spirals are to be attracted by the heterogeneity, as in our case the heterogeneity has a longer APD compared to the rest of the tissue.

Studies of the effect of heterogeneities on 2D wave propagation in various models of cardiac tissue were also performed in a series of publications [123, 122]. In particular, in [123], they studied dynamics of spiral waves in a low dimensional (Panfilov) model [95] and the ionic Luo-Rudy I model [78] of cardiac tissue in presence of squared ionic heterogeneities and inexcitable obstacles of 4 cm by 4 cm, placed at various locations in cardiac tissue. The observed dynamics include spiral turbulence, a rotating spiral and the quiescent state. They showed that a fractal-like boundary separates the basins of attraction of these regimes. One of the regimes observed was anchoring of spirals at the heterogeneity. In the follow-up study [122], they compared the dynamics of waves around squared inexcitable obstacles and ionic heterogeneities of 3 cm by 3 cm in four models of cardiac tissue [136, 11, 95, 78]. In all models they report various regimes of interaction of spirals with the obstacles. These regimes depend, in a complex way, on the obstacle location. In some situations they also observed anchoring of spiral waves. These papers give an excellent overview of possibilities which can occur in systems which contain an ionic heterogeneity or an inexcitable obstacle. It would be interesting to study which of these regimes can be realized with heterogeneities and obstacles of size and shape derived from direct experimental measurements.

Anchoring around 3D inexcitable obstacles was also studied in [142, 81, 131]. A study of the interaction of a spiral wave with a heterogeneity with a shorter APD in an anatomical model of the rabbit and pig heart was performed in [80]. It was shown that in that case, a spiral rotating close to the heterogeneity can anchor around it and that parts of this wave can enter the region in which this inhomogeneity is present. This is an interesting observation which shows that even heterogeneities with a shorter APD than the surrounding tissue can serve as anchoring sites for spirals (see also [122, 81]).

In this chapter we studied the possibility of anchoring of an existing spiral wave to a heterogeneity. In our previous study [24], we found that similar ionic heterogeneities can be

## CHAPTER 4. SMALL SIZE IONIC HETEROGENEITIES IN THE HUMAN HEART CAN ATTRACT SPIRAL WAVES

---

pro-arrhythmic and that spirals can be formed at such heterogeneities under high frequency external pacing. Note, that the final state in [24] was also a spiral rotating around the heterogeneity. In view of the results presented in this chapter, we can explain it as a consequence of attraction of the initiated spiral wave to the heterogeneity.

In our whole heart simulations the heterogeneity was located at different positions with respect to the endocardial and epicardial surface (compare for instance Fig. 4.11A with Fig. 4.11D). In all of these cases, we found that the spiral was anchored to the heterogeneity. Therefore, transmural location of the heterogeneity does not seem to affect the possibility of attraction of a spiral.

In our 2D simulations, we considered parallel fibers, and did not study the effect of more complex cases of fiber orientation on anchoring and attraction of a spiral wave by a heterogeneity. As anisotropy of cardiac tissue affects spiral wave dynamics, other types of fiber orientation could lead to more complex regions of attraction than these shown in Fig. 4.4.

We have studied the behavior of a single stable spiral in the presence of a single heterogeneity. It would be interesting to extend this study to the case when several heterogeneities are present in the heart, or to other regimes of spiral wave dynamics: for example to spiral breakup [99, 96], when multiple interacting spirals coexist in cardiac tissue.

In this chapter we considered only a stepwise change in  $G_{Kr}$  and  $G_{Ks}$  in single cell to model heterogeneities at tissue level. Although the change in APD values is stepwise at single cell level, it is gradual at tissue level, due to electrotonic effects. In our case the space constant for such changes is approximately 3-5 mm (we refer to [25] for a detailed discussion). Therefore, we expect that if instead of stepwise changes, more gradual changes at the single cell level would be used, it would not change the conclusion, provided these variations are less than the space constant for electrotonic coupling.

A limitation of this study is that it is based on heterogeneities in the subendocardial zone of the left ventricle, measured on the surface of a wedge, and the data do not provide depth information. This means that we don't have information on the 3D structure of the heterogeneity, which we nonetheless modeled in an anatomical model of the ventricles. It can also be that the amount of heterogeneity reported in [40] is overestimated if used for the whole heart, due to possible additional electrotonic load *in situ*. In addition, as the heterogeneity has some 3D structure, we do not know if the cut surfaces shown in [40] are really cut surfaces through the center of the heterogeneity. If this is not the case, the real heterogeneities can have a larger spatial scale. Thus although we extended the research for heterogeneities of various size and at various locations, this study should be considered as a starting point and more detailed investigations of the role of heterogeneity of various type, shape and origin on spiral wave dynamics in the heart are therefore needed.

Another limitation is that this study was conducted in only one model of the human ventricles. It would be interesting to test if the results obtained here could be confirmed in other human cell models [43, 94].

Overall we can conclude that ionic heterogeneities of small size can be preferred regions of localization of spirals. This means that ablation of these heterogeneities can be beneficial as it may reduce chances of stabilization of spiral waves at the heterogeneity. Alternatively, artificial creation of such heterogeneities close to the boundary of the heart, e.g. in a basal region, may attract the spirals to the boundaries and result in their elimination. Of course, this is a very controversial idea, which requires much more *in silico* and experimental verification.

---

# 5

## Global alternans instability and its effect on non-linear wave propagation: dynamical Wenckebach block and self-terminating spiral waves.

### Abstract

---

The most widely studied dynamical instability in cardiac tissue is the so-called alternans instability. It occurs if the slope of the APD-restitution curve is steeper than one. The APD-restitution curve relates the duration of the cardiac pulse (APD) to the time interval between the pulses, and can easily be measured in an experimental or even clinical setting. This alternans instability is considered as a possible mechanism for the onset of electrical turbulence in the heart, leading to sudden cardiac death. It had a paramount influence on modeling, experimental and clinical studies of cardiac arrhythmias and was a subject of many high profile publications. From a non-linear dynamics perspective, the alternans instability is associated with a local flip bifurcation and manifests itself as an alternating growth of small perturbations. In this chapter we reveal that APD-restitution can result in another dynamical instability, in which an initial perturbation of large amplitude extends in space. We coin this type of instability as global alternans instability (GAI). We first show the onset of this instability numerically in an ionic model for human cardiac cells, and then develop a basic theoretical framework explaining it semi-analytically. We formulate the conditions for the onset of this instability and show that unlike the alternans instability, the conditions for the onset of GAI are determined by the global shape of the APD restitution curve, and do not necessarily require that its local slope is steeper than one. The found instability can explain the results obtained in previous studies, in which we showed that under high frequency pacing an initial small scale heterogeneity can extend in space, and in this way can play an important role in the onset of cardiac arrhythmias, or influence the dynamics of existing spiral waves. We also report new findings that a GAI can result in the onset of dynamical Wenckebach block, formation of new sources, or termination of existing sources of arrhythmias.

### 1 Introduction

---

The pumping function of the heart is controlled by electrical waves of excitation, which propagate through the heart and initiate cardiac contraction. Abnormal propagation of these electrical waves can result in the formation of spiral waves which excite the heart with a high frequency and cause a cardiac arrhythmia, called tachycardia. In many cases, such spirals break down into a complex turbulent pattern and excitation of the heart becomes spatially

## CHAPTER 5. GLOBAL ALTERNANS INSTABILITY AND ITS EFFECT ON NON-LINEAR WAVE PROPAGATION: DYNAMICAL WENCKEBACH BLOCK AND SELF-TERMINATING SPIRAL WAVES.

---

asynchronous. Because of this, the effective contraction of the heart is disrupted, which results in ventricular fibrillation. Sudden cardiac death, due to ventricular fibrillation is one of the largest causes of death in the industrialized world, accounting for approximately one death in ten. Therefore the mechanisms behind the initiation of such spirals and the processes which can remove them from cardiac tissue are of great practical interest.

Early research showed that such spiral waves can be formed because of regional heterogeneity of the heart. One of the most exciting recent developments is the finding that such heterogeneity can be the result of dynamical instabilities in cardiac cells. It was shown that even in simple systems, for example during periodical forcing of a single cardiac cell, we may obtain either a non-periodic response, or a response with a period different from that of external forcing. These processes were investigated theoretically [93, 46] and experimentally [16] and have shown that the onset of such instability in many cases is related to the slope of the APD restitution curve. The APD restitution curve relates two parameters: the duration of the cardiac pulse (action potential duration, APD) and the diastolic interval (DI, the time between the end of the previous and the beginning of the new action potential). If we assume that this APD is just a function of DI (say  $F_{APD}(DI)$ ), then the process of periodic stimulation of a cardiac cell with a period  $T$  can be viewed as a discrete map  $APD_N = F_{APD}(DI_N) = F_{APD}(T - APD_N)$ , as for a periodic stimulation  $APD_N + DI_N = T$ . Such a map can lose stability of its equilibrium via a flip bifurcation if  $dF_{APD}/dDI > 1$  [93, 39]. This results in the onset of period two orbits (alternans) or more complex bifurcations, which can even lead to chaotic behavior.

Such dynamical instabilities obtained a lot of attention, because it was found that they result in the breakdown of a single spiral wave into a complex turbulent pattern of excitation [99, 62, 112]. These studies situated a lot of experimental studies of the restitution properties of cardiac tissue and it was finally shown that reduction of the slope of the restitution curve prevents the onset of ventricular fibrillation [114, 36]. In addition, a lot of new protocols and definitions of restitution relations were proposed, including dynamical restitution [72] and the restitution portrait [30]. However, they indicated that the situation is more complex than originally thought: instability is not only related to the slope of the restitution curve, but also to other parameters, e.g. dispersion relation of the waves [154]. Other types of instabilities were found as well, for example involving Ca-dynamics [126, 146]. Overall, the concept of dynamical instabilities is one of the most valuable contributions to the study of non-linear dynamics in cardiology. Currently, several types of instabilities are already tested in large scale clinical settings as possible predictors of sudden cardiac death [9, 149].

All studies listed above can be considered as studies of local dynamical instabilities. This means that there are some critical parameter values at which such instabilities occur. At the beginning, such an instability is usually just a small change, which grows and affects the global dynamics of the system. Mathematically this means that it is mainly determined by local properties of the tissue, expressed as derivatives of the functions, for example the slope of the restitution curve. In this chapter, we focus on similar phenomena, but extended to extreme values. The most extreme type of disturbance is a situation where properties of the tissue are changed to such an extent that the wave cannot propagate in a given region. Such regional blocks of propagation are extremely important, as wave block is the main mechanism of spiral wave formation and thus of initiation of cardiac arrhythmias. We study the following process. We consider homogeneous cardiac tissue and temporary block wave propagation at some region, so wave  $N$  cannot enter there. This block is temporal and the next wave (wave  $N+1$ ) can enter the region. However, we show that in a broad parameter range the next

wave (wave N+2) will be blocked again at the region without any external action, just due to restitution properties of cardiac tissue. Furthermore, we find that this region of initial block can grow in space and in some cases can result in the formation of new spiral waves, or removal of exciting spirals. Such behavior can be considered as an ultimate alternans instability or a global alternans instability (GAI), as it is determined by global restitution properties of the tissue (difference of APD at two points on the restitution curve, rather than slope of the restitution curve). In this chapter, we study this instability in detail. In the first section we study it in 1D and illustrate the growth of the wave-block region, find the velocity at which this region grows and the dependency on the forcing period. Next, we propose a semi-analytical theory, and demonstrate that it can describe the observed behavior with a high accuracy. Then, we show that in 2D this region extends in a similar way, and that it can result in the creation of new spiral waves or eventual removal of spirals from the tissue. Finally, we discuss our results and its possible consequences for the onset and dynamics of cardiac arrhythmias.

## 2 Materials and methods

---

*Model* - As in the previous chapters, we used the ionic TP06 model for human ventricular tissue [136, 139]. We refer to the materials and methods section of **chapter 2** for more details. Again, we used the default parameter settings from [139] for epicardial cells.

*Numerical methods* - For 1D and 2D simulations, the forward Euler method was applied to integrate Eq. (2.1). A space step of  $\Delta x = 0.25$  mm was used in 1D,  $\Delta x = 0.2$  mm in 2D, and a time step of  $\Delta t = 0.02$  ms was used. To integrate the Hodgkin-Huxley-type equations for the gating variables of the various time-dependent currents ( $m$ ,  $h$  and  $j$  for  $I_{Na}$ ;  $r$  and  $s$  for  $I_{to}$ ;  $x_{r1}$  and  $x_{r2}$  for  $I_{Kr}$ ;  $x_s$  for  $I_{Ks}$ ;  $d$ ,  $f$ ,  $f_2$  and  $f_{Cass}$  for  $I_{CaL}$ ), the Rush and Larsen scheme [117] was used.

*Anisotropy* - In one of our 2D simulations, the fibers are directed along the x-axis. In the other, we study the effect of rotational anisotropy, in that case the diffusion matrix is given by

$$\begin{cases} D_{xx} = D_L \cos^2 \theta + D_T \sin^2 \theta , \\ D_{xy} = D_{yx} = 0 , \\ D_{yy} = D_T , \end{cases} \quad (5.1)$$

with  $\theta(y) = \frac{y}{d}(\theta_2 - \theta_1) + \theta_1$ . Here  $d$  is the distance between epicardium and endocardium (in our simulations  $d = 20$  or  $16$  mm),  $\theta_1 = -60^\circ$ ,  $\theta_2 = 60^\circ$ ,  $D_L = 0.128 \frac{\text{mm}^2}{\text{ms}}$  and  $D_T = D_L/4$ . For 1D simulations,  $D_L = 0.154 \frac{\text{mm}^2}{\text{ms}}$  was used.

## 3 Results

---

### 3.1 GAI in 1D

In Fig. 5.1 we show the manifestation of what we call a global alternans instability (GAI). We consider a homogeneous cable of cardiac cells, which we pace at the left border with a period  $T = 220$  ms, corresponding to  $\text{APD} = 187$  ms. We temporary block wave propagation in the middle of the cable, so wave N cannot excite the cells to the right of this wave block location. However, this block is temporal, and wave N+1 again excites these cells. Due to restitution

**CHAPTER 5. GLOBAL ALTERNANS INSTABILITY AND ITS EFFECT ON NON-LINEAR WAVE PROPAGATION: DYNAMICAL WENCKEBACH BLOCK AND SELF-TERMINATING SPIRAL WAVES.**

---

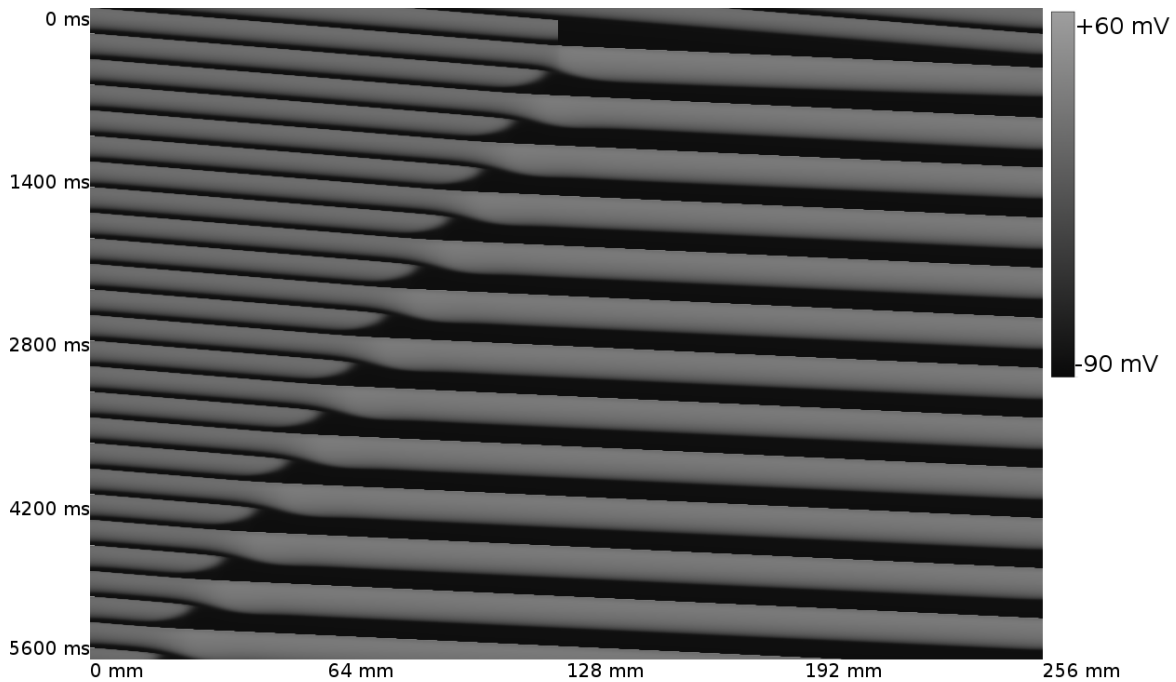


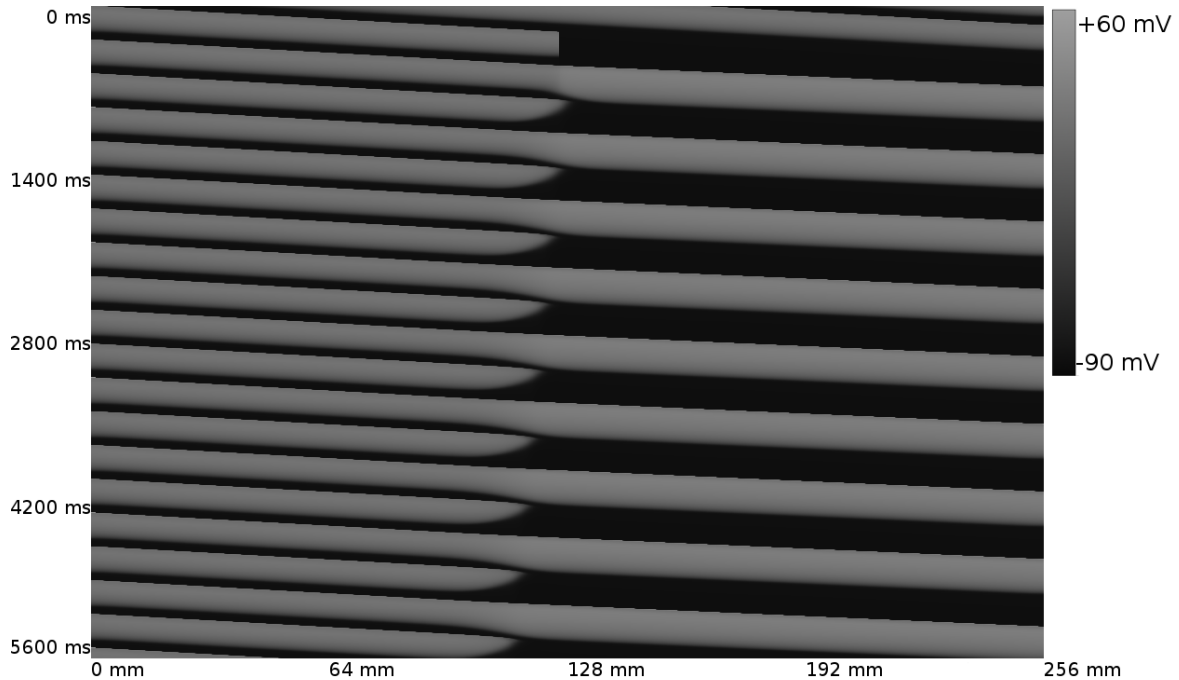
**Figure 5.1: GAI in a cable of cardiac cells.** The cable is paced at the left border with a period  $T = 220$  ms. The wave block region extends in space. Length of the cable is 256 mm.

effects, the duration  $APD_{N+1} = 278$  ms is substantially longer than the normal value. As a result, the next wave  $N+2$  is blocked again because cells are not recovered from the action potential  $N+1$ . In addition, if we look at Fig. 5.1 we observe that the point of the wave block is shifted to the left, in comparison to the previous point of block. In the same way, wave  $N+3$  will be able to excite the complete cable, and the process is repeated as  $APD_{N+3}$  will be longer again. So we see that in homogeneous tissue, due to initial conditions, we observe an area of wave block which extends in space in an alternating order. This is what we call a GAI.

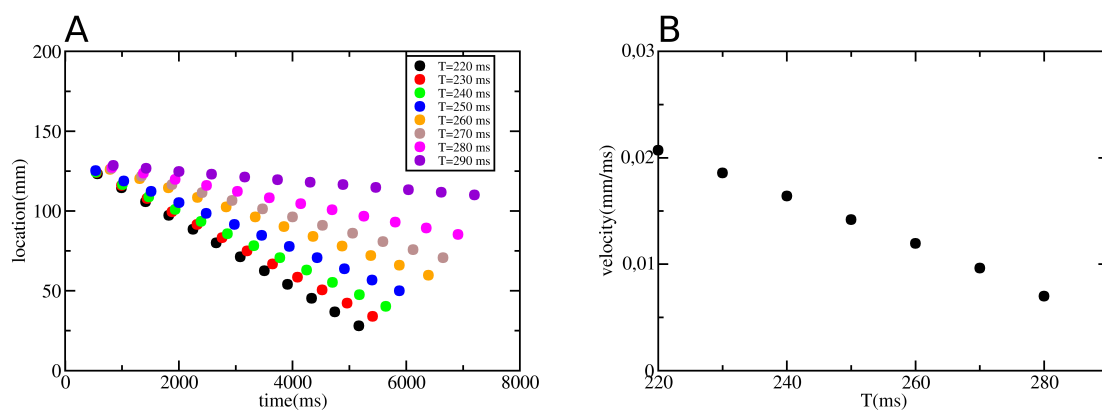
In Fig. 5.2 we show the same process but now for  $T = 290$  ms. We observe a similar growth of the wave block region, although in this case the rate at which it grows is lower than for  $T = 220$  ms.

Fig. 5.3A shows the dependence of the wave block point on the period of pacing  $T$ . The colored dots show the location of block for each second wave, for a certain  $T$ . Interestingly, as was already clear from Fig. 5.1 and Fig. 5.2, this shift of the wave block location is approximately constant. Next, we calculate the velocity at which the wave block region extends in space for different  $T$ . This is shown in Fig. 5.3B. We observe a linear dependency of the velocity on  $T$ . Also, we observe that there is a critical  $T$  (around 300 ms) for which this instability disappears. The reason for that is explained in the next section.





**Figure 5.2:** GAI in a cable of cardiac cells. The cable is paced at the left border with a period  $T = 290$  ms. The wave block region extends in space. Length of the cable is 256 mm.



**Figure 5.3:** Rate at which the wave block region extends in space. The colored dots in A show the location of the point of wave block versus time using the protocol as described in Fig. 5.1 and 5.2 for different  $T$ . In B, we show the velocity (in mm/ms) at which this instability extends in space. The velocity increases for shorter  $T$ .

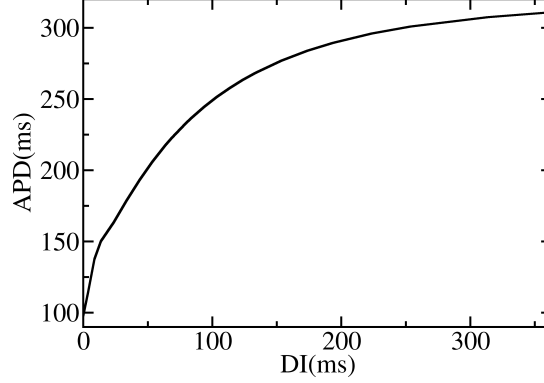


**Figure 5.4: Restitution curve.** DI versus APD.

## 3.2 Mechanism of GAI

### 3.2.1 General consideration

The critical period at which a GAI occurs can be estimated by a simple reasoning via the restitution curve (see Fig. 5.4). First, we note that if the cells located to the left of the point of block are stimulated with a certain period  $T$ , the cells inside the region of block are excited with a period  $2 \times T$ . Thus, if we neglect electrotonic effects, the APD for cells located outside this region is given via the restitution curve as  $APD_0$ , which is a solution of the implicit equation  $APD = F_{APD}(T - APD)$ , while the APD for the other cells is given by  $F_{APD}(2 \times T - APD_0)$ . Second, we will observe a wave block if the wave arrival time is smaller than the local refractory period (RP) of the cells. So, to find when a wave block will occur, and thus a GAI, we have to relate the RP to the APD. For this, we note that in cardiac tissue APD values are closely related to RP. We find that, in our model, APD measured at 90% is approximately equal to RP, so  $APD \approx RP$ . Finally, if we neglect conduction velocity changes, the arrival time to all points where the wave can reach is just equal to  $T$ . Combining these three remarks, we see that we will only have a GAI for those  $T$  for which:

$$T < F_{APD}(2 \times T - APD_0) \quad (5.2)$$

This simple formula based on the restitution curve shown in Fig. 5.4 gives us a critical  $T \approx 310$  ms, which is close to what we observed in our simulations.

### 3.2.2 Semi-analytical theory

Next, we show that we can also estimate the rate at which the wave block region grows by using an analytical-phenomenological approach. For this, let's say wave  $N$  was blocked at a certain location  $x_{\text{block}}$ . Then, as we already noted, for the next wave  $N+1$ , APD for  $x < x_{\text{block}}$  will be  $APD_1 = F_{APD}(T - APD)$ , while for  $x > x_{\text{block}}$  it will be  $APD_2 = F_{APD}(2 \times T - APD)$ . However, as this is an oversimplification due to electrotonic effects [141, 25, 119], we will have a spatially smooth transition from  $APD_1$  to  $APD_2$  and as shown in [25] it can be approximated

by

$$\text{APD}_{N+1}(x) = A_1 + A_2 \text{erf} \left( (x - A_0) \frac{1}{A_3} \right) , \quad (5.3)$$

with  $A_1 = \frac{\text{APD1} + \text{APD2}}{2}$ ,  $A_2 = \frac{\text{APD2} - \text{APD1}}{2}$  and  $A_3 = 7.8$  mm. This means that wave N+2 will propagate in a heterogeneous tissue with heterogeneity given by Eq. (5.3) and can be blocked at another location.

Now, we can easily describe the shift of the wave block point as an iterative process. For this we start from Eq. (5.3) (see black line in Fig. 5.5A, B, and C for  $T=220$ , 250 and 270 ms resp.) and try to find the APD distribution of wave N+2 and wave N+3 using the restitution curve (see Fig. 5.4). So, using Eq. (5.3), we find for the diastolic interval between wave N+1 and N+2 in each point  $x$ :

$$\text{DI}_{N+2}(x) = T - \text{APD}_{N+1}(x) . \quad (5.4)$$

From this we get via the restitution curve:

$$\text{APD}_{N+2}(x) = \text{APD}(\text{DI}_{N+2}(x)) . \quad (5.5)$$

This  $\text{APD}_{N+2}(x)$  gives us the APD distribution for the N+2th wave in the uncoupled system. To find the APD distribution of the N+2th wave in our system with propagating waves, we again need to take into account electrotonic effects. In [25] we showed that the APD distribution of the coupled system can be found from a complex underlying APD distribution of the uncoupled system, using a convolution with a Gaussian Green's function. In particular:

$$\overline{\text{APD}}_{N+2}(x) = \int_{-\infty}^{+\infty} \text{APD}_{N+2}(\alpha) e^{-\left((x-\alpha)\frac{1}{A_3}\right)} d\alpha , \quad (5.6)$$

with  $\overline{\text{APD}}_{N+2}(x)$  the predicted APD distribution of the N+2th wave in our system (see red line in Fig. 5.5A, B, and C). Because wave N+2 only excites the points before the point of block (thus if  $T > \text{APD}_{N+1}(x)$ ), the DI preceding wave N+3 is given by:

$$\begin{aligned} \text{DI}_{N+3}(x) &= T - \overline{\text{APD}}_{N+2}(x) \\ &\text{(if } T > \text{APD}_{N+1}(x) \text{ , i.e. before point of block) ,} \\ \text{DI}_{N+3}(x) &= T \times 2 - \text{APD}_{N+1}(x) \\ &\text{(if } T < \text{APD}_{N+1}(x) \text{ , i.e. after point of block) .} \end{aligned} \quad (5.7)$$

We can again use the restitution curve to find

$$\text{APD}_{N+3}(x) = \text{APD}(\text{DI}_{N+3}(x)) . \quad (5.8)$$

In the same way as in (5.6), we have

$$\overline{\text{APD}}_{N+3}(x) = \int_{-\infty}^{+\infty} \text{APD}_{N+3}(\alpha) e^{-\left((x-\alpha)\frac{1}{A_3}\right)} d\alpha , \quad (5.9)$$

with  $\overline{\text{APD}}_{N+3}(x)$  the desired APD distribution of the N+3th wave (see green line in Fig. 5.5A, B and C). We observe that the APD distribution obtained via our iterative method is very close to the APD distribution obtained via experiments.

We tested our iterative method for different  $T$ , and in Fig. 5.5D we show the velocity at which the wave block region extends in space for these  $T$ , both obtained via our iterative method (red dots), as observed in experiments (black dots).

**CHAPTER 5. GLOBAL ALTERNANS INSTABILITY AND ITS EFFECT ON NON-LINEAR WAVE PROPAGATION: DYNAMICAL WENCKEBACH BLOCK AND SELF-TERMINATING SPIRAL WAVES.**

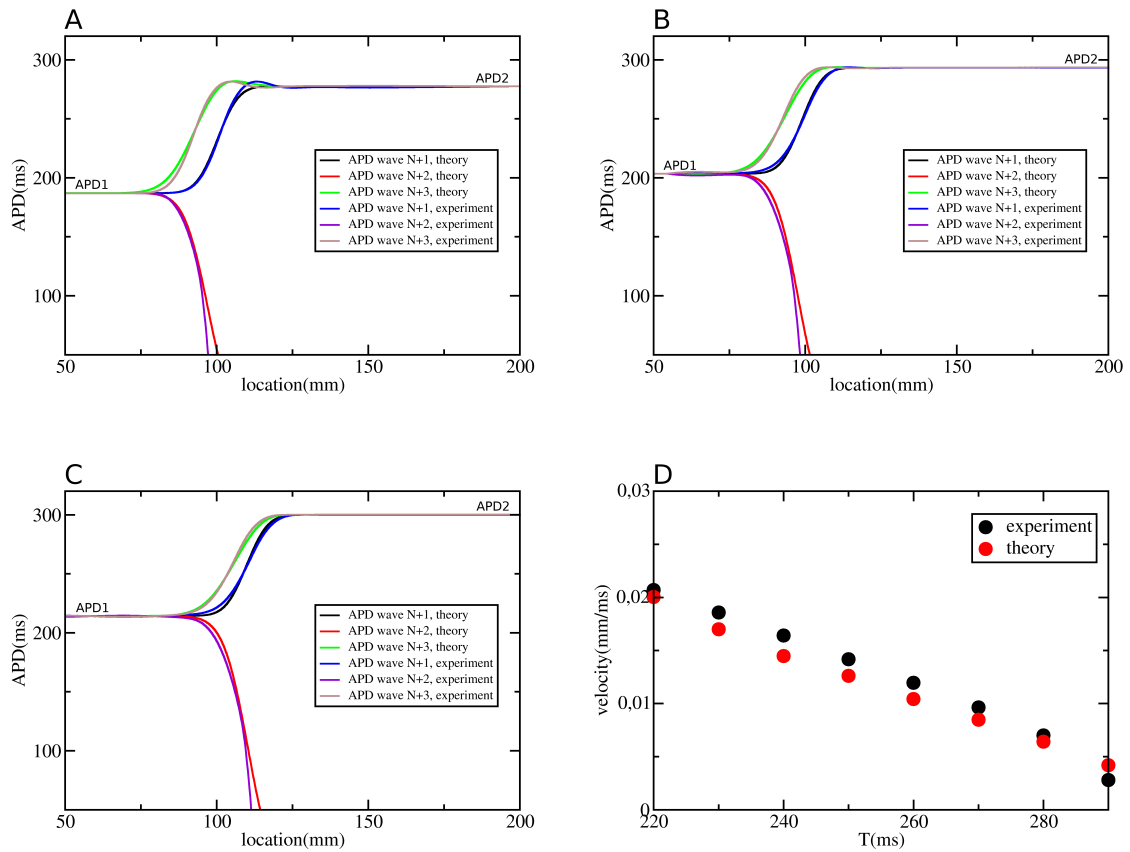


**Figure 5.5: Semi-analytical theory versus experiments.** Figure A, B and C show APD distribution of subsequent waves in our system, obtained both via our iterative method as in experiments, for a  $T$  equal to 220 ms, 250 ms and 270 ms, respectively. Black, red and green lines show APD distribution for the  $N+1$ th,  $N+2$ th and  $N+3$ th wave obtained via our iterative method. Blue, purple and brown lines show APD distribution for the  $N+1$ th,  $N+2$ th and  $N+3$ th wave obtained via simulations. D shows the velocity at which the wave block region extends in space, both found via our iterative method (red dots) and as observed in experiments (black dots).

### 3.3 GAI in 2D

In this section we show that similar effects occur in 2D models of cardiac tissue. For this, we consider a spiral wave in a transmural wedge of the heart (see Fig. 5.6). In Fig. 5.6 we show different timeframes, each consisting of two panels: the upper panel shows transmembrane voltage; the lower panel shows the period of excitation in each point. Similar to our 1D simulations, we temporarily block wave propagation (say wave  $N$ ) at a certain location in the tissue (see Fig. 5.6, time=840 ms, time=940 ms). There we block wave excitation at a point close to the right boundary of the tissue. As in 1D, this block is temporal, so wave  $N+1$  can excite these cells again (time=1080 ms, upper panel), however the period of excitation of this region is substantially longer (time=1080 ms, lower panel). As a consequence, the APD duration in the previously blocked region will be longer, and we see that wave  $N+2$  is blocked at a certain location (time=1260 ms, 1320 ms). This process is repeated, and we see that, similar to 1D, the wave block region (which corresponds to the region of period doubling) is shifted to the left (compare time=1680 ms with time=2300, 8840 ms). So, we have a persisting heterogeneity which, as was the case in 1D, shifts in space. We also see that when the block region approaches the core of the spiral it starts affecting its dynamics (see time=8840 ms). Eventually, interaction of the spiral wave with the wave block region (time=9220 ms, time=9280 ms) results in annihilation of the spiral from the tissue (time=9420 ms). Note, that the waveblock which we observe here, is what is called Wenckebach block in electrophysiology [147]. We see that in our case it is dynamic, as the area of the block shifts in space.

The simulation shown in Fig. 5.6 was performed for homogeneous cardiac tissue. We also did simulations in a more realistic setup, representing a transmural wedge in which the fibers rotate counterclockwise from endocardium to epicardium from -60 degrees at the epicardium to 60 degrees at the endocardium [132]. We refer to the method section for the diffusivity matrix under rotational anisotropy. So, we consider a similar situation as in Fig. 5.6, but now in a medium with rotational anisotropy (see Fig. 5.7).

We follow the same protocol as in Fig. 5.6 and show results of the simulations in Fig. 5.7. We block a wave (at time=800 ms), and again observe that a persisting heterogeneity is created (time=1060 ms). In the same way as in Fig. 5.6, this region extends in space (compare for instance time=1060 ms with time=1920, 5120 ms). However, as the region approaches the core of the spiral wave, dynamics become more complex than in Fig. 5.6: at time=5180, 5240 ms, we see that a new spiral is formed and we get two counterrotating spiral waves (time=5240, 5380, 5540, 5660 ms). However, after a few rotations these spiral waves eliminate each other, and we end up with the quiescent state.

We note that we did many similar simulations, in which we varied the position of the initial spiral (closer, or further away from the boundaries of the medium), and each time we observed the same pattern: the wave block region approaches the core of the spiral wave, and eventually the spiral is removed from the tissue.

Finally, we also investigate the effect of a partial wave propagation block, as this may be considered as a more realistic situation (we refer to Fig. 5.8). At time=940 ms, we partially block wave excitation (time=1020, 1080 ms). When the next wave arrives at the wave block region, we remove the obstacle, and as in the previous cases a dynamical heterogeneity is created (time=1200, 1280, 1380 ms). Interaction of this heterogeneity with the next excitation wave leads to the formation of wavebreaks (time=1480 ms). However, these wavebreaks propagate around the dynamical heterogeneity and excite the cells inside this region the

**CHAPTER 5. GLOBAL ALTERNANS INSTABILITY AND ITS EFFECT ON NON-LINEAR WAVE PROPAGATION: DYNAMICAL WENCKEBACH BLOCK AND SELF-TERMINATING SPIRAL WAVES.**

---

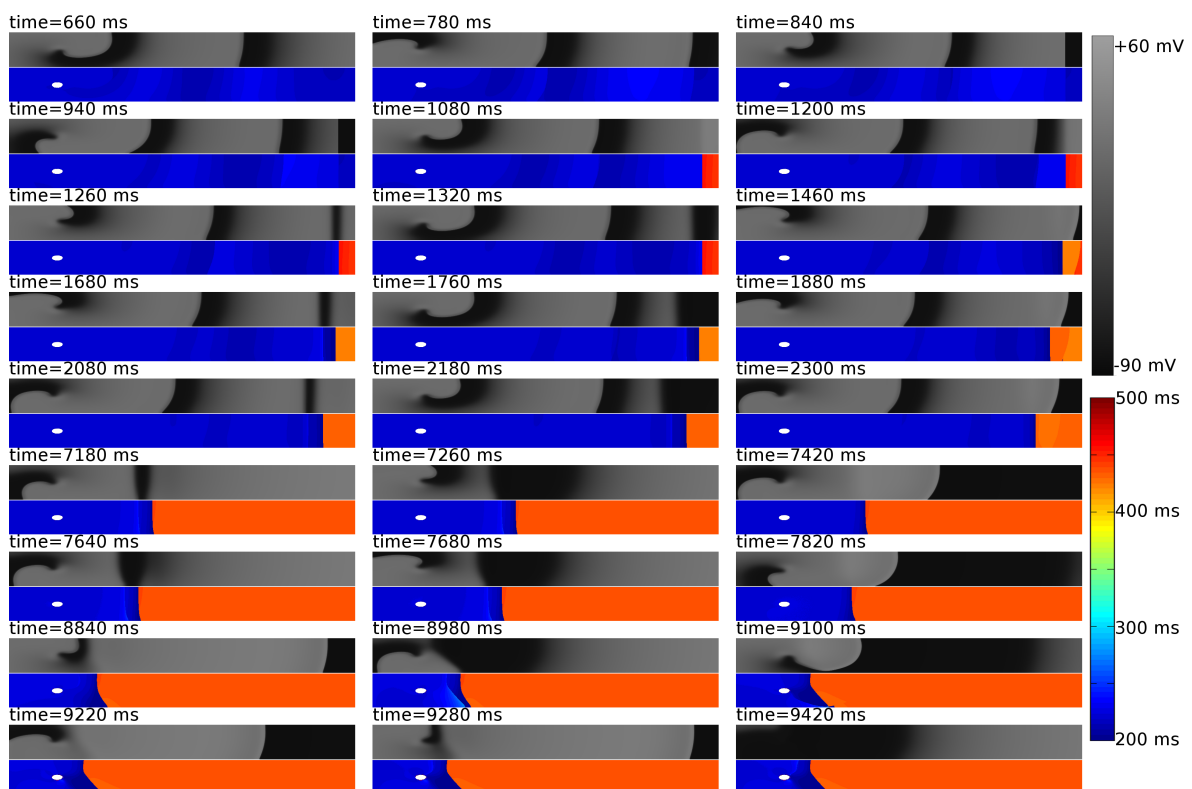


**Figure 5.6: GAI in a 2D medium.** Spiral wave dynamics after temporal block of excitation at time=780 ms (shown by timeframes time=840 ms, time=940 ms). Upper panel of each timeframe shows transmembrane voltage; lower panel shows period of excitation. Size of the medium is  $20 \times 2$  cm.

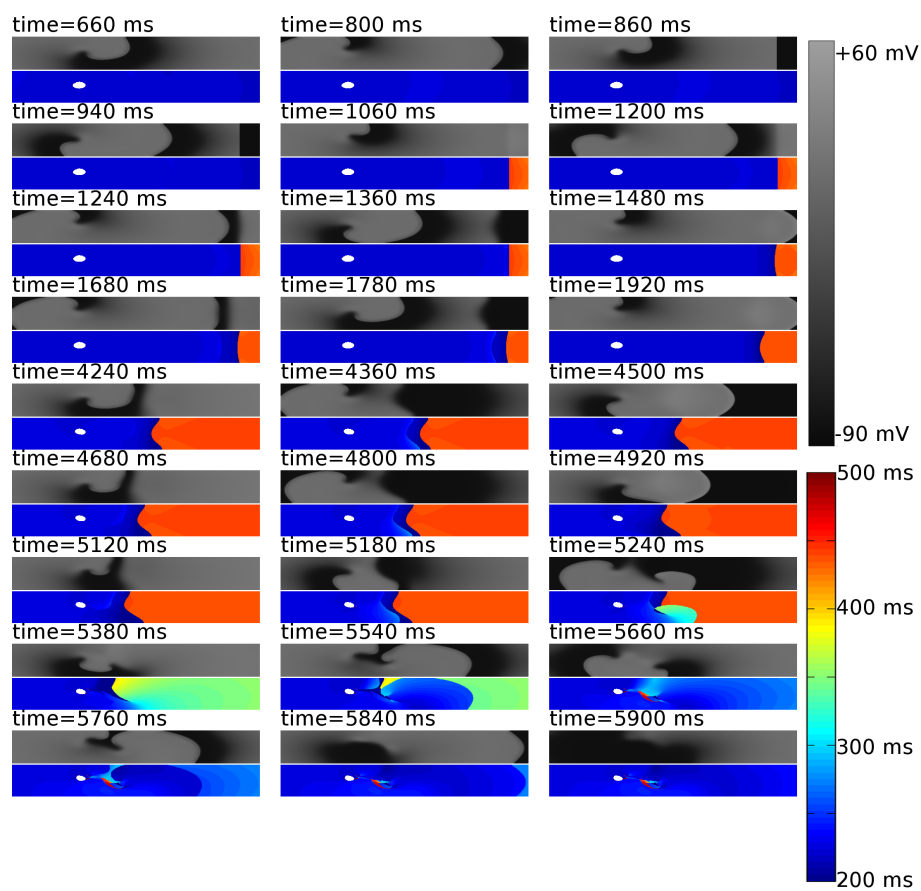


**Figure 5.7: GAI in a 2D medium with rotational anisotropy.** Spiral wave dynamics after temporal block of excitation at time=800 ms (shown by timeframes time=860 ms, time=940 ms). Upper panel of each timeframe shows transmembrane voltage; lower panel shows period of excitation. Size of the medium is  $12 \times 1.6$  cm.

## CHAPTER 5. GLOBAL ALTERNANS INSTABILITY AND ITS EFFECT ON NON-LINEAR WAVE PROPAGATION: DYNAMICAL WENCKEBACH BLOCK AND SELF-TERMINATING SPIRAL WAVES.

---

moment the refractory period ends there (time=1560 ms). As a consequence, the initial heterogeneity disappears (time=1700, 1800 ms, lower panel). Interestingly, these wavebreaks create new dynamical heterogeneities (time=1800, 2900 ms) which extend in space (compare lower panel of time=3060ms and time=3280, 3440 ms), and eventually one of the breaks disappears, and we end up with two counterrotating spiral waves: the original spiral wave and a new one (time=3440, 3560, 4220 ms). After some time, interaction of these two spirals results into the annihilation of the newly formed spiral wave (time=4280, 4420 ms) and a new dynamical heterogeneity is created (time=4680, 4740 ms). Again, interplay of this heterogeneity with the spiral leads to the formation of wavebreaks (time=4900, 4980 ms). This small dynamical heterogeneity extends in space (compare the light blue region in the lower panel at time=5120 ms with time=5860, 7300 ms) and moves to the core of the spiral wave. Eventually, interaction of the spiral with this small heterogeneity and boundaries of the medium results in spiral wave annihilation (time=7400, 7500, 7560, 7720 ms).

We conclude that a GAI is also present in 2D and has a substantial effect on spiral wave formation, or eventual removal of spirals. From the spatial frequency distribution, we again see that we have a clear (dynamical) Wenckebach 1:2 block. Interestingly, this block occurs in homogeneous tissue and extends in space. In case of a partial wave propagation block, the dynamics are more complex as we have interaction of different wavebreaks. However, also in that case we observe dynamical heterogeneities which extend in space, reminiscent of GAI, and eventually remove the spirals.

## 4 Discussion

---

In this chapter we show that disturbances of wave propagation, such as temporal block of propagation, may have important effects on spiral wave dynamics, and can lead, for example, to spiral wave termination. They can also substantially affect spatial excitation patterns and result in dynamical Wenckebach blocks for wave propagation.

In our simulations such blocks were created artificially. However, they can also occur in natural conditions. For example Sharifov et al. [125] showed that parasympathetic excitation and local release of acetylcholine can result in local temporal blocks of propagation and can even induce new spiral waves in the heart. Here we show that such processes can be affected by restitution properties of cardiac cells and can result in the spatial extension of initially induced block areas, making them more prone to spiral wave formation. Mechanism of this spatial extension was investigated here in details (see section 3.2). Indeed we showed that because of restitution properties we obtain a dynamic heterogeneity in cardiac tissue, and due to electrotonic effects it shifts and extends in space.

Note that although we studied a homogeneous medium, our results are also applicable for heterogeneous tissue. In that case, we can have an initial block of excitation occurring at the heterogeneity, for example due to the general mechanism described in [87, 73]. What is important here is that due to restitution effects such initial areas of block will extend in space and thus will result in larger heterogeneities which can more likely induce spirals. This result is very important, as recent experimental studies showed small size heterogeneities in transmural wedges of the human heart [40, 77]. We studied these type of heterogeneities in previous publications [24, 26], and we indeed found that they can create spiral waves but only after they had extended in space. In this chapter, we illustrate that GAI is the possible mechanism of this spatial extension of the heterogeneity.



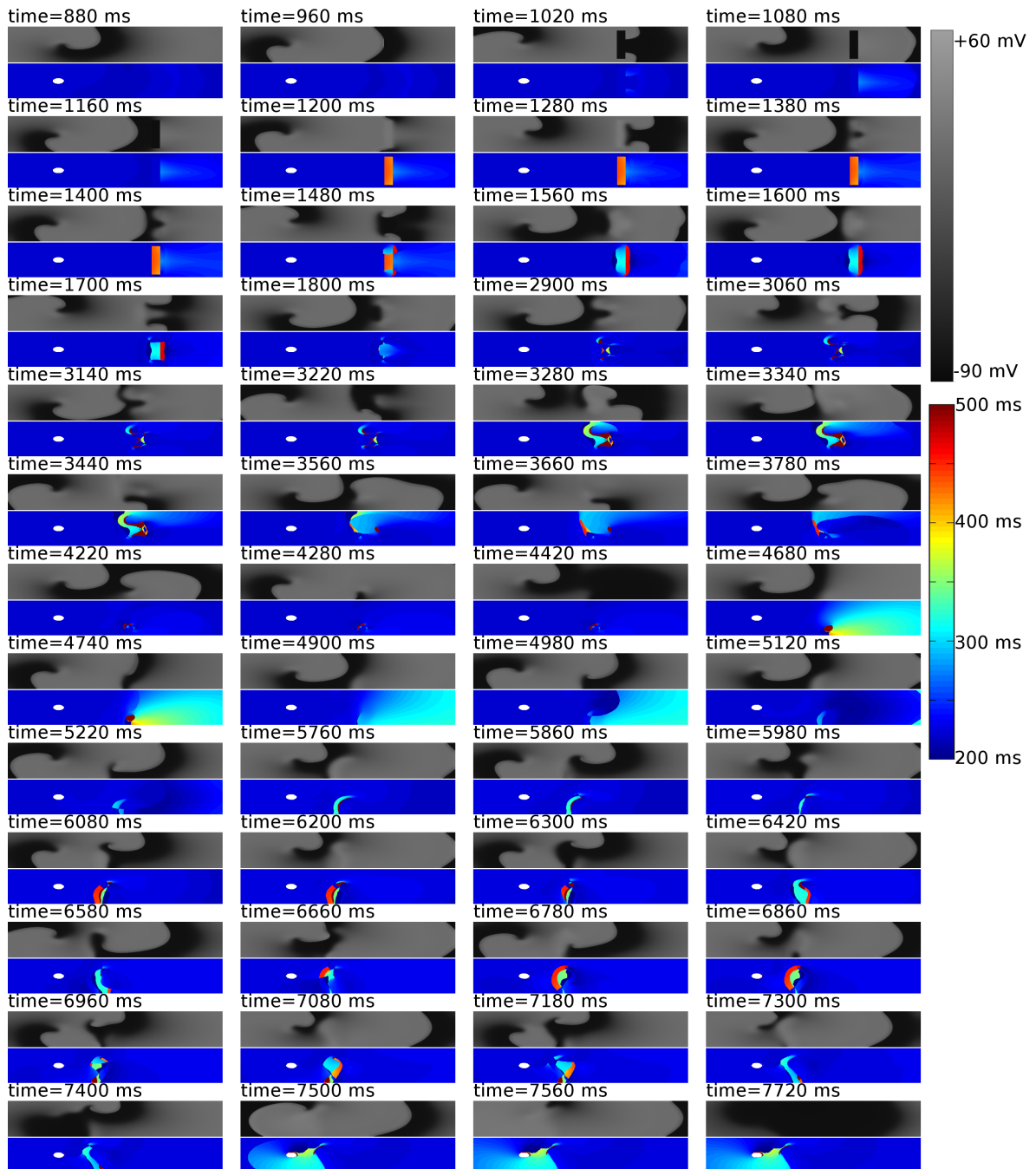


**Figure 5.8: GAI in a 2D medium with rotational anisotropy.** Spiral wave dynamics after temporal and partial block of excitation at time=940 ms (shown by timeframes time=1020 ms, time=1080 ms). Upper panel of each timeframe shows transmembrane voltage; lower panel shows period of excitation. Size of the medium is  $12 \times 2$  cm.

## **CHAPTER 5. GLOBAL ALTERNANS INSTABILITY AND ITS EFFECT ON NON-LINEAR WAVE PROPAGATION: DYNAMICAL WENCKEBACH BLOCK AND SELF-TERMINATING SPIRAL WAVES.**

---

Restitution properties of cardiac tissue were always considered as an important mechanism underlying the formation of spiral waves. Multiple studies [62, 112, 114, 36] showed that steep restitution can result in dynamical instabilities, possibly leading to fibrillation. Here, we show that substantial effects of restitution at the global level can also be expected according to formula (5.2). Thus, we show that, although steep restitution gives rise to dynamical instabilities, it is not a necessary condition: the global shape of the restitution curve also plays an important role. It would be interesting to investigate formula (5.2) on a patient specific restitution curve, and study if it is related to the onset of cardiac arrhythmias.

---

# 6

## Setting up a database structure for modeling the human heart

### 1 Introduction

---

In recent years, the amount of data available from human hearts has grown exponentially. For example, one of the leading groups in the world on experimental cardiac electrophysiology, the group of Prof. Efimov from the Department of Biomedical Engineering at Washington University in St. Louis, already performed experiments on more than 200 human hearts (see Fig. 6.1), both on failing and non failing human hearts (Fig. 6.2).

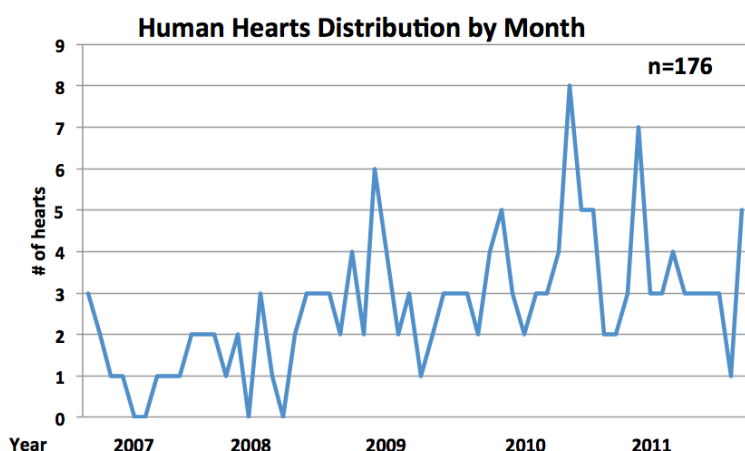


**Figure 6.1:** Number of human hearts on which the group of Prof. Efimov already performed experiments.

Because of this increasing amount of data, it becomes very useful to collect these data in one database. This would allow research groups to compare their data to data measured by other groups; upload data in a standardized way; download data from the database. Because this database would give a good overview of the data available, it would act as a bridge between experimental and modeling groups.

Here, we describe the first steps in the development of this platform. We started developing this database in close collaboration with the group of Prof. Efimov. Together with this group we decided on the general structure of the database. This structure was created via the content management system Drupal. We describe the structure of the database in the first section. In the second section, we describe how data can be added to the database. Starting

## CHAPTER 6. SETTING UP A DATABASE STRUCTURE FOR MODELING THE HUMAN HEART

from this structure and data, we created a website where users can search for specific data and download the sought data, which we highlight in the last section.

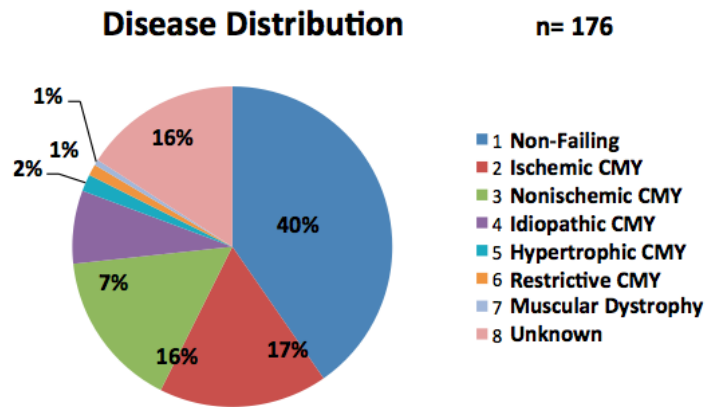


**Figure 6.2:** Disease distribution of the human hearts on which the group of Prof. Efimov performed experiments.

## 2 Structure of the database

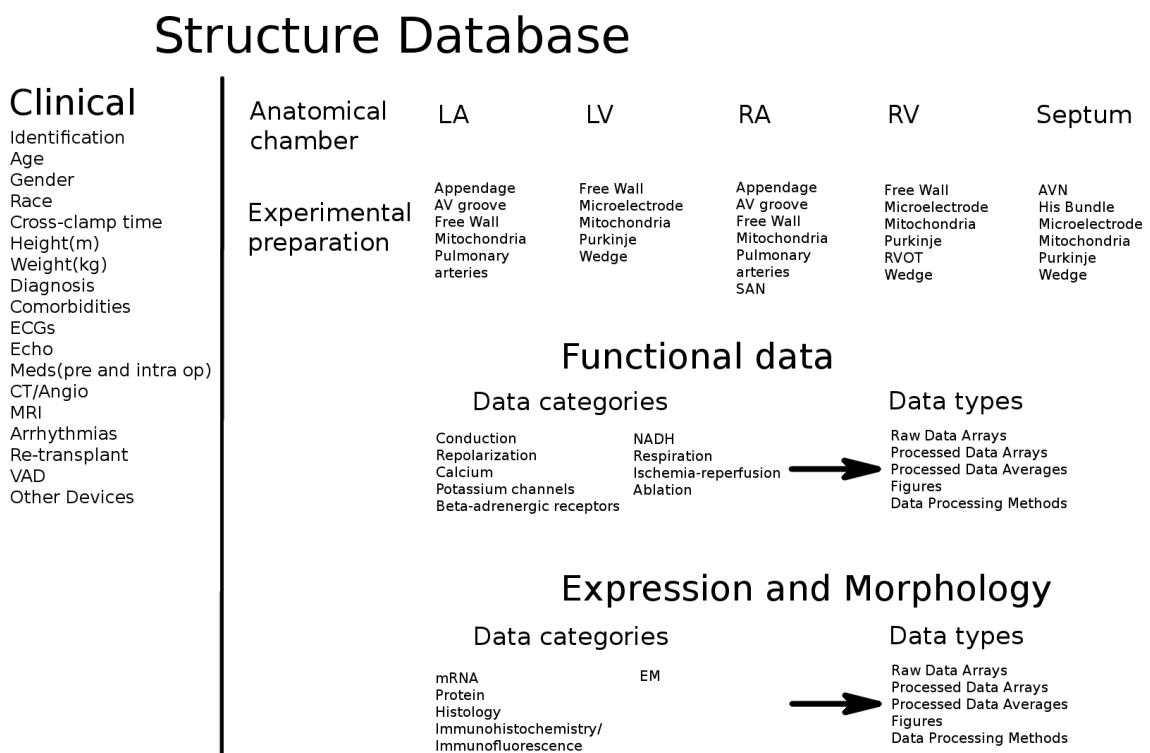


**Figure 6.3:** A schematic overview of the structure of the database.

### 3. FEATURES OF THE DATABASE

In close collaboration with the group of Prof. Efimov, we've set up a structure for the database. In Fig. 6.3, we show a schematic overview of this structure. As is shown in Fig. 6.3, we store many different types of data: clinical data; positional information; different types of experimental preparations; functional data; data obtained from expression and morphology experiments.

The clinical data which will be stored in the database is listed in Fig. 6.3. These clinical parameters are fields which can be filled in when a new heart (which is a content type in our database) is added to the database (see Fig. 6.4).

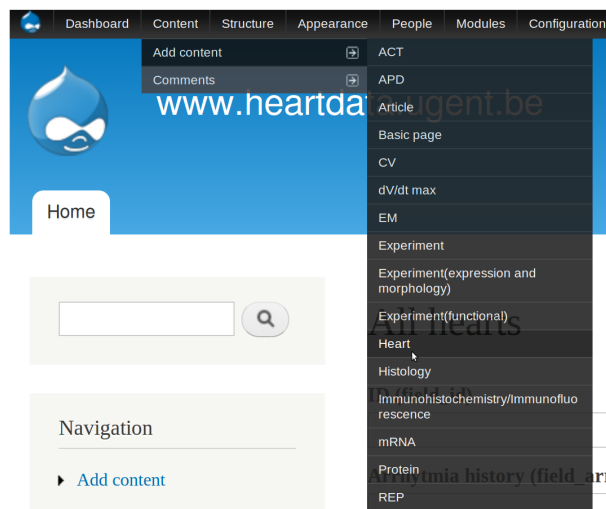


**Figure 6.4:** We show how to add content to the database using Drupal.

When a heart is added to the database, it is possible to add experiments which were performed on this heart. As is shown in Fig. 6.3 and Fig. 6.4, two different types of experiments can be added to a heart: functional experiments and experiments on expression and morphology. The data categories of these two types are listed in Fig. 6.3. Information on the anatomical chamber where the experimental preparation originated from, and the type of experimental preparation can be added as data to each experiment. The different anatomical chambers and the possible experimental preparations for each chamber are listed in Fig. 6.3.

For each data category different data types can be uploaded: raw data, processed data, figures and also data processing methods. This last type should describe the experimental protocol used to generate the data.

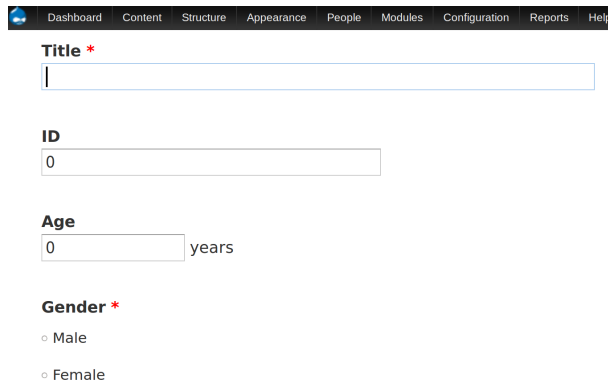
## 3 Features of the database

### 3.1 Upload data

In this paragraph, we describe how to upload data to the database using Drupal. We start by explaining how to upload a new heart and the corresponding clinical data. As already shown in Fig. 6.4, a new heart can be added to the database by navigating to the menu 'Content', and then by clicking on 'Heart'.

## CHAPTER 6. SETTING UP A DATABASE STRUCTURE FOR MODELING THE HUMAN HEART

---

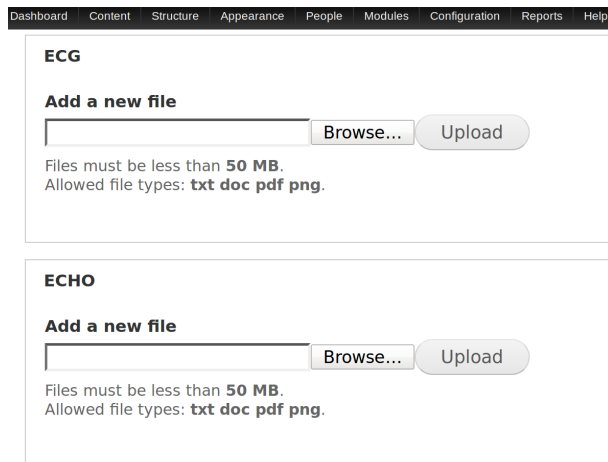


The screenshot shows a Drupal administration interface with a navigation menu at the top containing 'Dashboard', 'Content', 'Structure', 'Appearance', 'People', 'Modules', 'Configuration', 'Reports', and 'Help'. Below the menu is a form for adding a new heart. The form contains the following fields:

- Title \***: A text input field.
- ID**: A text input field containing the value '0'.
- Age**: A text input field containing the value '0', followed by the text 'years'.
- Gender \***: Two radio button options: 'Male' and 'Female'.

**Figure 6.5:** We show how to add clinical data when adding a new heart to the database.

If we do this, we arrive at a form we need to fill out. This form handles all the parameters listed in Fig. 6.3 in the section ‘Clinical’. In Fig. 6.5 and Fig. 6.6, we show how this form looks like in Drupal.



The screenshot shows a Drupal administration interface with a navigation menu at the top containing 'Dashboard', 'Content', 'Structure', 'Appearance', 'People', 'Modules', 'Configuration', 'Reports', and 'Help'. Below the menu is a form for adding clinical data. The form contains two sections:

- ECG**: A section titled 'Add a new file' with a text input field, a 'Browse...' button, and an 'Upload' button. Below the input field, it says 'Files must be less than 50 MB. Allowed file types: txt doc pdf png.'
- ECHO**: A section titled 'Add a new file' with a text input field, a 'Browse...' button, and an 'Upload' button. Below the input field, it says 'Files must be less than 50 MB. Allowed file types: txt doc pdf png.'

**Figure 6.6:** We show how to add clinical data when adding a new heart to the database.

This clinical data ranges from simple information like ‘Gender’, ‘Age’, an ‘ID’ number (Fig. 6.5), to more complex information like ‘ECG’ and ‘ECHO’ (Fig. 6.6). For each of these clinical parameters, we made it possible to store information in the most self-evident way. For example, for ‘Age’, we just need to fill in a number, and for ‘ECG’, ‘ECHO’, ‘CT’, ‘MRI’ we can upload a figure or a text file. Data for parameters like ‘Arrhythmia history’, ‘Medication’ is stored as text. For these parameters there are a lot of possible values (e.g. one type of arrhythmia can sometimes be described in different ways), but the autocomplete option makes sure that information for these parameters remains consistent between hearts.

In the last part of the form, it is possible to link experiments performed on the heart we upload (see Fig. 6.7). To do this, we need to create an experiment first.

### 3. FEATURES OF THE DATABASE



**Figure 6.7:** We illustrate how to link experiments to a particular heart.

This is done in the same way as for the content type ‘Heart’. So, as shown in Fig. 6.4, we should navigate to the menu ‘Content’, and then click on ‘Experiment(functional)’ or ‘Experiment(expression and morphology)’, depending on which type of experiment we want to add. If we do this, we arrive at a form, which we need to fill in. There we can provide information regarding this experiment. This includes the anatomical chamber where the experimental preparation originated from; the type of experimental preparation; the data category; description of data processing methods; links to the different measurements performed in this experiment. For anatomical chamber, type and data category we just need to tick a box (or boxes). See Fig. 6.8. Input of description of data processing methods is done by uploading a (text) file to the database.

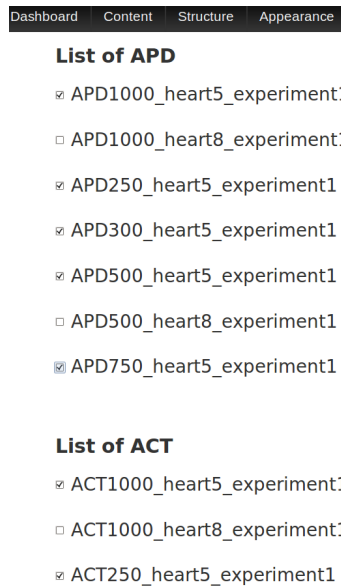
Anatomical chamber	Experimental preparation	Data category
<input type="checkbox"/> N/A	<input type="checkbox"/> N/A	<input type="checkbox"/> N/A
<input type="checkbox"/> LA	<input type="checkbox"/> Appendage	<input type="checkbox"/> Ablation
<input checked="" type="checkbox"/> LV	<input type="checkbox"/> Atrioventricular groove	<input type="checkbox"/> Beta-adrenergic receptors
<input type="checkbox"/> RA	<input checked="" type="checkbox"/> Free wall	<input type="checkbox"/> Calcium
<input type="checkbox"/> RV	<input type="checkbox"/> His Bundle	<input checked="" type="checkbox"/> Conduction
<input type="checkbox"/> Septum	<input type="checkbox"/> Microelectrode	<input type="checkbox"/> Ischemia-reperfusion
	<input type="checkbox"/> Mitochondria	<input type="checkbox"/> NADH
	<input type="checkbox"/> Pulmonary arteries	<input type="checkbox"/> Potassium channels
	<input type="checkbox"/> Purkinje	<input checked="" type="checkbox"/> Repolarization
	<input type="checkbox"/> Right ventricular outflow tract	<input type="checkbox"/> Respiration
	<input type="checkbox"/> Sinoatrial node	
	<input type="checkbox"/> Wedge	

**Figure 6.8:** Input of information on anatomical chamber, type of experimental preparation and data category for a certain experiment is done by ticking a box (or boxes).

In the same way as we did for the content type ‘Heart’, we can link measurements performed in the experiment using this form (for instance, we can add action potential duration (APD) measurements or activation (ACT) measurements to an experiment: see Fig. 6.9).

## CHAPTER 6. SETTING UP A DATABASE STRUCTURE FOR MODELING THE HUMAN HEART

---



Dashboard | Content | Structure | Appearance

**List of APD**

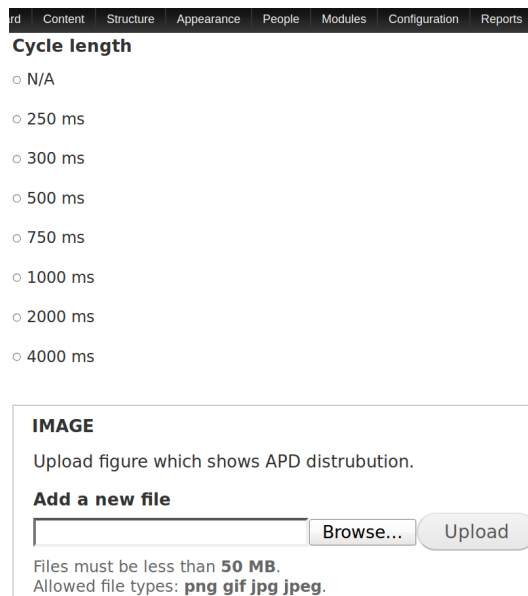
- APD1000\_heart5\_experiment1
- APD1000\_heart8\_experiment1
- APD250\_heart5\_experiment1
- APD300\_heart5\_experiment1
- APD500\_heart5\_experiment1
- APD500\_heart8\_experiment1
- APD750\_heart5\_experiment1

**List of ACT**

- ACT1000\_heart5\_experiment1
- ACT1000\_heart8\_experiment1
- ACT250\_heart5\_experiment1

**Figure 6.9:** We show how to link measurements performed in an experiment to a particular experiment.

To do this, we first need to make content of the type we want to link to the experiment (this content was already made in the screenshot in Fig. 6.9). In this case, this would mean that we add content of type ‘APD’ and ‘ACT’ to the database. This is done in the same way as it was done for content of type ‘Heart’ and ‘Experiment(functional)’ or ‘Experiment(expression and morphology)’ (see Fig. 6.4). Again, if we navigate to the menu ‘Content’ and click on ‘APD’ (or ‘ACT’), we arrive at a form we can fill in (see Fig. 6.10).



rd | Content | Structure | Appearance | People | Modules | Configuration | Reports

**Cycle length**

- N/A
- 250 ms
- 300 ms
- 500 ms
- 750 ms
- 1000 ms
- 2000 ms
- 4000 ms

**IMAGE**

Upload figure which shows APD distribution.

**Add a new file**

Files must be less than **50 MB**.  
Allowed file types: **png gif jpg jpeg**.

**Figure 6.10:** We show how to add a measurement performed on a certain experimental preparation to the database.

In the case we want to upload data on APD, we can upload information on cycle length;



### 3. FEATURES OF THE DATABASE

figure(s); raw data; processed data. In a similar way, we can add other measurements to an experiment (and to a certain heart) using Drupal.

#### 3.2 Download data from the website

Next to uploading data to the database, it is also possible to search in the database and download data from the database. If we go to ‘www.heartdata.ugent.be’, we arrive at the opening page as shown in Fig. 6.11. There, we see a list of all the hearts uploaded to the database, info on gender of the heart, and if the heart was a failing or a non-failing heart. Via the search bars (with autocomplete option), it is possible to filter the data. For instance, if we fill in ‘Ischemic-cardiomyopathy’ in the search bar ‘Diagnosis’, only the hearts with ischemic-cardiomyopathy will be listed.

Title	Failing / Non failing	Gender
Heart2	Failing	Female
Heart3	Failing	Male
Heart7	Failing	Male
Heart8	Non-Failing	Male

**Figure 6.11:** Opening page of the website ‘www.heartdata.ugent.be’ shows a list of all the hearts uploaded to the database. Via the search bars it is possible to filter the data.

Next, if we click on a heart (say, for example ‘Heart5’) listed on the opening page, we arrive at the next layer of our website (see Fig. 6.12). There we get a list of all the clinical parameters we filled in for this heart, as explained in the previous section. Next to that, we get an overview of all experiments performed on this heart. In this case, only one experiment was performed, namely a functional experiment.

## CHAPTER 6. SETTING UP A DATABASE STRUCTURE FOR MODELING THE HUMAN HEART

---

### Heart5

[View](#) [Edit](#)

Submitted by [agdefauw](#) on Wed, 10/02/2013 - 10:52

**Age:**  
20.00years

**Gender:**  
Male

**Failing / Non failing:**  
Non-Failing

**Diagnosis:**  
[Non-failing](#)

**Cause of death:**  
[Drug overdose](#)

**Arrhythmia history:**  
[N/A](#)

**Ventricular assist device:**  
No

**Other devices:**  
[N/A](#)

**Re-transplant:**  
No

**Experiments(functional):**  
[Experiment\(functional\)\\_heart5](#)

**Figure 6.12:** Overview of all clinical parameters for, and experiments performed on, ‘Heart5’.

Again, if we click on an experiment, we go to the following layer of our database (see Fig. 6.13). In Fig. 6.13, we see a list of all the measurements performed in this experiment and also information on anatomical chamber, type of experimental preparation and the data category. This particular experiment contains several measurements on: action potential duration (APD), activation (ACT), repolarization time (REP). These measurements are all listed in the corresponding category, i.e: ‘List of APD’, ‘List of ACT’ and ‘List of REP’.

## Experiment(functional)\_heart5

View Edit

Submitted by [agdefauw](#) on Thu, 03/20/2014 - 08:37

Anatomical chamber:  
[LV](#)

Experimental preparation:  
[Wedge](#)

Data category:  
[Conduction](#) [Repolarization](#)

**List of APD:**  
[APD1000\\_heart5\\_experiment1](#)  
[APD250\\_heart5\\_experiment1](#)  
[APD300\\_heart5\\_experiment1](#)  
[APD500\\_heart5\\_experiment1](#)  
[APD750\\_heart5\\_experiment1](#)

**List of ACT:**  
[ACT1000\\_heart5\\_experiment1](#)  
[ACT250\\_heart5\\_experiment1](#)  
[ACT500\\_heart5\\_experiment1](#)

**List of REP:**  
[REP1000\\_heart5\\_experiment1](#)  
[REP300\\_heart5\\_experiment1](#)

**Figure 6.13:** Overview of information on anatomical chamber, type of experimental preparation, data category and measurements performed in this experiment.

Now, we can click on a measurement. This brings us to the lowest layer of our database. In Fig. 6.14, we show an example of such a measurement (APD). We see at which cycle length the measurement of APD was performed. As discussed in the previous section, we also get a figure and a file with raw data which can both be downloaded by the user. Other measurements, like ACT, REP or data on expression and morphology can be accessed in a similar way.

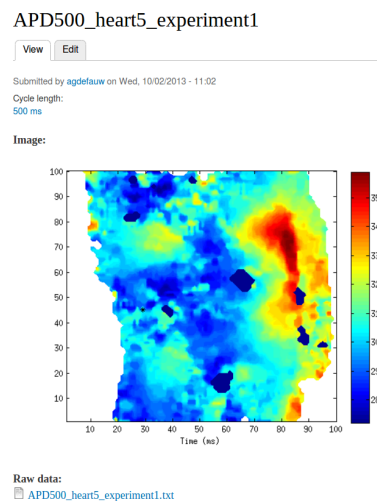


**Figure 6.14:** We show all the data available for an action potential duration measurement performed during a certain experiment. We see information on cycle length, a figure and raw data.

### 4 Conclusion and future perspective

---

In the previous sections we explained the general structure of the database, and illustrated how data can be added to, or downloaded from the database. It should be clear that Drupal makes it easy for the user to manage the content of the database. We also note that Drupal allows it for the user to change the structure of the database up to a certain degree, if this would be necessary. For example, it is easy to add other fields to store ‘Clinical’ data, other types of ‘Experimental preparation’, ‘Data categories’ etc.

However, we note that the prototype of the database is still under development, and has several limitations, which would be interesting to overcome in future work. The most obvious limitation of the prototype is that it does not allow to perform statistics on the data. Allowing the user to compare the different data stored in the database, in a systematic way, would be both valuable for modelers as for experimentalists. It would also be useful to make it possible for the user to upload data in an automated way. For instance data on gene expression tend to be very extensive, so uploading such data to a database by hand can easily become a time consuming task for the user. Finally, another future direction would be to link data stored in the database to models of the human heart. For example, data on spatial expression of genes coding ion channels, exchangers and pumps could be linked to different parameters of ionic models of the human heart. It would thus be valuable to also store the different parameter sets of the models which can fit, or correspond to, a particular experimental measurement.

---

# 7

## Summarizing discussion

---

### 1 A review

---

In this thesis we study the effect of heterogeneities on electrical waves of excitation in the human heart. In particular, in **chapters 2, 3, 4**, we study APD heterogeneity of cardiac tissue and its role in initiation of spiral waves. We also study the dynamics of spiral waves around these heterogeneities. Then, in **chapter 5** we focus on the effect of a dynamical heterogeneity due to restitution effects on wave propagation and spiral wave dynamics, and apply it to explain the mechanisms of the effects considered in **chapters 3, 4**. **Chapter 6** is devoted to the collection of data on human heart heterogeneity, as used in this thesis.

In **chapter 2**, we show that electrotonic effects in heterogeneous cardiac tissue can with good accuracy be described using a linear Green's function approach and with a good approximation the Green's function is given by a Gaussian. In particular, we show that APD at tissue level can be found by a convolution of APD distribution at cell level with a bell-shaped Gaussian function (forward problem). We also use this formalism to develop an approach to find properties of individual cells from measurements at tissue level (inverse problem). We can solve the forward problem with a reasonable high accuracy, and even for steep gradients, we can predict the maximal value of APD in the coupled system, which is important for characterization of the extent of heterogeneity. Regarding the inverse problem, our solution is also promising. However, for steep gradients, we have an additional oscillatory component outside the heterogeneity, because of which we can not determine the maximal amplitude with sufficient degree of certainty. This oscillatory component is a well known feature of inverse solutions. However, we note that we applied the simplest method for solution of the inverse problem and that it is one of the most studied in applied mathematics, so our solution can certainly be improved. For example, different norms of Tikhonov regularization could be used. This would require specific investigation and the development of non-standard software, which is outside the scope of this thesis. The main value of this chapter for applications, is that we can relate heterogeneity at cellular and tissue levels. We can predict properties of cardiac cells from tissue measurements or estimate how given heterogeneity of cardiac cells will manifest itself in tissue. Note that this is a non-trivial problem as heterogeneity at cell level can be 200 to 500 % more than at tissue level (see e.g. Fig. 2.11 from **chapter 2**).

In **chapter 3**, we use the TP06 model for human cardiac tissue to model small size ionic heterogeneities, similar to those measured by Glukhov et al. [40] in wedge preparations of the human left ventricle. For an initial estimate of the underlying properties of the cells inside these heterogeneities, we use the approach developed in **chapter 2**. We study the effects of these type of heterogeneities on the onset of spiral waves and the dynamics of spiral waves around such heterogeneities. We find that under high frequency forcing, spiral waves can be

formed. However, these new sources are not only initiated by break formation as in classical mechanisms [73, 102], but also by interaction of wavebreaks with other upcoming waves, eventually leading to the formation of a single spiral wave anchored around the heterogeneity. We study the dynamics of these anchored spiral waves and find that we have two distinct values of period of excitation: one inside and one outside the heterogeneity. We also show that each of these periods is mainly determined by properties of cardiac tissue at the corresponding region: increase of the refractory period results in increase of the period. Interestingly, we find that, when we increase the extent of heterogeneity, the increase in period is not gradual. At this bifurcation point, the period suddenly increases around 1.3 times.

In previous modeling studies [1, 102, 2], the main effects of heterogeneity on spiral wave dynamics is drift along the heterogeneity boundary. Here, the main effect is anchoring of the spiral to the heterogeneity. Also, we get a torsades de pointes like ECG and an ECG reminiscent of polymorphic tachycardia. However, in our case it is a result of a different frequency of excitation of tissue inside and outside the heterogeneity and not a result of shift of the excitation source in space.

Anchoring of spiral waves to obstacles was already studied intensively, both in 2D and 3D [22, 142, 152, 81, 156, 81, 131]. However, in all these cases, spirals were anchored to inexcitable obstacles. In **chapter 3** we show that a heterogeneity which is excitable can also anchor spirals, and that anchoring results in more complex dynamics compared to anchoring around inexcitable obstacles, because of a direct influence of the heterogeneity on wave rotation.

We checked that our results on the dynamics of a spiral wave around a heterogeneity are general, and also hold for heterogeneities of different size, shape and induced by modification of different parameters of our model. Our results are also valid for tissue with rotational anisotropy.

Overall, in **chapter 3** we explain possible wave dynamics at realistic heterogeneities measured in the human heart, in terms of formation of new sources of arrhythmias in 2D models of cardiac tissue.

In **chapter 4**, we continue our research on the effect of small size ionic heterogeneities on spiral wave dynamics. Again, we model heterogeneities with a size and magnitude similar to these measured by Glukhov et al. in [40], but now both in 2D and in an anatomical model of the human ventricles. We show that such heterogeneities can not only anchor, as we found in **chapter 3**, but can also attract spirals rotating at a substantial distance from the heterogeneity. In particular, in 2D these type of heterogeneities can attract and eventually anchor a spiral rotating within 6 cm along the fibers, 4 cm across the fibers and around 5 cm at 45 degrees. In the whole heart, if the degree of heterogeneity is large enough, it is always anchored (or eventually removed). Thus, the basin of attraction of these ionic heterogeneities is very substantial in comparison to the typical size of the human heart, whose height is around 10 cm. Interestingly, this attraction over large distances is a property of ionic heterogeneities alone, i.e. it does not hold for inexcitable obstacles. Also, in our anatomical model of the ventricles, we demonstrate that if the heterogeneity is located close to the base, it can not only attract and anchor a spiral wave, but can also remove it. This is an interesting result, as it suggests that some types of heterogeneities have an anti-arrhythmic effect.

The mechanism of attraction of spiral waves to heterogeneities can be attributed to a generic behavior of spirals in heterogeneous tissue. In [116, 102, 138] it was shown that spirals tend to drift to the regions of longer period of rotation. Longer period of rotation of a spiral is normally associated with a longer APD [100, 138]. Thus it is very natural to expect that in our simulations the spirals are to be attracted by the heterogeneity, as in our

case the heterogeneity has a longer APD compared to the rest of the tissue. Remarkably, the process of attraction observed here is not a continuous process in which the spiral slowly drifts towards the heterogeneity, as reported in these previous studies, but a stepwise process in which the spiral is shifted closer to the heterogeneity due to a complex interaction with the heterogeneity.

In [123] the authors investigated the dynamics of spiral waves in a low dimensional (Panfilov) model [95] and the ionic Luo-Rudy I model [78] of cardiac tissue in presence of large squared ionic heterogeneities and inexcitable obstacles, placed at various locations in cardiac tissue. Different dynamics, including spiral turbulence, a rotating spiral and the quiescent state were reported. It was shown that a fractal-like boundary separates the basins of attraction of these regimes. One of the regimes observed was anchoring of a spiral wave around the heterogeneity. In a follow up study [122], they compared the dynamics of waves around large squared inexcitable obstacles and ionic heterogeneities in four models of cardiac tissue [136, 11, 95, 78]. In all models they report various regimes of interaction of spirals with the obstacles. These regimes depend, in a complex way, on the obstacle location. In some situations they also observed anchoring of spirals. It would be interesting to study which of the reported regimes in [123, 122] are found when heterogeneities and obstacles of size and shape derived from direct experimental measurements would be used.

In [80] the authors studied the interaction of a spiral wave with a heterogeneity with a shorter APD in an anatomical model of the rabbit and the pig heart. There it was shown that a spiral rotating close to the heterogeneity can anchor around it and that parts of this wave can enter the region in which this inhomogeneity is present. So it seems that even heterogeneities with a shorter APD than the surrounding tissue can serve as anchoring sites for spiral waves (see also [122, 81]).

Overall, in **chapter 4** we studied the possibility of anchoring of an existing spiral wave to heterogeneities of realistic size. This is a continuation of the research performed in **chapter 3**, but now focused on the aspect of anchoring of spiral waves and performed using anatomically accurate models. A new unexpected result here is that such heterogeneity can attract spiral waves and in some cases such attraction can terminate the arrhythmia.

In **chapter 5**, we study dynamical heterogeneities in homogeneous cardiac tissue created due to APD-restitution effects. We show that a region of temporal block of wave propagation can result in dynamical Wenckebach blocks which grow in space. This type of instability is called a GAI and can have important effects on spiral wave dynamics: it can lead to formation of new spirals or spiral termination. Restitution properties of cardiac tissue were always considered as related to observed instabilities, underlying the formation, or breakup of spiral waves. In particular, multiple studies [62, 112, 114, 36] showed that steep restitution can result in dynamical instabilities, possibly leading to fibrillation. In **chapter 5**, we show that also substantial effects of restitution at the global level can be expected. Thus we show that, although steep restitution gives rise to dynamical instabilities, it is not a necessary condition: also the global shape of the restitution curve plays an important role.

Looking back to **chapter 3** and **4**, we can now also understand why the initial small size ionic heterogeneities extend themselves in space under high frequency pacing: the possible mechanism behind this growth, because of which spirals could be initiated, or attracted, is GAI. In addition, this mechanism may be essential for a general theory of cardiac arrhythmias, for example those occurring under parasympathetic stimulation of the heart, as reported in [125].

Then in **chapter 6** we introduce our prototype of a database to collect data obtained from

experiments on human hearts, which we set up using the content management system Drupal. The prototype is based on data developed by the group of Prof. Efimov. We discuss the general structure of the database, and how users can both upload and download data obtained from experiments on human hearts. This system is still under development, however, all the main components of the database and corresponding website are already tested, and it will be filled in with data shortly.

## 2 Model complexity and limitations

---

In this thesis, we used the TP06 model for human ventricular cells [139]. In **chapter 2, 3 and 5** we used this model to describe human cardiac tissue, and in **chapter 4**, we combined this model with an anatomically based model of the human ventricles including fiber direction anisotropy [54]. The TP06 model is based on (recent) experimental data on most of the major ionic currents: the fast sodium, L-type calcium, transient outward, rapid and slow delayed rectifier, and inward rectifier currents, and it includes an extensive description of intracellular calcium handling. It fits experimentally measured APD restitution properties of human myocardium, which is a very important property for the occurrence and stability of reentrant arrhythmias. Also, regarding the anatomical model of the human ventricles, a good agreement was shown between simulated and clinical data in terms of ECG pattern, ECG frequency, surface wave patterns and occurrence of epicardial reentry [135]. These arguments prove the model used in this thesis to be a valuable model to study cardiac arrhythmias.

However, in recent years, new models for human ventricular cells were developed, based on more recent experimental data, and describe some ionic currents in more detail. Of interest, with respect to the results obtained in this thesis, is that Fink et al. [32] modified the TP06 model to include updated  $I_{Kr}$  and  $I_{K1}$  formulations, based on human ventricular measurements. In comparison to the TP06 model, the rate of repolarization is more accurate in this model. But, because a Markov formulation is used for  $I_{Kr}$ , this model sacrifices runtime speed. In a major part of this thesis we focused on the effect of changes in the repolarization currents on spiral initiation and dynamics, so it would be interesting to check if our results are still valid if such a modified description of these currents would be used.

Another interesting model, is the model developed by Iyer et al. [58]. This model accurately fits APD restitution properties of human ventricular myocytes, addresses whole-cell Ca homeostasis carefully and accurately reproduces diverse aspects of ECG. However, the most relevant ionic currents are formulated with Markovian chains, which make this model much more complex than the TP06 model, computationally more demanding, and hence less suited for tissue and whole heart simulations.

We also mention the model developed by Grandi et al. [43] (GB). This model relies on the framework of a rabbit myocyte model, and models ion channels and transporters on the basis of recent experimental data from human ventricular myocytes. It reformulates  $K^+$  currents, includes an additional subsarcolemmal compartment and provides a detailed description of  $Ca^{2+}$  handling. It is important to note that in the GB model, the effect of a block of the  $I_{Kr}$  or  $I_{Ks}$  current is slightly different than in the TP06 model. Also, in [43] the authors show that when the  $I_{Ks}$  current is blocked, the AP is less lengthened in the GB model than in the TP06 model. Furthermore, in the TP06 model, when the frequency is increased, a greater AP prolongation is observed upon block of the  $I_{Kr}$  current, while in the GB model, a reverse-rate dependence of  $I_{Kr}$  block was found. It should be clear that it would be interesting to examine



if these differences in the dynamics of these main repolarization currents have an effect on the results presented in this thesis.

Finally, we mention one of the most recent developed models for human ventricular cells, namely the ORd (O'Hara-Rudy dynamic) model [94]. The authors combined data obtained from new measurements for the L-type  $Ca^{2+}$  current,  $K^+$  currents, and  $Na^+/Ca^{2+}$  exchange current from undiseased human ventricle with data from previously published experiments, to build this model. In comparison to the GB model and the TP06 model, this model includes an extra current, namely the late  $I_{Na}$  current, and is based on more data for the  $I_{CaL}$  current. One of the most important aspects of this model is its close correspondence to experimental measurements of APD measured at not only 90% repolarization, but also at 50% and 30%, and this at all physiological relevant pacing rates. Compared to this model, the rate dependence of APD30 and APD50 of the TP06 model is less accurate [94]. This difference in repolarization rate between the ORd and the TP06 model is caused by the use of new data for the  $I_{CaL}$ ,  $I_{NaCa}$ ,  $I_{Kr}$  and  $I_{Ks}$  current. The altered dynamics of these repolarization currents also affect early after depolarization (EAD) formation. Indeed, recent studies observed, for example, a decreased repolarization reserve in the ORd model, making this model more prone to EADs [160]. The altered dynamics of these currents also have an effect on other phenomenon related to reentrant arrhythmia [56]. So again, it is evident that it should be checked if these differences between the models have an effect on our results.

We also note that in this thesis, current flow was modeled using a monodomain description of cardiac tissue. Another widely used model for cardiac tissue is the bidomain model [108]. In a monodomain description only the transmembrane currents and potentials are represented, while in a bidomain model both intracellular and extracellular currents and potentials are described. For simulations for which an external stimulus is applied, e.g. defibrillation, it is generally accepted that bidomain models are required. Although, for all our simulations, which did not include modeling of defibrillation, it was sufficient to use the computationally much more efficient monodomain modeling approach.

Another limitation to our modeling approach, is that only the cardiac excitation process is modeled. These waves of excitation initiate contraction, but not only excitation is coupled to the deformation of the medium; also the deformation of the heart affects cellular excitation processes. This phenomenon is called 'mechano-electrical-feedback' (MEF), and may have both pro-rhythmic and arrhythmogenic consequences [71]. For example, it has been shown that mechanical deformation alters the electrical properties of myocytes [130] and plays an important role in ventricular arrhythmias [35]. The effect of these feedback mechanisms on excitation lies outside the scope of this thesis.

### 3 Future directions

---

In this thesis, we studied APD heterogeneity of cardiac tissue, its role in initiation of spiral waves, and the influence of these ionic heterogeneities on the dynamics of spiral waves. Also heterogeneities created due to APD-restitution effects were studied. We believe that our work was a large step forward in the understanding of both the effect of electrotonic coupling on (APD) heterogeneity, spiral wave dynamics around (ionic) heterogeneities and heterogeneities created due to temporal inexcitability of cardiac tissue. However, our study contains a number of limitations, which would be interesting to overcome in future work.

We start with the future research directions opened up by the results presented in **chapter**

2. First of all, it is evident that it would be interesting to apply the approach presented there, i.e. evaluate APD heterogeneity of cardiac tissue using a Gaussian Green's function approach, to experimental studies. However, in order to extend our computational study to experimental work, several important issues still need to be investigated. The most important of them is to determine the space constant of the Green's function. The best approach here would be direct measurement of spatial distribution of repolarization in tissues with known heterogeneity. This heterogeneity might be static or dynamic (e.g. by local injection of currents into cardiac cells).

Also, computational [119] and recent experimental data [144] show that the extent of electrotonic effects depends on the shape of the action potential. It would thus be interesting to investigate the possibility to determine the space constant of the Green's function from measured action potential shapes.

Next, our solution of the inverse problem (find APD at single cell level, starting from measurements at tissue level) is not perfect for steep gradients of heterogeneity: the solution contains an oscillatory component, because of which we can not predict the underlying heterogeneity with a sufficient degree of certainty. Although, we note that in this thesis we used the most straightforward approach to solve the inverse problem, so this solution can certainly be improved if specific research would focus on this problem. Definitely because the inverse problem presented in **chapter 2** is one of the most studied in applied mathematics.

In **chapter 3 and 4**, we modeled small size ionic heterogeneities, similar to those measured in human cardiac tissue, and studied dynamics of spirals around these heterogeneities. Again, it would be interesting to study if results on initiation and anchoring of spiral waves could be confirmed via experimental studies. In [13], some experimental evidence for our results can be found. There, the authors applied several premature stimuli to a sheet of epicardial tissue of a rabbit heart containing a region with prolonged APD, created through regional cooling. They observed the formation of wavebreaks, which after further pacing, resulted in a spiral rotating around the heterogeneity, similar as observed in our simulations. Also in [155], anchoring of spirals to regions of prolonged APD, again created through regional cooling, was observed. Unfortunately neither of these studies provided a spatial distribution of the period of excitation, as we did in **chapter 3**. Therefore, it would be interesting to perform similar experiments with a protocol including the measurement of the period of excitation. In this way it would be easier to compare the results we obtained here with experimental results. Also, it would be of interest to check if similar ECG patterns as in our computational study are found in experiments, when a spiral is anchored around an ionic heterogeneity.

Finding the bifurcation described in **chapter 3** in an experimental study might be more challenging. This would require a gradual change of the extent of heterogeneity, which is difficult to obtain in experiments. However, it might be possible to use cell cultures of neonatal rat ventricular myocytes, such as in [12, 14], where heterogeneities of different size can be created. Gradual change of the extent of the heterogeneity can then be achieved by the application of drugs which change the refractory period of cardiac tissue.

In **chapter 4** we showed that small size ionic heterogeneities can not only anchor spirals, but can also attract spirals rotating at a substantial distance from the heterogeneity. It is clear that this property of these type of heterogeneities should be tested in an experimental set-up. Also, in our anatomical model of the ventricles, we demonstrate that if the heterogeneity is located close to the base, it can not only attract and anchor a spiral wave, but can also remove it. It would be interesting to study this attraction, anchoring, and eventual removal of a spiral, when the heterogeneity is created in the same way as studied here. Such heterogeneity

could for example be created by changing the local expression of genes responsible for the conductance of the  $I_{Ks}$  and  $I_{Kr}$  currents.

Also, in **chapter 4** we investigated the dynamics of a single spiral in the presence of a single heterogeneity. It would be interesting to investigate what would be the effect of several heterogeneities on a spiral wave; or the effect of an ionic heterogeneity on other regimes of spiral wave dynamics, such as spiral breakup.

Another limitation of our results presented in **chapter 3 and 4** is that the exact underlying reason of the APD heterogeneity measured in [40] is not known. In our studies we choose to change the conductance of the  $I_{Ks}$  and  $I_{Kr}$  currents (and in **chapter 3** also of the  $I_{CaL}$  current). The same APD heterogeneity could also be obtained for other parameter values. Although we checked that our main results are still valid for different sets of parameters, it would be interesting to find out the exact parameter set responsible for the observed APD heterogeneity. A possible way to achieve this, would be to use data on mRNA expression of genes responsible for the conductances of various channels, such as measured in [8]. Observed regional differences in mRNA expression could then be translated into our model by changing the conductances of the various currents in these regions. However, up to now, the regional differences reported in studies as [8] were not large enough to explain the observed (APD) heterogeneities at the tissue level. It is also possible that during the translation process from mRNA to proteins, or because of post-translational changes (e.g. phosphorylation), regional differences between the cells are created or enhanced. Also the coupling between the cells could be higher, or lower for different (transmural) locations in the heart, resulting in differences at the tissue level. It should thus be clear that a lot of work is still to be done to understand the exact mechanism causing the reported APD heterogeneity observed in studies as [40].

Next, the parameter setting used in this thesis to describe cardiac cell behavior corresponds to healthy human myocardium. Also the heterogeneities modeled in **chapters 3 and 4**, are based on data from non failing human hearts. However, the occurrence of ventricular tachycardia and fibrillation is strongly coupled to diseases such as myocardial infarction, cardiomyopathies, and heart failure. It is known that during these diseases extensive fibrosis formation [23] and gap junction remodeling [106] takes place, thereby increasing cardiac heterogeneity. Therefore, it would be interesting to incorporate these type of heterogeneities to our model, and investigate the possible additional effects on spiral wave dynamics.

Furthermore, apart from islands of increased APD heterogeneity, as studied and modeled here, there also exist transmural [10], and apex-base gradients [113]. These gradients will likely add additional effects which are important for the initiation and dynamics of spiral waves and organization of fibrillation.

In **chapter 5**, we showed that substantial effects of restitution at the global level can be expected according to formula (5.2). Thus, in **chapter 5** we showed that although steep restitution gives rise to dynamical instabilities, also the global shape of the restitution curve plays an important role. So, it would be interesting to investigate formula (5.2) on a patient specific restitution curve, and study if it is related to the onset of cardiac arrhythmias. It would also be interesting to investigate if the observed growth of the wave block region (GAI), as reported here, can be confirmed in an experimental set-up.

Finally, the prototype of the database, as introduced and discussed in **chapter 6**, has several limitations, which would be useful to overcome in future work. The most obvious limitation of the database is that it does not allow the users to compare the different experimental data stored in the database in a systematic way. It would thus be valuable to make it

possible for the user to perform statistics on the stored data. Another clear limitation is that the prototype does not allow the user to upload data in an automated way, as data on, for example, gene expression tend to be very extensive. Finally, another future direction would be to link data stored in the database to models of the human heart. For example, data on spatial expression of genes coding ion channels, exchangers and pumps could be linked to different parameters of ionic models of the human heart. It would thus be valuable to also store the different parameter sets of the models which can fit, or correspond to, a particular experimental measurement.

## 4 Conclusion

---

In this thesis we investigated APD heterogeneity of cardiac tissue and its influence on spiral wave dynamics. We also studied heterogeneity created by APD-restitution effects. We obtained several interesting results. In the first part of this thesis, we showed that the effect of cell coupling on APD heterogeneity can be described mathematically using a Gaussian Green's function approach. Using this approach, we can predict properties of cardiac cells from tissue measurements or vice versa. This is a non-trivial problem as heterogeneity at cell level can be 200 to 500 % more than at tissue level. We believe this is an exciting result, as it relates the problem of electrotonic interactions to a wide range of classical problems in physics, chemistry and biology, for which robust methods exist. So, although our method does not give a perfect solution for the (inverse) problem, we think it is promising. Then in the following chapter, we modeled small size ionic heterogeneities, similar to those observed in experiments, and showed that these heterogeneities can be pro-arrhythmic under high frequency external pacing. Interestingly, we found that spirals can be anchored around these small regions of increased APD. Next, we also found that these heterogeneities can attract spirals rotating at a substantial distance from the heterogeneity, both in 2D as in an anatomical model of the human ventricles. We also showed how a temporal block of wave propagation can have important effects on spatial excitation patterns and spiral wave dynamics. In particular, we showed that it results in dynamical Wenckebach blocks, which extend in space, and which we called global alternans instability or GAI. Interesting, we illustrate that GAI is the possible mechanism behind the growth of the small size ionic heterogeneities, leading to spiral wave initiation and attraction, observed in previous chapters. Finally, we introduced and discussed a prototype of the database we created to store data obtained from experiments, as used in this thesis.

## List of publications

---

A. Defauw, I.V. Kazbanov, H. Dierckx, P. Dawyndt, and A.V. Panfilov. Action potential duration heterogeneity of cardiac tissue can be evaluated from cell properties using Gaussian Green's function approach. *PLoS one*, 8(11):e79607, 2013.

A. Defauw, P. Dawyndt, and A.V. Panfilov. Initiation and dynamics of a spiral wave around an ionic heterogeneity in a model for human cardiac tissue. *Phys. Rev. E*, 88:062703, 2013.

A. Defauw, N. Vandersickel, P. Dawyndt, and A.V. Panfilov. Small size ionic heterogeneities in the human heart can attract rotors. *Am. J. Physiol. Heart Circ. Physiol.*, 307:1456-1468, 2014.

A. Defauw, N. Vandersickel, P. Dawyndt, and A.V. Panfilov. Global alternans instability and its effect on non-linear wave propagation: dynamical Wenckebach block and self terminating spiral waves. *Submitted*.

N. Vandersickel, I.V. Kazbanov, A. Defauw, D.A. Pijnappels, A.V. Panfilov. Decreased repolarization reserve increases defibrillation threshold by favoring early afterdepolarizations in an in silico model of human ventricular tissue. *Heart Rhythm*, 2015.



- [1] J.A. Abildskov and R.L. Lux. The mechanism of simulated torsade de pointes in a computer model of propagated excitation. *J. Cardiovasc. Electrophysiol.*, 2:224–237, 1991.
- [2] J.A. Abildskov and R.L. Lux. Simulated torsade de pointes - the role of conduction defects and mechanism of qrs rotation. *J. Electrocardiol.*, 33:55–64, 2000.
- [3] K. Agladze, J.P. Keener, S.C. Muller, and A.V. Panfilov. Rotating spiral waves created by geometry. *Science*, 264:1746–1748, 1994.
- [4] R.R. Aliev and A.V. Panfilov. Modeling of heart excitation patterns caused by a local inhomogeneity. *J. Theor. Biol.*, 181:33–40, 1996.
- [5] R.R. Aliev and A.V. Panfilov. A simple two-variable model of cardiac excitation. *Chaos, Solitons and Fractals*, 7:293–301, 1996.
- [6] M.A. Allesie, F.I.M. Bonke, and F.J.G. Schopman. Circus movement in rabbit atrial muscle as a mechanism of tachycardia. *Circ. Res.*, 33:54–62, 1973.
- [7] M.A. Allesie, W.J.E.P. Lammers, F.I.M. Bonke, and J. Hollen. *Experimental evaluation of Moe's multiple wavelet hypothesis of atrial fibrillation*. In: D.P. Zipes and J. Jalife, eds. *Cardiac Electrophysiology and Arrhythmias*. Grune and Stratton, 1985.
- [8] C.M. Ambrosi, K.A. Yamada, J.M. Nerbonne, and I.R. Efimov. Gender differences in electrophysiological gene expression in failing and non-failing human hearts. *PLoS one*, 8(1):e54635, 2013.
- [9] G. Amit, D.S. Rosenbaum, D.M. Super, and O. Costantini. Microvolt T-wave alternans and electrophysiologic testing predict distinct arrhythmia substrates: implications for identifying patients at risk for sudden cardiac death. *Heart Rhythm*, 7(6):763–768, 2010.
- [10] C. Antzelevitch, S. Sicouri, S.H. Litovsky, A. Lukas, S.C. Krishnan, J.M.D. Diego, G.A. Gintant, and D. Liu. Heterogeneity within the ventricular wall. *Circ. Res.*, 69:1427–1449, 1991.
- [11] O. Bernus, R. Wilders, C.W. Zemlin, H. Verschelde, and A.V. Panfilov. A computationally efficient electrophysiological model of human ventricular cells. *Am. J. Physiol. Heart Circ. Physiol.*, 282:H2296–H2308, 2002.
- [12] B.O. Bingen, S.F. Askar, M.J. Schaliij, I.V. Kazbanov, D.L. Ypey, A.V. Panfilov, and D.A. Pijnappels. Prolongation of minimal action potential duration in sustained fibrillation decreases complexity by transient destabilization. *Cardiovasc. Res.*, 97:161–70, 2013.
- [13] L. Boersma, Z. Zetelaki, J. Brugada, and M. Allesie. Polymorphic reentrant ventricular tachycardia in the isolated rabbit heart studied by high density mapping. *Circulation*, 105:3053–61, 2002.
- [14] K. Campbell, C.J. Calvo, S. Mironov, T. Herron, O. Berenfeld, and J. Jalife. Spatial gradients in action potential duration created by regional magnetofection of hERG are

## BIBLIOGRAPHY

---

- a substrate for wavebreak and turbulent propagation in cardiomyocyte monolayers. *J. Physiol.*, 590:6363–6379, 2012.
- [15] J. Chen, R. Mandapati, O. Berenfeld, A.C. Skanes, and J. Jalife. High-frequency periodic sources underlie ventricular fibrillation in the isolated rabbit heart. *Circ. Res.*, 86:86–93, 2000.
- [16] D.R. Chialvo and J. Jalife. Non-linear dynamics of cardiac excitation and impulse propagation. *Nature*, 330:749–752, 1987.
- [17] M.K. Chung, S.M. Pogwizd, D.P. Miller, and M.E. Cain. Three-dimensional mapping of the initiation of nonsustained ventricular tachycardia in the human heart. *Circulation*, 95:2517–2527, 1997.
- [18] R.H. Clayton, O. Bernus, E.M. Cherry, H. Dierckx, F.H. Fenton, L. Mirabella, and A.V. Panfilov. Models of cardiac tissue electrophysiology: Progress, challenges and open questions. *Prog. Biophys. Mol. Biol.*, 104:22–48, 2011.
- [19] M. Courtemanche, J.P. Keener, and L. Glass. A delay equation representation of pulse circulation on a ring of excitable media. *SIAM J. Appl. Math.*, 56:119–142, 1996.
- [20] B.T. Daniel. *Migraine*. AuthorHouse, 2010.
- [21] J.M. Davidenko, P.F. Kent, D.R. Chialvo, D.C. Michaels, and J. Jalife. Sustained vortex-like waves in normal isolated ventricular muscle. *Proc. Natl. Acad. Sci. U.S.A.*, 87:8785–9, 1990.
- [22] J.M. Davidenko, A.V. Pertsov, R. Salomonsz, W. Baxter, and J. Jalife. Stationary and drifting spiral waves of excitation in isolated cardiac muscle. *Nature*, 355:349–51, 1992.
- [23] J.M. de Bakker and H.V. van Rijen. Electrocardiographic manifestation of anatomical substrates underlying post-myocardial infarction tachycardias. *J. Electrocardiol.*, 40:21–25, 2007.
- [24] A. Defauw, P. Dawyndt, and A. V. Panfilov. Initiation and dynamics of a spiral wave around an ionic heterogeneity in a model for human cardiac tissue. *Phys. Rev. E*, 88:062703, 2013.
- [25] A. Defauw, I.V. Kazbanov, H. Dierckx, P. Dawyndt, and A. V. Panfilov. Action potential duration heterogeneity of cardiac tissue can be evaluated from cell properties using Gaussian Green’s function approach. *PLoS one*, 8(11):e79607, 2013.
- [26] A. Defauw, N. Vandersickel, P. Dawyndt, and A.V. Panfilov. Small size ionic heterogeneities in the human heart can attract rotors. *Am. J. Physiol. Heart Circ. Physiol.*, 307:1456–1468, 2014.
- [27] G. Dupont, A. Goldbeter, R. Salomonsz, W. Baxter, and J. Jalife. Oscillations and waves of cytosolic calcium: insights from theoretical models. *Bioessays*, 14:485–493, 1992.
- [28] I.R. Efimov, V.P. Nikolski, and G. Salama. Optical imaging of the heart. *Circ. Res.*, 95:21–33, 2004.



- [29] V.G. Fast and A.M. Pertsov. Drift of a vortex in the myocardium. *Biophysics*, 35:489–494, 1990.
- [30] F. Fenton, S.J. Evans, and H.M. Hastings. Memory in an excitable medium: A mechanism for spiral wave breakup in the low-excitability limit. *Phys. Rev. Lett.*, 83:3964–3967, 1999.
- [31] F. Fenton and A. Karma. Vortex dynamics in three-dimensional continuous myocardium with fiber rotation: Filament instability and fibrillation. *Chaos*, 8:20–47, 1998.
- [32] M. Fink, D. Noble, L. Virag, A. Varro, and W.R. Giles. Contributions of HERG K<sup>+</sup> current to repolarization of the human ventricular action potential. *Prog. Biophys. Mol. Biol.*, 96:357–376, 2008.
- [33] R. FitzHugh. Thresholds and plateaus in the hodgkin-huxley nerve equations. *J. Gen. Physiol.*, 43:867–896, 1960.
- [34] R. FitzHugh. Impulses and physiological states in theoretical models of nerve membrane. *Biophys. J.*, 1:445–466, 1961.
- [35] M.R. Franz, R. Cima, D Wang, D Profitt, and R. Kurz. Electrophysiological effects of myocardial stretch and mechanical determinants of stretch-activated arrhythmias. *Circulation*, 86:968–978, 1992.
- [36] A. Garfinkel, Y.H. Kim, O. Voroshilovsky, Z. Qu, J.R. Kil, M.H. Lee, H.S. Karagueuzian, J.N. Weiss, and P.S. Chen. Preventing ventricular fibrillation by flattening cardiac restitution. *Proc. Natl. Acad. Sci. U.S.A.*, 97:6061–6066, 2000.
- [37] W. Garrey. The nature of fibrillary contraction of the heart: its relation to tissue mass and form. *Am J Physiol*, 33:397–414, 1914.
- [38] G. Gerisch. Periodische signale steuern die musterbildung in zellverbanden. *Naturwissenschaften*, 58:430–438, 1971.
- [39] L. Glass, M.R. Guevara, A. Shrier, and R. Perez. Bifurcation and chaos in a periodically stimulated cardiac oscillator. *Physica D*, 7:89–101, 1983.
- [40] A.V. Glukhov, V.V. Fedorov, Q. Lou, V.K. Ravikumar, P.W. Kalish, R.B. Schuessler, N. Moazami, and I.R. Efimov. Transmural dispersion of repolarization in failing and nonfailing human ventricle. *Circ. Res.*, 106:981–91, 2010.
- [41] A.S. Go, D. Mozaffarian, V.L. Roger, E.J. Benjamin, J.D. Berry, W.B. Borden, D.M. Bravata, S. Dai, E.S. Ford, C.S. Fox, S. Franco, H.J. Fullerton, C. Gillespie, S.M. Hailpern, J.A. Heit, V.J. Howard, M.D. Huffman, B.M. Kissela, S.J. Kittner, D.T. Lackland, J.H. Lichtman, L.D. Lisabeth, D. Magid, G.M. Marcus, A. Marelli, D.B. Matchar, D.K. McGuire, E.R. Mohler, C.S. Moy, M.E. Mussolino, G. Nichol, N.P. Paynter, T. Poutrincourt, P.J. Schreiner, P.D. Sorlie, J. Stein, T.N. Turan, S.S. Virani, N.D. Wong, D. Woo, and M.B. Turner. Heart disease and stroke statistics - 2013 update. A report from the American Heart Association. *Circulation*, 127:6–245, 2012.
- [42] N.A. Gorelova and J. Bures. Spiral waves of spreading depression in the isolated chicken retina. *J. Neurobiol.*, 14:353–363, 1983.

## BIBLIOGRAPHY

---

- [43] E. Grandi, F.S. Pasqualini, and Bers D.M. A novel computational model of the human ventricular action potential and ca transient. *J. Mol. Cell. Cardiol.*, 48:112–121, 2010.
- [44] R.A. Gray, J. Jalife, A.V. Panfilov, W.T. Baxter, C. Cabo, J.M. Davidenko, and A.M. Pertsov. Mechanisms of cardiac fibrillation. *Science*, 270:1222–1223, 1995.
- [45] R.A. Gray, J. Jalife, A.V. Panfilov, W.T. Baxter, C. Cabo, J.M. Davidenko, and A.M. Pertsov. Nonstationary vortexlike reentrant activity as a mechanism of polymorphic ventricular tachycardia in the isolated rabbit heart. *Circulation*, 91:2454–69, 1995.
- [46] M.R. Guevara, A. Ward, A. Shrier, and L. Glass. Electrical alternans and period doubling bifurcations. *IEEE Comp. Cardiol.*, 562:167–170, 1984.
- [47] M. Haïssaguerre, P. Jaïs, D.C. Shah, A. Takahashi, M. Hocini, G. Quiniou, S. Garrigue, A. Le Mouroux, P. Le Métayer, and J. Clémenty. Spontaneous initiation of atrial fibrillation by ectopic beats originating in the pulmonary veins. *N. Eng. J. Med.*, 339:659–666, 1998.
- [48] P.C. Hansen. *Regularization tools: a Matlab package for analysis and solution of discrete ill-posed problems*. 2008.
- [49] P.C. Hansen, J.G. Nagy, and D.P. O’leary. *Deblurring images: Matrices, Spectra and Filtering*. SIAM, 2006.
- [50] W. Harvey. On the motion of the heart and blood in animals. 1628.
- [51] J. Hayase, R. Tung, S.M. Narayan, and D.E. Krummen. A case of a human ventricular fibrillation rotor localized to ablation sites for scar-mediated monomorphic ventricular tachycardia. *Heart Rhythm*, 10(12):1913–1916, 2013.
- [52] C.S. Henriques. Simulating the electrical behavior of cardiac tissue using the bidomain model. *Crit. Revs. Biomed. Eng.*, 21:1–77, 1993.
- [53] A. Hodgkin and A.F. Huxley. A quantitative description of membrane current and its application to conduction and excitation in nerve. *J. Physiol.*, 117:500–544, 1952.
- [54] R. Hren. A realistic model of the human ventricular myocardium: Applications to the study of ectopic activation. *PhD thesis*, 1996.
- [55] J. Huang, G.P. Walcott, C.R. Killingsworth, S.B. Melnick, J.M. Rogers, and R.E. Ideker. Quantification of activation patterns during ventricular fibrillation in open-chest porcine left ventricle and septum. *Heart Rhythm*, 2:720–728, 2005.
- [56] T.J. Hund, N.F. Otani, and Y. Rudy. Dynamics of action potential head-tail interaction during reentry in cardiac tissue: ionic mechanisms. *Am. J. Physiol. Heart Circ. Physiol.*, 279:1869–1879, 2000.
- [57] R.E. Ideker and J. Huang. Our search for the porcine mother rotor. *Ann. Noninvasive Electrocardiol.*, 10:7–15, 2005.
- [58] V. Iyer, R. Mazhari, and R.L. Winslow. A computational model of the human left-ventricular epicardial myocyte. *Biophys J.*, 87:1507–1525, 2004.

- [59] S. Jacubith, H.H. Rotermund, W. Engel, A. Von Oertzen, and G. Ertl. Spatiotemporal concentration patterns in a surface-reaction - propagating and standing waves, rotating spirals and turbulence. *Phys Rev Lett*, 65:3013–3016, 1990.
- [60] J. Jalife. Déjà vu in the theories of atrial fibrillation dynamics. *Cardiovasc. Res.*, 89:766–775, 2011.
- [61] J. Jalife, M. Delmar, J. Anumonwo, O. Berenfeld, and O. Kalifa. *Basic cardiac electrophysiology for the clinician, second edition*. Wiley-Blackwell, 2009.
- [62] A. Karma. Spiral breakup in model equations of action potential propagation in cardiac tissue. *Phys. Rev. Lett.*, 71:1103–1106, 1993.
- [63] A. Karma. Electrical alternans and spiral wave breakup in cardiac tissue. *Chaos*, 4:461–472, 1994.
- [64] M.W. Kay, G.P. Walcott, Gladden J.D., S.B. Melnich, and J.M. Rogers. Lifetimes of epicardial rotors in panoramic optical maps of fibrillating swine ventricles. *Am. J. Physiol. Heart. Circ. Physiol.*, 291:H1935–H1941, 2006.
- [65] J.P. Keener and J. Sneyd. *Mathematical Physiology*. Springer-Verlag, 1998.
- [66] R.H. Keldermann, K.H.W.J. ten Tusscher, M.P. Nash, C.P. Bradley, R. Hren, P. Taggart, and A.V. Panfilov. A computational study of mother rotor VF in the human ventricles. *Am. J. Physiol., Heart. Circ. Physiol.*, 296:370–379, 2009.
- [67] R.H. Keldermann, K.H.W.J. ten Tusscher, M.P. Nash, R. Hren, P. Taggart, and A.V. Panfilov. Effect of heterogeneous APD restitution on VF organization in a model of the human ventricles. *Am. J. Physiol.*, 294:764–774, 2008.
- [68] Y.H. Kim, F. Xie, M. Yashima, T.J. Wu, M. Valderrábano, M.H. Lee, T. Ohara, O. Voroshilovsky, R.N. Doshi, M.C. Fishbein, Z. Qu, A. Garfinkel, J.N. Weiss, H.S. Karagueuzian, and P.S. Chen. Role of papillary muscle in the generation and maintenance of reentry during ventricular tachycardia and fibrillation in isolated swine right ventricle. *Circulation*, 100:1450–1459, 1999.
- [69] A.G. Kleber and Y. Rudy. Basic mechanisms of cardiac impulse propagation and associated arrhythmias. *Physiol Rev*, 84:431–488, 2004.
- [70] B.Y. Kogan, W.J. Karplus, B.S. Billett, A.T. Pang, H.S. Karagueuzian, and S.S. Khan. The simplified fitzhugh-nagumo model with action potential duration restitution: effects on 2d wave propagation. *Physica D*, 50:327–340, 1991.
- [71] P. Kohl, P. Hunter, and D. Noble. Stretch-induced changes in heart rate and rhythm: Clinical observations, experiments and mathematical models. *Prog. Biophys. Molec. Biol.*, 71:91–138, 1999.
- [72] M. Koller, M.L. Riccio, and R.F. Gilmour Jr. Dynamic restitution of action potential duration during electrical alternans and ventricular fibrillation. *Am. J. Physiol., Heart. Circ. Physiol.*, 275:1635–1642, 1998.

## BIBLIOGRAPHY

---

- [73] V.I. Krinsky. Spread of excitation in an inhomogeneous medium (state similar to cardiac fibrillation). *Biophysics*, 11:776–784, 1966.
- [74] J.I. Laughner, F.S. Ng, M.S. Sulkin, R.M. Arthur, and I.R. Efimov. Processing and analysis of cardiac optical mapping data obtained with potentiometric dyes. *Am. J. Physiol. Heart Circ. Physiol.*, 303:H753–H765, 2012.
- [75] A.A.P. Leao. Spreading depression of activity in the cerebral cortex. *Journal of Neurophysiology*, 7:359–390, 1944.
- [76] J. Lechleiter, S. Girard, E. Peraltal, and D. Clapham. Spiral calcium wave propagation and annihilation in *Xenopus Laevis* oocytes. *Science*, 252:123–126, 1991.
- [77] Q. Lou, V.V. Fedorov, A.V. Glukhov, N. Moazami, V. Fast, and I.R. Efimov. Transmural heterogeneity and remodeling of ventricular excitation-contraction coupling in human heart failure. *Circulation*, 123:1881–1890, 2011.
- [78] C.H. Luo and Y. Rudy. A model of the ventricular cardiac action potential. Depolarization, repolarization, and their interaction. *Circ. Res.*, 68:1501–1526, 1991.
- [79] C.H. Luo and Y. Rudy. A dynamic model of the cardiac ventricular action potential. i. Simulations of ionic currents and concentration changes. *Circ. Res.*, 74:1071–1096, 1994.
- [80] R. Majumder. *Spiral and scroll wave dynamics in ionically and anatomically realistic mathematical models for mammalian ventricular tissue*. Phd thesis, Indian Institute of science, Bangalore, 2014.
- [81] R. Majumder, A.R. Nayak, and R. Pandit. Scroll wave dynamics in human cardiac tissue: lessons from a mathematical model with inhomogeneities and fiber architecture. *PLOS one*, 6(4):e18052, 2011.
- [82] S. Masse, E. Downar, V. Chauhan, E. Sevapsidis, and K. Nanthakumar. Ventricular fibrillation in myopathic human hearts: mechanistic insights from in vivo global endocardial and epicardial mapping. *Am. J. Physiol.*, 292:H2589–H2597, 2007.
- [83] J. Mayer. Rhythmical pulsation in Scyphomedusae. Washington, DC: Carnegie Institute of Washington. Publication number 47. pages 1–62, 1906.
- [84] G.R. Mines. On dynamic equilibrium in the heart. *J Physiol (Lond)*, 46:349–383, 1913.
- [85] G.R. Mines. On circulating excitations in heart muscles and their possible relation to tachycardia and fibrillation. *Trans R Soc Can*, 4:43–52, 1914.
- [86] G.K. Moe. On the multiple wavelet hypothesis of atrial fibrillation. *Arch. Int. Pharmacodyn. Ther.*, 140:183–188, 1962.
- [87] G.K. Moe, W.C. Rheinbolt, and J.A. Abildskov. A computer model of atrial fibrillation. *Am. Heart J.*, 67:200–220, 1964.
- [88] S.M. Narayan, D.E. Krummen, and W. Rappel. Clinical mapping approach to diagnose electrical rotors and focal impulse sources for human atrial fibrillation. *J. Cardiovasc. Electrophysiol.*, 23(5):447–454, 2012.

- 
- [89] S.M. Narayan, D.E. Krummen, K. Shivkumar, P. Clopton, W. Rappel, and J.M. Miller. Treatment of atrial fibrillation by the ablation of localized sources. *J. Am. Coll. Cardiol.*, 60(7):628–636, 2012.
- [90] M.P. Nash, A. Mourad, R.H. Clayton, P.M. Sutton, C.P. Bradley, M. Hayward, D.J. Paterson, and P. Taggart. Evidence for multiple mechanisms in human ventricular fibrillation. *Circulation*, 114:536–542, 2006.
- [91] D. Noble. A modification of the Hodgkin-Huxley equations applicable to Purkinje fibres action and pacemaker potential. *J. Physiol. (Lond.)*, 160:317–352, 1962.
- [92] D. Noble, A. Varghese, P. Kohl, and P. Noble. Improved guinea-pig ventricular cell model incorporating a diadic space, IKr and IKs, and length- and tension-dependent processes. *Can. J. Cardiol.*, 14:123–134, 1998.
- [93] J.B. Nolasco and R.W. Dahlen. A graphic method for the study of alternation in cardiac action potentials. *J. Appl. Physiol.*, 25:191–196, 1968.
- [94] T. O’Hara, L. Virag, A. Varro, and Y. Rudy. Simulation of the undiseased human cardiac ventricular action potential: model formulation and experimental validation. *PLoS Comput. Biol.*, 7(5):e1002061, 2011.
- [95] A.V. Panfilov. Spiral breakup as a model of ventricular fibrillation. *Chaos*, 8:57–64, 1998.
- [96] A.V. Panfilov. Three-dimensional organization of electrical turbulence in the heart. *Phys. Rev. E*, 59:6251–6254, 1999.
- [97] A.V. Panfilov. Is heart size a factor in ventricular fibrillation? or how close are rabbit and human hearts? *Heart Rhythm*, 3:862–864, 2006.
- [98] A.V. Panfilov and P. Hogeweg. Spiral break up in a modified FitzHugh Nagumo model. *Phys. Lett. A*, 176:295–299, 1993.
- [99] A.V. Panfilov and A.V. Holden. Self-generation of turbulent vortices in a two-dimensional model of cardiac tissue. *Phys. Lett. A*, 147:463–466, 1990.
- [100] A.V. Panfilov and A.V. Holden. Computer simulation of reentry sources in myocardium in two and three dimensions. *J. Theor. Biol.*, 161:271–285, 1993.
- [101] A.V. Panfilov and J.P. Keener. Effects of high frequency stimulation on cardiac tissue with an inexcitable obstacle. *J. Theor. Biol.*, 163:439–448, 1993.
- [102] A.V. Panfilov and B.N. Vasiev. Vortex initiation in a heterogeneous excitable medium. *Physica D*, 49:107–113, 1991.
- [103] D. Pazo, L. Kramer, A. Pumir, S. Kanani, I. Efimov, and V. Krinsky. Pinning force in active media. *Phys. Rev. Lett.*, 93:168303, 2004.
- [104] A.M. Pertsov, J.M. Davidenko, R. Salomontsz, W. Baxter, and J. Jalife. Spiral waves of excitation underlie reentrant activity in isolated cardiac muscle. *Circulation*, 72:631–650, 1993.

## BIBLIOGRAPHY

---

- [105] A.M. Pertsov, M. Wellner, M. Vinson, and J. Jalife. Topological constraint on scroll wave pinning. *Phys. Rev. Lett.*, 84:2738–2741, 2000.
- [106] J.M. Pinto and P.A. Boyden. Electrical remodeling in ischemia and infarction. *Cardiovasc. Res.*, 42:284–297, 1999.
- [107] S.M. Pogwizd, J.P. McKenzie, and M.E. Cain. Mechanisms underlying spontaneous and induced ventricular arrhythmias in patients with idiopathic dilated cardiomyopathy. *Circulation*, 98:2404–2414, 1998.
- [108] M. Potse, B. Dubé, A. Vinet, and R. Cardinal. A comparison of monodomain and bidomain propagation models for the human heart. *Conf Proc IEEE Eng Med Biol Soc.*, 1:3895–8., 2006.
- [109] L. Priebe and D.J. Beuckelmann. Simulation study of cellular electrical properties in heart failure. *Circ. Res.*, 82:1206–1223, 1998.
- [110] Z. Qu, A. Garfinkel, and J.N. Weiss. Vulnerable window for conduction block in a one-dimensional cable of cardiac cells, 1: single extrasystoles. *Biophys. J.*, 91:793–804, 2006.
- [111] Z. Qu, A. Garfinkel, and J.N. Weiss. Vulnerable window for conduction block in a one-dimensional cable of cardiac cells, 2: multiple extrasystoles. *Biophys. J.*, 91:805–815, 2006.
- [112] Z. Qu, J.N. Weiss, and A. Garfinkel. Cardiac electrical restitution properties and stability of reentrant spiral waves: a simulation study. *Am. J. Physiol. Heart Circ. Physiol.*, 276:269–283, 1999.
- [113] C. Ramanathan, P. Jia, R. Ghanem, K. Ryu, and Y. Rudy. Activation and repolarization of the normal human heart under complete physiological conditions. *PNAS*, 103(16):6309–6314, 2006.
- [114] M.L. Riccio, M.L. Koller, and R.F. Gilmour Jr. Electrical restitution and spatiotemporal organization during ventricular fibrillation. *Circ. Res.*, 84:955–963, 1999.
- [115] J.M. Rogers, Huang J., S.B. Melnick, and R.E. Ideker. Sustained reentry in the left ventricle of fibrillating pig hearts. *Circ. Res.*, 92:539–545, 2003.
- [116] A.N. Rudenko and A.V. Panfilov. Drift and interaction of vortices in two-dimensional heterogeneous active medium. *Studia Biophysica*, 98:183–188, 1983.
- [117] S. Rush and H. Larsen. A practical algorithm for solving dynamic membrane equation. *IEEE Trans Biomed Eng.*, 25:389–392, 1978.
- [118] F. Samie, O. Berenfeld, J. Anumonwo, S.F. Mironov, S. Udassi, J. Beaumont, S. Taffet, A.M. Pertsov, and J. Jalife. Rectification of the background potassium current: a determinant of rotor dynamics in ventricular fibrillation. *Circ. Res.*, 89:1216–1223, 2001.
- [119] K.J. Sampson and C.S. Henriquez. Electrotonic influences on action potential duration dispersion in small hearts: a simulation study. *Am J Physiol Heart Circ Physiol*, 289:350–360, 2005.

- [120] P. Sanders, O. Berenfeld, M. Hocini, P. Jaïs, R. Vaidyanathan, L.F. Hsu, S. Garrigue, Y. Takahashi, M. Rotter, F. Sacher, C. Scavée, R. Ploutz-Snyder, J. Jalife, and M. Haïssaguerre. Spectral analysis identifies sites of high-frequency activity maintaining atrial fibrillation in humans. *Circulation*, 112:789–797, 2005.
- [121] O. Selfridge. Studies on flutter and fibrillation; some notes on the theory of flutter. *Arch. Inst. Cardiol. Mex.*, 18:177–187, 1948.
- [122] T.K. Shajahan, A.R. Nayak, and R. Pandit. Spiral wave turbulence and its control in the presence of inhomogeneities in four mathematical models of cardiac tissue. *PLOS one*, 4(3):e4738, 2009.
- [123] T.K. Shajahan, S. Sinha, and R. Pandit. Spiral wave dynamics depend sensitively on inhomogeneities in mathematical models of ventricular tissue. *Phys. Rev. E*, 75:011929, 2007.
- [124] T.K. Shajahan, S. Sinha, and R. Pandit. Spiral wave dynamics depend sensitively on inhomogeneities in mathematical models of ventricular tissue. *Phys. Rev. E*, 75:011929, 2007.
- [125] O.F. Sharifov, V.V. Fedorov, G.G. Beloshapko, A.V. Glukhov, A.V. Yushmanova, and L.V. Rosenshtraukh. Roles of adrenergic and cholinergic stimulation in spontaneous atrial fibrillation in dogs. *J. Am. Coll. Cardiol.*, 43:483–490, 2004.
- [126] Y. Shiferaw, M.A. Watanabe, A. Garfinkel, J.N. Weiss, and A. Karma. Model of intracellular calcium cycling in ventricular myocytes. *Biophys. J.*, 85(6):3666–3686, 2003.
- [127] W. Shimizu and C. Antzelevitch. Cellular basis for the ECG features of the LQT1 form of the long-QT syndrome: effects of beta-adrenergic agonists and antagonists and sodium channel blockers on transmural dispersion of repolarization and torsade de pointes. *Circulation*, 98:2314–2322, 1998.
- [128] W. Shimizu and C. Antzelevitch. Differential effects of beta-adrenergic agonists and antagonists in LQT1, LQT2 and LQT3 models of the long QT syndrome. *J. Am. Coll. Cardiol.*, 35:778–786, 2000.
- [129] F. Siegert and C.J. Weijer. Three-dimensional scroll wave organize Dictyostelium slugs. *Proc. Natl. Acad. Sci. U.S.A.*, 89:6433–6437, 1992.
- [130] W. Sigurdson, A. Ruknudin, and F. Sachs. Calcium imaging of mechanically induced fluxes in tissue-cultured chick heart: role of stretch-activated ion channels. *Am. J. Physiol.*, 262:1110–1115, 1992.
- [131] S. Sridhar, A. Ghosh, and S. Sinha. Critical role of pinning defects in scroll wave breakup in active media. *Europhys. Lett.*, 103:50003, 2013.
- [132] D. Streeter. *Handbook of Physiology, Sec. 2. Vol. I. The Heart*. Bethesda, Maryland: Am Physiol Soc, 1979.
- [133] S. Takagi, A. Pumir, D. Pazo, I. Efimov, V. Nikolski, and V. Krinsky. Unpinning and removal of a rotating wave in cardiac muscle. *Phys. Rev. Lett.*, 93:058101, 2004.

## BIBLIOGRAPHY

---

- [134] K.H.W. ten Tusscher. *Spiral wave dynamics and ventricular arrhythmias*. Phd thesis, Universiteit Utrecht, 2004.
- [135] K.H.W. ten Tusscher, R. Hren, and A.V. Panfilov. Organization of ventricular fibrillation in the human heart. *Circ. Res.*, 100(12):87–101, 2007.
- [136] K.H.W. ten Tusscher, D. Noble, P.J. Noble, and A.V. Panfilov. A model for human ventricular tissue. *Am. J. Physiol. Heart Circ. Physiol.*, 286:1573–1589, 2004.
- [137] K.H.W. ten Tusscher and A.V. Panfilov. Influence of nonexcitable cells on spiral breakup in two-dimensional and three-dimensional excitable media. *Phys. Re. E*, 68:062902, 2003.
- [138] K.H.W. ten Tusscher and A.V. Panfilov. Reentry in heterogeneous cardiac tissue described by the Luo-Rudy ventricular action potential model. *Am. J. Physiol.*, 284:542–548, 2003.
- [139] K.H.W. ten Tusscher and A.V. Panfilov. Alternans and spiral breakup in a human ventricular tissue model. *Am. J. Physiol. Heart Circ. Physiol.*, 291:1088–1100, 2006.
- [140] M. Valderrabano, M.H. Lee, T. Ohara, A.C. Lai, M.C. Fishbein, S.F. Lin, H.S. Karagueuzian, and P.S. Chen. Dynamics of intramural and transmural reentry during ventricular fibrillation in isolated swine ventricles. *Circulation*, 88(8):839–848, 2001.
- [141] A. Vinet. Quasiperiodic circus movement in a loop model of cardiac tissue: multistability and low dimensional equivalence. *Ann. Biomed. Eng.*, 28:704–720, 2000.
- [142] M. Vinson, A. Pertsov, and J. Jalife. Anchoring of vortex filaments in 3d excitable media. *Physica D*, 72:119–134, 1994.
- [143] C.R. Vogel. *Computational methods for inverse problems*. SIAM, 2002.
- [144] R.D. Walton and O. Bernus. Electrotonic effects on action potential duration in perfused rat hearts. *Conf Proc IEEE Eng Med Biol Soc*, pages 4190–4193, 2009.
- [145] L.D. Weise. *Spiral wave initiation in reaction-diffusion mechanics systems*. Phd thesis, Universiteit Utrecht, 2012.
- [146] J.N. Weiss, A. Karma, Y. Shiferaw, P.S. Chen, A. Garfinkel, and Z. Qu. From pulsus to pulseless: the saga of cardiac alternans. *Circ. Res.*, 98(10):1244–1253, 2006.
- [147] K.F. Wenckebach. On the analysis of irregular pulses. *Z. Klin. Med.*, 37:475–488, 1899.
- [148] N. Wiener and A. Rosenblueth. The mathematical formulation of the problem of conduction of impulses in a network of connected excitable elements, specifically in cardiac muscle. *Arch. Inst. Cardiol. Mex.*, 16:205–265, 1946.
- [149] S.C. Wijers, M.A. Vos, and M. Meine. Microvolt t-wave alternans in an unselected heart failure population: pros and cons. *Eur. J. Heart Fail.*, 14(4):344–347, 2012.
- [150] A.T. Winfree. Spiral waves of chemical activity. *Science*, 175:634–636, 1972.



- 
- [151] A.T. Winfree. Scroll-shaped waves of chemical activity in three dimensions. *Science*, 7:937–939, 1973.
- [152] T. Wu, M. Yashima, F Xie, C.A. Athill, Y. Kim, M.C. Fishbein, Z. Qu, A. Garfinkel, J.N. Weiss, H.S. Karagueuzian, and P. Chen. Role of pectinate muscle bundles in the generation and maintenance of intra-atrial reentry. *Circ. Res.*, 83:448–462, 1998.
- [153] T.J. Wu, S.F. Lin, A. Baher, Z. Qu, A. Garfinkel, J.N. Weiss, C.T. Ting, and P.S. Chen. Mother rotors and the mechanisms of D600-induced type 2 ventricular fibrillation. *Circulation*, 110:2110–2118, 2004.
- [154] Y. Xie, G. Hu, D. Sato, J.N. Weiss, A. Garfinkel, and Z. Qu. Dispersion of refractoriness and induction of reentry due to chaos synchronization in a model of cardiac tissue. *Phys. Rev. Lett.*, 99(11):118101, 2007.
- [155] M. Yamazaki, H. Honjo, T Ashihara, M. Harada, I. Sakuma, K. Nakazawa, N. Trayanova, M. Horie, J. Kalifa, J. Jalife, K. Kamiya, and Kodama I. Regional cooling facilitates termination of spiral-wave reentry through unpinning of rotors in rabbit hearts. *Heart Rhythm*, 9(1):107–114, 2012.
- [156] C.W. Zemlin and A.M. Pertsov. Anchoring of drifting spiral and scroll waves to impermeable inclusions in excitable media. *Phys. Rev. Lett.*, 109:038303, 2012.
- [157] A.M. Zhabotinsky and A.N. Zaikin. Space effects in a self-oscillating chemical system. *Oscillatory Processes in Biological and Chemical Systems*, 2:279–283, 1971.
- [158] A.M. Zhabotinsky and A.N. Zaikin. Autowave processes in a distributed chemical system. *J. Theor. Biol.*, 40:45–61, 1973.
- [159] Z.J. Zheng, J.B. Croft, W.H. Giles, and G.A. Mensah. Sudden cardiac death in the United States, 1989 to 1998. *Circulation*, 104:2158–2163, 2001.
- [160] S. Zimik, N. Vandersickel, A.R. Nayak, A.V. Panfilov, and R. Pandit. A comparative study of EAD-mediated fibrillation in the ORd and TP06 models. *In preparation*.